

Optical techniques for broadband in-building networks

Citation for published version (APA):

Yang, H. (2011). *Optical techniques for broadband in-building networks*. [Phd Thesis 1 (Research TU/e / Graduation TU/e), Electrical Engineering]. Technische Universiteit Eindhoven. <https://doi.org/10.6100/IR694369>

DOI:

[10.6100/IR694369](https://doi.org/10.6100/IR694369)

Document status and date:

Published: 01/01/2011

Document Version:

Publisher's PDF, also known as Version of Record (includes final page, issue and volume numbers)

Please check the document version of this publication:

- A submitted manuscript is the version of the article upon submission and before peer-review. There can be important differences between the submitted version and the official published version of record. People interested in the research are advised to contact the author for the final version of the publication, or visit the DOI to the publisher's website.
- The final author version and the galley proof are versions of the publication after peer review.
- The final published version features the final layout of the paper including the volume, issue and page numbers.

[Link to publication](#)

General rights

Copyright and moral rights for the publications made accessible in the public portal are retained by the authors and/or other copyright owners and it is a condition of accessing publications that users recognise and abide by the legal requirements associated with these rights.

- Users may download and print one copy of any publication from the public portal for the purpose of private study or research.
- You may not further distribute the material or use it for any profit-making activity or commercial gain
- You may freely distribute the URL identifying the publication in the public portal.

If the publication is distributed under the terms of Article 25fa of the Dutch Copyright Act, indicated by the "Taverne" license above, please follow below link for the End User Agreement:

www.tue.nl/taverne

Take down policy

If you believe that this document breaches copyright please contact us at:

openaccess@tue.nl

providing details and we will investigate your claim.

Optical Techniques for Broadband In-Building Networks

PROEFSCHRIFT

ter verkrijging van de graad van doctor aan de
Technische Universiteit Eindhoven, op gezag van de
rector magnificus, prof.dr.ir. C.J. van Duijn, voor een
commissie aangewezen door het College voor
Promoties in het openbaar te verdedigen
op dinsdag 11 januari 2011 om 16.00 uur

door

Hejie Yang

geboren te Tianjin, China

Dit proefschrift is goedgekeurd door de promotor:

prof.ir. A.M.J. Koonen

Copromotor:

dr.ir. E. Tangdionga

This Ph.D. thesis has been approved by a committee with the following members:

prof.dr.ir. A.C.P.M. Backx (chairman), Technische Universiteit Eindhoven
prof.ir. A.M.J. Koonen (first promotor), Technische Universiteit Eindhoven
dr.ir. E. Tangdionga (copromotor), Technische Universiteit Eindhoven
prof.dr.ir. P.G.M. Baltus, Technische Universiteit Eindhoven
prof.dr. B. Cabon, Grenoble Institute of Technology
dr.-ing. O. Ziemann, Georg-Simon-Ohm-Fachhochschule Nuernberg
prof.dr. J. Capmany, Universidad Politécnica de Valencia
dr.-ing. A. Stöhr, Universität Duisburg Essen

A catalogue record is available from the Eindhoven University of Technology Library

Optical techniques for broadband in-building networks

Hejie Yang. - Eindhoven : Technische Universiteit Eindhoven, 2011.

Proefschrift. - ISBN: 978-90-386-2423-5

NUR 959

Trefwoorden: optische telecommunicatie / radio-over-glasvezel / magnetron fotonica /
plastic optische vezel.

Subject headings: optical fibre communication / radio-over-fibre / microwave photonics /
plastic optical fibre.

Copyright © 2011 by Hejie Yang

All rights reserved. No part of this publication may be reproduced, stored in
a retrieval system, or transmitted in any form or by any means without the
prior written consent of the author.

Typeset using L^AT_EX, printed in The Netherlands.

天行健，君子以自強不息；
地勢坤，君子以厚德載物。
——《周易》，公元前3世紀

As heaven maintains vigor through movements,
a gentleman should constantly strive for self-perfection.

As earth's condition is receptive devotion,
a gentleman should hold the outer world with broad mind.

—— I Ching (Yi Jing), 3rd century BC

Abstract

Essays on Optical Techniques for Broadband In-Building Networks

Optical fibres, which has been shown to be capable of conveying bandwidth demand, have been rolled out to more than 32 million homes and professional buildings worldwide up to 2010. The basic technological and economical challenges of fibre-to-the-home (FTTH) has been solved. The current FTTH technology can now provide baseband Gbit Ethernet and high definition TV services to the doorstep. Thus, the bottleneck for delivery of broadband services to the end users is shifting from the access to the in-building network. In the meantime, the need for high-capacity transmission between devices inside the building, e.g. between desktop PC and data services, are also rapidly increasing. How to bring high bandwidth to the mobile terminals such as laptops, PDAs or cell phones as well as to the fixed terminals such as desktop PCs and HDTV equipment in an all-in-one network infrastructure is a challenge we are facing. Building on the flexibility of the wireless access networks and the latent vast bandwidth of fibre infrastructure, radio-over-fibre (RoF) techniques have been proposed as a cost-effective solution for the future integration of broadband services into in-building networks.

This thesis investigates techniques to deliver high data rate wireless services via in-building networks: high capacity RoF links employing optical frequency multiplication (OFM) and sub-carrier multiplexing (SCM) techniques, with single- or multi-carrier signal formats. The orthogonal frequency division multiplexing (OFDM) format is investigated for the RoF transmission system, particularly with respect to the optical system nonlinearity. For low-cost short-range optical backbone networks, RoF transmission over large-core diameter plastic optical fibre (POF) links has been studied, including the transmission of the WiMedia-compliant multiband OFDM ultra-wideband (UWB) signal over bandwidth-limited large-core POFs as well as a full-duplex bi-directional UWB transmission over POF.

In order to improve the functionalities for the delivery of wireless services of in-building networks, techniques to introduce flexibility into the network architecture and to create dynamic capacity allocation have been investigated. By employing optical switching techniques based

on optical semiconductor amplifiers (SOA), an optically routed RoF system has been studied. The dynamic capacity allocation is addressed by investigating one and two-level routing using electrical SCM and optical wavelengths.

In addition, next to RoF networking, this thesis explores techniques for wired delivery of baseband high capacity services over POF links by employing a multi-level signal modulation format, in particular discrete multi-tone (DMT) modulation. Transmission of 10 Gbit/s data over 1 mm core diameter PMMA POF links is demonstrated as a competitor to more expensive fibre solutions such as silica single and multimode fibre. A record transmission rate of more than 40 Gbit/s is presented for POF whose core diameter is comparable with silica multimode fibre.

Finally, from the network perspective, the convergence of wired and wireless multi-standard services into a single fibre-based infrastructure has been studied. Techniques have been designed and demonstrated for in-building networks, which can convey both high capacity baseband services and broadband radio frequency (RF) services over a POF backbone link. The multi-standard RoF signals carry different wireless services at different radio frequencies and with different bandwidths, including WiFi, WiMax, UMTS and UWB. System setups to transport them together over the same multimode optical fibre based network have been designed and experimentally shown.

All the concepts, designs and system experiments presented in this thesis underline the strong potential of multimode (silica and plastic) optical fibre techniques for the delivery of broadband services to wired and wireless devices for in-building networks, in order to extend to the end user the benefits of the broadband FTTH networks which are being installed and deployed worldwide.

Contents

Abstract	v
1 Introduction	1
1.1 Broadband In-Building Networks	2
1.1.1 Wireless services	2
1.1.2 Radio-over-fibre techniques	5
1.2 Optical Backbone: Plastic Optical Fibre (POF)	7
1.3 Scope of Thesis	10
2 High Capacity Radio-over-Fibre Transmission Systems	13
2.1 Optical Frequency Multiplication	13
2.1.1 Principle of operation	13
2.1.2 Influence of phase noise	16
2.2 Radio-over-Fibre Distribution using SCM and OFM	18
2.2.1 Broadcast architecture: system design and experiment	20
2.2.2 Parameters and trade-off	22
2.3 OFM Transmitter Nonlinearity	24
2.3.1 Orthogonal frequency division multiplexing	24
2.3.2 Effects of MZM nonlinearity on single-carrier QAM and OFDM-QAM signals . . .	26
2.4 Summary	30
3 Ultra-Wideband Wireless Service over POF Systems	33
3.1 Ultra-Wideband Signal and Multi-Band OFDM	33
3.1.1 Multi-band OFDM UWB versus impulse radio UWB	33
3.1.2 Industrial standard on multi-band OFDM	34
3.1.3 UWB-over-POF system	36
3.2 High Capacity Gbit/s UWB Transmission over PMMA POF	36

CONTENTS

3.2.1	Baseband OFDM: discrete multi-tone modulation	37
3.2.2	Experimental setup and results	38
3.3	WiMedia-compliance UWB Transmission over PMMA POF	40
3.3.1	Principle of operation	41
3.3.2	Experimental results	43
3.4	Bi-directional Transmission of WiMedia-compliance UWB over PF POF	45
3.4.1	Experimental setup	45
3.4.2	Experimental results	46
3.5	Summary	48
4	Optical Dynamic Routing in Radio-over-Fibre Links	51
4.1	Principle of Operation	52
4.1.1	Wavelength conversion techniques	52
4.1.2	XGM effect on analogue RF signal in SOA	53
4.1.3	Optical routing using SOA	55
4.2	Experimental Study	57
4.2.1	One-level dynamics with optical routing	57
4.2.2	Two-level dynamics with optical routing and electrical SCM	61
4.3	Inter-room Communication via Optical Cross-connect	65
4.4	Summary	67
5	High Capacity Baseband Data Links over POF	69
5.1	Bit-Loading in DMT	69
5.2	Transmission over PMMA GI-POF Employing Different Photo-detectors	71
5.2.1	4.5 Gbit/s over 50 m PMMA GI-POF using APD	71
5.2.2	12.7 Gbit/s over 35 m PMMA GI-POF using PIN Diode	74
5.2.3	Discussion	76
5.3	Transmission over 50 m PMMA Multi-core SI-POF	76
5.4	47.4 Gbit/s Transmission over 100 m PF GI-POF	80
5.4.1	Experimental setup	80
5.4.2	Transmission results	81
5.4.3	Effect of parameters	82
5.5	Summary	86

6	Converged Multi-standard In-Building Networks	89
6.1	Multi-standard Wireless Distribution System over MMF	90
6.1.1	Experimental setup	90
6.1.2	Experimental results	91
6.2	Wired and Wireless Multi-standard System over POF	93
6.2.1	Experimental setup	94
6.2.2	Experimental results and discussion	95
6.3	Summary	98
7	Conclusions and Recommendations	99
7.1	Summary and Conclusion	99
7.2	Outlook and Future Work	104
A	Modeling of XGM Effect on an Analogue RF Signal in SOA	107
B	UWB WiMedia Analysis Report	109
	References	126
	Acronyms	126
	List of publications	130
	Acknowledgements	137
	Curriculum vitae	139

CONTENTS

Chapter 1

Introduction

Fibre-to-the-home (FTTH) has become a reality. In 2010, more than 50 million households over the world have been connected by optical fibre, of which 38.9 million are located in the Asia-Pacific region, 3.4 million in Europe and 7.9 million in U.S. [1]. South Korea, ranked as the top in the FTTH market (with 7157 thousand FTTH connection), has deployed fibre to connect to 44.2% of their households in 2009 [2]. Today, fully symmetric, 1 Gbit/s connection including Ethernet, telephony and Internet protocol television (IPTV) services have already appeared on the market costing only \$35 a month in Hong Kong [3].

Next to fixed terminals like personal computers, television, mobile terminals such as laptops, personal digital assistant (PDA) or cell phones are being widely used in the residential buildings, shopping malls, trains, airport terminals, etc. The connection speed of the mobile terminals, depending on wireless standards, vary from 10 kbit/s to hundreds of Mbit/s. In contrast with the optical Gbit/s Ethernet mentioned above, a typical 54 Mbit/s IEEE 802.11a/b/g wireless router costs approximately \$40 in the market today. Moreover, this router is most commonly connected to a digital subscriber line (DSL) modem via twisted pair copper cables in the access networks which only can offer a maximum of 100 Mbit/s per user. However, a decade from now, 100 Mbit/s or even 500 Mbit/s will not satisfy the bandwidth hunger. For example, downloading a 3D blue-ray DVD movie (file size of 25 GBytes) to a mobile phone with satisfactory user experience could easily require 2.5 Gbit/s bandwidth or more [3].

Therefore, copper cables which are a 100-year-old transmission media in the home, can hardly meet the high demand of bandwidth or the large capacity required by various network services in the future. Due to in-home applications such as fibre-to-the-display and multi-service inter-room communications, the in-home network capacity can easily overreach the capacity available in access networks [4]. How to bring the high bandwidth to both mobile and fixed terminals preferably in an all-in-one network

1. INTRODUCTION

infrastructure, as well as providing the high bandwidth for data exchange within the home networks, are the challenges we are facing. Today, the convergence of optical techniques with wireless networks enables an attractive solution for such a cost-effective, integrated and flexible architecture. For in-building networks, the technology of remotely delivering radio frequency (RF) services such as wireless fidelity (WiFi) or worldwide inter-operability for microwave access (WiMax) from residential gateway through optical fibre to a remote antenna unit (RAU), is named radio-over-fibre (RoF) techniques. There are basically two scenarios for the application of RoF techniques depending on the network design. First one is to deliver wireless services such as WiFi via optical fibre to the *public* environment such as railway stations, a shopping areas in a city or WiMax services for fixed wireless access. The other type of RoF system is deployed for *private* wireless access, such as WiFi, ultra-wideband or 60 GHz personal area network services to a residential building, e.g. hospitals, enterprises offices, shops, etc. Depending on different scenarios, the type of optical fibres, intensity of the antenna units, distance between residential gateways and antenna units, network management etc. will be different.

By combining the large bandwidth of optical fibres with the flexibility of the wireless services, RoF techniques not only simplify the RAUs significantly, but also overcome the broadband connection bottleneck for both wired and wireless services for in-building networks [5]. For instance, RoF techniques enable the cheap installation, maintenance and upgrading of remote antennas, consolidate the head-end station very much by moving most of the complex signal processing from the antenna to the residential gateway [6, 7].

The following section gives an overview of the current and emerging wireless broadband services and networks, showing the bandwidth requirement of the services, which motivate the RoF techniques as an advanced broadband converged network solution. After reviewing the state-of-the-art of the RoF techniques, the vision of future home networks is discussed by introducing the low-cost home backbone of plastic optical fibre (POF) in section 1.2. Finally in the section 1.3, the scope and the outline of this thesis are explained.

1.1 Broadband In-Building Networks

1.1.1 Wireless services

Trends of wireless services: With the rapid growth of personal electronics devices, wireless communications have been able to provide flexible, low-cost and comfortable services according to the consumer's desire. Since the emergence of the second generation digital cellular global system for mobile communications (GSM) network 20 years ago, varieties of technologies and systems have been developed to cover the

whole range of wide, local and personal area networks, as illustrated in Figure 1.1. GSM and universal mobile telecommunication system (UMTS) are dominating the wireless wide area network (WWAN), providing data rates up to 1 Mbit/s for voice, internet and broadband data services. With the spread of digital subscriber line (DSL), wireless local area network (WLAN) has also been developed to extend the broadband services to the end users in home and office environments. The IEEE 802.11 family has been successful in providing the experience of internet anywhere, anytime nowadays by providing WiFi services up to 100 Mbit/s, while increasing the carrier frequency to 2.4 GHz and 5 GHz bands [8]. Within the last 5 years, the demand on bandwidth and data throughput has been increasing exponentially in the wireless personal area network (WPAN). Bluetooth technology providing up to 3 Mbit/s data rate is no longer satisfying the bandwidth hunger [9]. Similarly with the evolution of IEEE 802.11 family, higher carrier frequencies have been required to enable larger bandwidths thus higher data rates in the WPAN. The 40 and 60 GHz bands have been utilised by IEEE 802.15 and 802.16 standards. As an update of WiFi standards, WiMax has been able to provide up to 1 Gbit/s data rate and has been identified as an alternative solution to cable and DSL technologies in wireless [10]. Next to IEEE 802.16 standard, IEEE 802.15 has also been feverishly developed, targeting at a ultra-wideband (UWB) low-power-density solution in the spectral domain and providing 480 Mbit/s in the 3-10 GHz band and up to 2 Gbit/s in the 60 GHz band [11]. While the high-definition multimedia interface (HDMI) is evolving to be the standard interface for high-definition TVs, the key advantage and main motivation of 60 GHz technology is to provide secure and uncompressed high-definition video distribution via wireless links.

In summary, the trend of providing higher data rate for wireless access networks has always been driving the development of the technologies, as shown in Figure 1.1. With the increase of the data rate from 10 kbit/s to more than 1 Gbit/s, the RF carrier frequency has increased from less than 1 GHz to the 60 GHz region, resulting in a reduced wireless cell size - the wireless pico-cells. Taking the UWB and millimeter wave 60 GHz radio as examples, the operation principle of such high data rate wireless communications is based on the line-of-sight. Together with high air attenuation, this restricts the coverage area to the in-home and in-building environment ($\leq 10\text{m}$).

Why radio-over-fibre: Due to the high carrier frequency and high data rate of such services, conventional unshielded twisted-pair (UTP) cable broadband access networks are no longer qualified for delivering such services as it was. Moreover, the design of electronics for the high frequency or ultra-broadband implementation is high in cost, leading to a high price for the media converters at the user end where baseband signals are converted to RF domain. Therefore, the distribution of high data rate wireless access services to the end users or between different users raise a critical challenge for broadband

1. INTRODUCTION

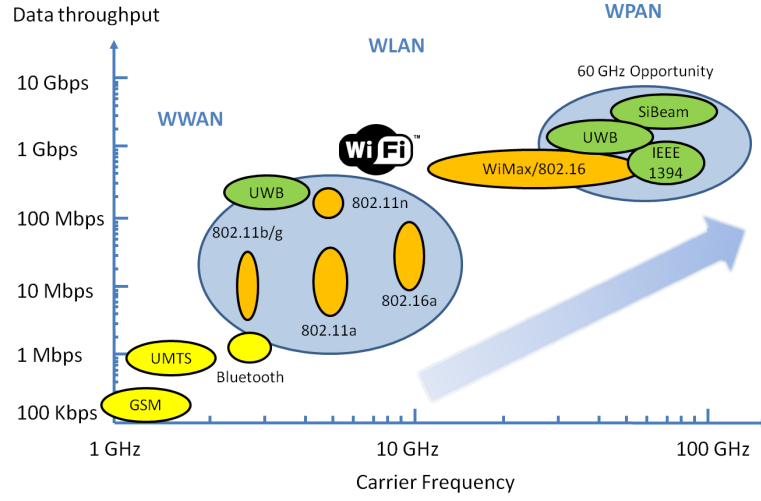


Figure 1.1: Current and emerging wireless services

in-building networks. And this will become more and more severe with the development of the wireless technology in the future, due to the rapidly increasing demand of the consumer electronics. To distribute such in-building broadband networks in a reliable infrastructure, apparently optical fibre, which can easily handle any bandwidth demand, is a future-proof solution, compared to the copper cable technology. RoF technology is such a technology that can deliver, in principle, any RF or millimeter wave service at any bandwidth demand from a remote residential gateway to different end users, therefore enabling the consolidation of the most expensive equipment in the residential gateway and simplifying the RAU to a single optical-electrical (O/E) converter [12, 13]. Moreover, the centralised network management optimises the network resource and capacity allocation, while making the network maintenance and upgrading much easier [14]. Additionally, the inherent advantages of fibre optics besides the large transmission bandwidth, such as low loss, light weight and immunity against electromagnetic interference, makes the optical fibre a well-suited medium for the home environment. Another future-proof advantage of deploying fibre infrastructure in the building is that, thanks to its huge bandwidth, optical fibre is the only transmission medium that can provide reliable converged wired and wireless services (known as multi-standard system) over a single physical medium. Comparisons between conventional copper cable¹ broadband access and proposed RoF broadband access are summarised in Table 1.1 for different types of fibres². A variety of RoF applications employing different types of fibres will be addressed in the following chapters.

¹UTP catalogue 5 cable: the bandwidth of Cat. 5 cable is 100 MHz and 350 MHz for Cat. 5e cable for 100 m distance.

²POF cable summarised in Table 1.1 is standard 50 m long step-index PMMA POF. Table 1.1 only provides a very general and basic comparison.

Copper cable (UTP)	Silica SMF	Silica MMF	POF
Bandwidth ≤ 100 MHz	Unlimited bandwidth	Limited bandwidth	Bandwidth ≤ 300 MHz
Baseband only	Multi-services	Multi-services	Baseband only
Signal processing	Simplified RAU	Simplified RAU	Signal processing
Large loss	Very low loss	Very low loss	Low loss
Complex connector	Difficult installation	Easy installation	Very easy installation
Difficult to upgrade	Future-proof	Semi-future-proof	Difficult to upgrade

Table 1.1: Comparison on broadband access network approaches: unshielded twisted pair (UTP) (Cat. 5 and below) vs. silica sing-mode fibre (SMF), multi-mode fibre (MMF) and plastic optical fibre (POF). Coaxial cable, which generally supports 300 MHz for 100 m distance, is not listed in this table due to its price and size unsuitability for home networks.

1.1.2 Radio-over-fibre techniques

The data rate and bandwidth demand derived from broadband wireless access networks have led to the development of a great variety of RoF techniques to generate and deliver the RF signals to the RAUs. Some commercial cases of RoF implementations have been reported. In 2000, an RoF indoor and outdoor system was deployed at the Sydney Olympic Games, allowing 15000 athletes and millions of spectators attending the Games to use their mobile phones. In 2010, a dedicated fibre-optics system was employed by Bell to offer critical network and communications services at Vancouver Winter Olympic Games, including high-speed wireless data and a broadband TV network. Among different RoF techniques, there are mainly two families: **RF intensity modulation** and **optical heterodyning** approaches.

RF Intensity Modulation: The simplest method to deliver an RF signal through fibres is to modulate the intensity of a continuous lightwave (CW) by the RF signal with a sub-carrier, either by direct [15] or external modulation [16], so that the signal resides on the double sideband (DSB) of the optical carrier, with a separation of the electrical sub-carrier frequency between the optical carrier and the sideband. At the receiver end of the RAU, simply an O/E converter namely a photo-detector is required to detect the envelope of the optical signal. The significant advantage of this type of RoF system is the simplicity at both the residential gateway and RAU sides, which constitutes the most cost-effective solution. Therefore, for typical WWAN or WLAN applications such as UMTS or WiFi service which has carrier frequency less than 5 GHz, RF direct intensity modulation is desired given that the fibre transmission length is relatively short so that fibre chromatic dispersion does not play a major role. However, the intensity modulation approach could give rise to problems if the carrier frequency of the desired RF signals goes beyond 5 GHz or even is in 60 GHz millimeter wave band. In that case, the requirement of high-frequency electronics

1. INTRODUCTION

to directly modulate the CW source, both at the gateway and the RAU side, leads to a considerably expensive RoF system [17]. Another issue in such DSB system is the fading effects of the signal due to the fibre chromatic dispersion when the bandwidth of the signal is very large, for instance in 60 GHz RoF systems [18].

In contrast, single sideband (SSB) modulation has also been implemented in RoF systems, either by dual-driving the Mach-Zehnder modulator (MZM) [19] or hybrid intensity and phase modulation [20], to combat the fading effect from fibre chromatic dispersion. Due to high complexity of the system, this method has been considered unsuitable for in-building networks and has been ruled out in recent years.

Optical Heterodyning: In contrast with the RF intensity modulation, an RoF system employing an optical heterodyning method does not only make use of the sub-carrier of the wireless signal, but also is able to remotely generate the desired electrical carrier at the photo-detector, by means of the optical heterodyning between one CW optical signal and one data-modulated optical carrier at different wavelengths [21]. The advantage of this method is the flexible and remote generation of an RF carrier or a millimeter wave carrier at any desired RF frequency, ranging from GHz to THz. The generated RF carrier frequency is determined by the separation of the two optical wavelengths. However, due to the different order of magnitude of optical frequencies and RF frequencies, any wavelength shift which is considered small in optical frequency can easily cause a major shift in RF frequency in the heterodyning process, therefore resulting in a high requirement on the accuracy of CW wavelengths [22]. The spectral linewidth of generated RF carrier depends on the summation of two CW optical linewidths, which is normally in the order of MHz and not qualified as an RF carrier. As a consequence, to obtain a high-quality RF carrier, phase control mechanisms such as the optical phase lock loop (OPLL) must be applied in optical heterodyning schemes to synchronise in the phase of all optical sources [23, 24]. Therefore, although the optical heterodyning method can generate and deliver the RF service in principle at any arbitrary frequencies, the system complexity introduced by the phase control sub-system greatly degrades the feasibility of real implementation of such RoF systems for in-building applications.

Optical Frequency Multiplication: As a deviation of optical heterodyning, microwave generation using a frequency-modulation to intensity-modulation (FM-IM) conversion scheme employs a phase modulation of the CW signal, resulting in an optical frequency "comb" in the spectral domain. The beating effect between the different harmonics of the phase modulated optical signal, in some instances, gives rise to an FM-IM conversion thus generating microwave waves at the desired RF frequency [25–28]. By using such FM-IM conversion, frequency up-conversion or optical frequency multiplication (OFM) can be realised. The principle of microwave generation using OFM is the same as the optical heterodyning,

while both of which employ the carrier beating in the optical domain as the fundamental mechanism to generate an RF carrier. Compared with a typical optical heterodyning approach, OFM method does not require any external phase control mechanism, due to the inherent phase locking between different harmonics of the single phase-modulated optical source. Moreover, OFM method only requires a single optical source instead of two.

An example of such OFM systems can be easily obtained when an MZM is biased at its null point (minimum transmission point) and modulated by a sinusoidal signal, so that the CW light going through the MZM is phase modulated by ± 180 degrees each time that the sinusoidal signal goes across the null point or inflexion point of the MZM [29, 30]. The efficiency of the OFM can be largely improved by an external modulator which is dedicated for the phase modulation [31]. Another well-known method to generate RF carrier by OFM method is to employ a notch filter at the CW wavelength after phase modulating the CW signal, so that the beating effect for even harmonics on the photo-detector is enhanced while for odd harmonics depressed [32]. Moreover, OFM system can also be realised by phase modulating a CW laser and optically band-pass filtering [28]. In such systems, the linewidths of the generated RF carriers are only limited by the linewidth of the sinusoidal signal which modulates the CW signal, instead of CW optical source linewidth. Another advantage of using the OFM method to generate RF carriers, compared with the RF intensity modulation, is that the OFM method combines the delivery of RF signals together with the RF carrier generation, therefore the data at low frequency is up-converted to a higher RF carrier, in such a way that RF services can be transported over fibres cost-effectively. Additionally, due to the high conversion efficiency of OFM method, only a low frequency synthesiser is required at the residential gateway to obtain an RF carrier at much higher frequency band. Details of the OFM approach employing a periodic optical filter will be discussed in Section 2.1.1.

1.2 Optical Backbone: Plastic Optical Fibre (POF)

The vision of this thesis on the future broadband in-building networks is illustrated in Figure 1.2 [14, 33]. Similarly with the present FTTH market, optical fibres, most often large capacity single-mode fibre, are connected to the building (or airport terminal, shopping mall or hospital, etc.) until the point of the home residential gateway (RG) [34]. At present, broadband in-building access is supported by telephone line (twisted pair) or UTP cable, which has been shown in Table 1.1 to be no longer suitable for the upcoming broadband in-building networks. In the proposed fibre-based future home network, RoF techniques will provide various wireless access services as well as digital TV or Ethernet services, as shown in Figure 1.2 [7, 35, 36]. Such optical backbone infrastructure will not only provide connections from the RG to the end users but also support inter-room communication [14]. Research and development

1. INTRODUCTION

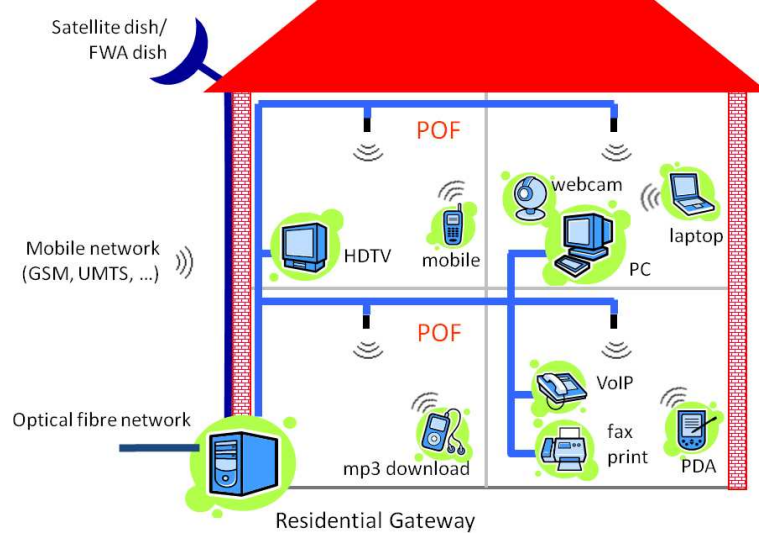


Figure 1.2: Optical backbone for future home networks

have been carried out also at the protocol level of the future home networks, in order to integrate high capacity wireless service such as 60 GHz into the multi-radio home networking environment [37]. The ad-hoc infrastructure and the cognitive plane in the control and management level of such networks have been studied in detail [38]. In the physical layer, plastic optical fibre (POF) has shown its significant advantages in the suitability for in-building/in-home environment, mainly due to its large core diameter and material properties [33, 39].

For a long time, automobile manufacturers have been implementing in-vehicle fibre networks with high-bandwidth links, low costs and complete reliability, by employing POF to provide high data rate TV, video or gaming services for the in-car electronic devices, known as the media-oriented systems transport (MOST). For example, BMW has developed a 10 Mbit/s POF system called ByteFlight [40], which it uses to support the rapidly growing number of sensors, actuators and electronic control units within cars. For the last 10 years, POF has also been playing an important role in other short-range communications using fibre-optics to replace electrical cables in many different applications, for instance short-range high speed connections for consumer electronics [41] and intercomputer connections [42]. Currently, POF vendor communities as well as telecom operators are working together towards providing a future-proof broadband home network by employing POFs [43–46].

Due to the very large core diameter of POF, the installation of POF links in home can be very simple compared to single mode fibres, enabling do-it-yourself installation and maintenance therefore significantly reduce the infrastructure cost of the home networks. Moreover, the bending radius of POF is inherently

smaller than that of standard SMF (G652d)¹ with typically less than 25 mm [47] for loss increment less than 0.5 dB, which is another advantage for in-home wiring compared with standard SMF. POF systems also require low-cost optical transceivers (\$2–4) therefore permits cost-effective solutions [48]. Another practical issue that makes POF suitable for in-building application is the fact that POF can be properly fitted into the ducts which were intended for powerlines or telephony lines [49], thus replacing copper cable by POF or deploying POF together with power-line in the building can efficiently reduce the installation cost. The other advantages of POF network in the installation cost over other infrastructures have also been reported recently [7].

There are mainly two types of POF available on the market: poly-methyl-methacrylate (PMMA) POF with the core diameter of 0.98 mm² (normally cited as 1 mm) and perfluorinated (PF) POF with typical core diameters of 50 and 80 μm ³. Comparing with 9 μm core diameter of SMF, the larger core diameter and the larger numerical aperture (NA) of the POF gives rise to larger connector tolerances where small misalignments can be easily ignored, while the alignment design of the SMF has to be very precise. For PMMA POF, there are also different designs on the index profile, namely step-index (SI) and graded-index (GI). Due to the index design PMMA GI-POF has more bandwidth compared with the SI-POF because of the less modal dispersion [39]. Moreover, another design of multiple core within the 1 mm diameter of PMMA SI-POF has also been commercially available, in order to reduce the bending radius of the POF. In this multi-core design, many cores (19 to over 200) are put together in production in such a way that they together fill a round cross-section of 1 mm diameter. The individual cores are arranged in a hexagonal shape [39]. More explanations are explicitly presented in Chapter 5 for SI-, GI- and multi-core PMMA POFs.

The attenuation characteristics for the two main types of POF are summarised in Figure 1.3, compared with the conventional SMF. As shown in the figure, the curve of PMMA SI-POF shows an opened transmission window around 400 to 700 nm, which is the visible wavelength region. This leads to an advantage for installing and maintaining POF networks in home environment because consumers are able to observe whether the service is on or off, by looking at the optical transmitters are emitting light or not. Consequently, the light source employed in the PMMA POF system can be a light emitting diode (LED), resonant-cavity (RC) LED, edge-emitting laser diode, or vertical cavity surface emitting laser (VCSEL), which operate at visible wavelengths. Due to the large core diameter and large NA of the PMMA POF, which is approximately 0.5 (for standard PMMA SI-POF), large area silicon PIN photo-detectors are

¹Novel types of bend-insensitive SMF allows bends with less than 0.1 dB loss at 5 mm radius.

²according to IEC 60793-2-40, optical fibres - part 2-40: product specifications

³There are also PF graded-index POFs with specified core diameters of 62.5, 120 and 200 μm , while 50 and 80 μm are most commonly used diameters.

1. INTRODUCTION

normally used with a detecting area varying from 200 μm to 800 μm . In contrast of PMMA POF, PF POF has a much lower attenuation at longer wavelength, e.g. at 850 or 1310 nm region. This allows the PF POF system to make use of the common SMF transceivers available for 1310 nm region [39].

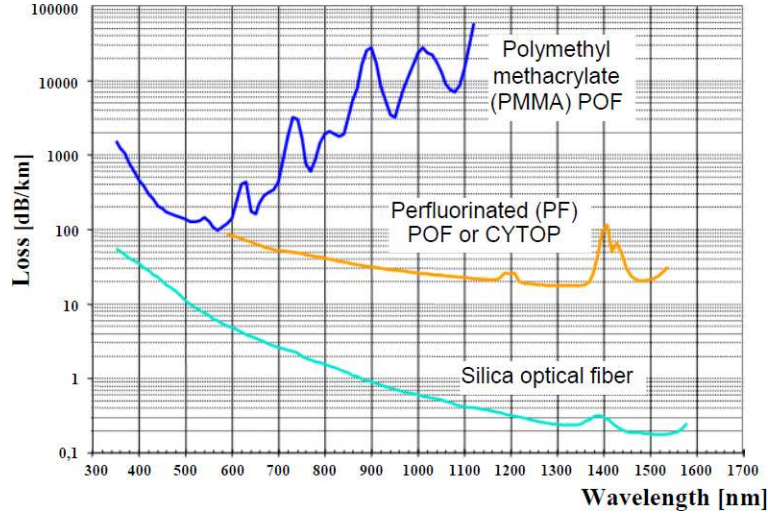


Figure 1.3: Attenuation characteristics of POF and silica fibre [50].

1.3 Scope of Thesis

The research work reported in this thesis has been performed in Eindhoven University of Technology, within the framework of "Future Home Network" project, supported by the Innovation Oriented research Program (IOP) Generieke Communicatie (GenCom) Program of the Senter Novem agency within the Dutch Ministry of Economics Affairs. The aim of the project is to explore the concept of ambient intelligence in buildings where Gbit/s data capacity is provided through either an optical infrastructure or radio relays. In this project, the research activity at Eindhoven University of Technology focussed on providing such Gbit/s capacity by means of optical fibre infrastructure. With the proposal of employing POF for the in-building networks, the work reported in this thesis have also largely contributed to the European Framework Program 7 (FP7) POF-PLUS in the respect of radio-over-fibre system using POF as well as high capacity transmission over POF.

The objective of this thesis is to explore different optical techniques to enable an easy installed, maintained and user-friendly in-building infrastructure, providing microwave and baseband network services to the personal terminals. Such networks and infrastructures should also provide easy network configura-

tion and control the data throughput adaptively according to the traffic demand. The main contributions of this thesis are given below:

- Low-cost silica MMF and POF are employed to realise the easy installation and maintenance for in-building networks.
- Different techniques are explored for the delivery of microwave and baseband signals.
- Routing techniques are discussed for the control of the traffic throughput of microwave signals.
- Convergence of both baseband and microwave services are realised by optical techniques.

This thesis is organised as follows. Chapter 2 presents the high capacity RoF techniques, optical frequency multiplication, by means of theoretical and experimental analysis. Based on this technique, multi-carrier RoF transmission is demonstrated using sub-carrier multiplexing (SCM) increasing the RoF link capacity up to more than 200 Mbit/s. The transmitter nonlinearity is also investigated in this chapter by comparing single-carrier and multi-carrier signals. Chapter 3 focuses on the radio-over-POF link targeting at the multi-band OFDM ultra-wideband (UWB) signal. It addresses the challenge of transporting such ultra broad-band signal over a dispersive multi-mode medium, showing the feasibility of transmitting WiMedia-compliance signal (standard signal employed by wireless-USB) over both PMMA and PF POF. A first demonstration of full duplex bi-directional transmission of UWB over POF is reported.

After presenting investigations of the transmission systems in Chapter 2 and 3, Chapter 4 explores the RoF network functionalities in the physical layer, by the optical approach. It studies the dynamic capacity allocation using SOA-based optical routing. By combining both optical routing and SCM, the dynamics capacity allocation is proposed and experimentally demonstrated. Chapter 5 is dedicated to reporting multi-Gbit/s baseband transmission over PMMA POF, aiming at providing baseband services such as HDTV or Gbit/s Ethernet for in-building networks. Applications targeting for data center interconnection at more than 40 Gbit/s is also shown in Chapter 5 by employing PF POF and an advanced modulation format. After that, Chapter 6 presents an experimental demonstration of providing converged baseband and RF services over a single fibre infrastructure over either POF or multi-mode silica fibre. Finally, Chapter 7 summarises the main contributions of the work and envisages possible future research interests.

1. INTRODUCTION

Chapter 2

High Capacity Radio-over-Fibre Transmission Systems

This chapter presents a high capacity radio-over-fibre (RoF) system by employing the sub-carrier multiplexing (SCM) and the optical frequency multiplication (OFM) technique. First, in Section 2.1, the analysis of the OFM approach is presented in the frequency domain. Section 2.2 presents the experimental investigation of RoF systems using OFM and SCM. The trade-off on different system parameters is also discussed in this section. In Section 2.3, after introducing the orthogonal frequency division multiplexing (OFDM), both simulation and experimental study on the impact of signal formats, i.e. single-carrier format and OFDM format, on the OFM transmitter nonlinearity are addressed.

2.1 Optical Frequency Multiplication

2.1.1 Principle of operation

Optical frequency multiplication (OFM) is an optical approach of RF harmonic generation, or in other words frequency up-conversion, by means of phase-modulation (PM) to intensity modulation (IM) conversion. Theoretical analysis of the OFM scheme have been presented in literatures such as [6, 27, 28, 33, 54–56]. These OFM analysis are performed using computation in the time domain [28]. In this section, an alternative theoretical explanation about the OFM is presented in the frequency domain [52]. A schematic diagram of the basic OFM setup is illustrated in Figure 2.1(a). It consists of a continuous wave (CW) optical source with central optical frequency ω_0 , which is phase modulated by a sinusoidal signal with a radial frequency of ω_{sw} , an optical filter and a photodetector (PD). For the external data modulation, a Mach-Zehnder modulator (MZM) is also shown in front of the optical filter in Figure 2.1(a). To start

This chapter is based on the results published in [51], [52] and [53]

2. HIGH CAPACITY RADIO-OVER-FIBRE TRANSMISSION SYSTEMS

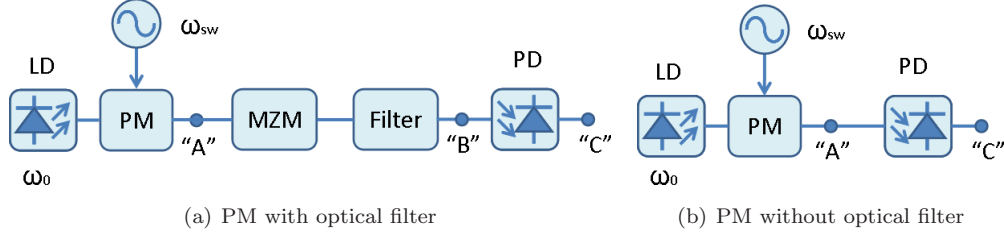


Figure 2.1: Schematic diagram of OFM principle: (a) with optical filter and (b) without optical filter.

the analysis, let us assume initially that the optical filter and the MZM are not present, as shown in Figure 2.1(b).

Phase modulation without filter: The envelope of the electrical field of the phase modulated signal at point "A" in Figure 2.1(b) is given by

$$e_{pm}(t) = E_0 e^{j(\omega_0 t + \phi)} e^{j\beta \sin(\omega_{sw} t)} = E_0 e^{j\phi} e^{j[\omega_0 t + \beta(\sin(\omega_{sw} t))]} \quad (2.1)$$

where E_0 is the amplitude of the field of the CW signal, β the phase modulation index and ϕ is the constant phase term of the CW signal. For simplicity, normalising $E_0 = 1$ V/m so that the amplitude spectrum of $e_{pm}(t)$, i.e. the Fourier transform of e_{pm} can be written as [57]

$$\frac{E_{pm}(\omega)}{E_0(\omega)} = e^{j\phi} \sum_{n=-\infty}^{n=\infty} J_n(\beta) \delta(\omega - \omega_0 - n\omega_{sw}) \quad (2.2)$$

where $J_n(\beta)$ is the n^{th} order Bessel function of the first kind. According to Equation 2.2, $E_{pm}(\omega)$ consists of multiple components in the spectrum domain that are equally spaced by ω_{sw} and have amplitude of $J_n(\beta)$. In Figure 2.1(b), the phase modulated signal is detected by a PD. The normalised photo-current $i(t)$ is given by

$$i(t) = R_d \cdot e(t) \cdot e^*(t) \quad (2.3)$$

where R_d is the photodiode responsivity. Assuming $R_d = 1$ A/W and transforming Equation 2.3 to frequency domain, the photo-current can be written as the convolution of the field and its complex conjugate, given by [58]

$$I(\omega) = E(\omega) \otimes E^*(-\omega) = \int_{-\infty}^{\infty} E(\xi) E^*(\xi - \omega) d(\xi) \quad (2.4)$$

Substituting Equation 2.2, Equation 2.4 can then be written as [52]

$$\begin{aligned}
I(\omega) &= \int_{-\infty}^{\infty} \{ [e^{j\phi} \sum_{n=-\infty}^{\infty} J_n(\beta) \delta(\xi - \omega_0 - n\omega_{sw})] \\
&\quad \cdot [e^{-j\phi} \sum_{m=-\infty}^{\infty} J_m(\beta) \delta(\xi - \omega_0 - m\omega_{sw})] \} d(\xi) \\
&= \sum_{n=-\infty}^{\infty} \sum_{m=-\infty}^{\infty} J_n(\beta) J_m(\beta) \delta(\omega - (n - m)\omega_{sw}) \\
&= \sum_{n=-\infty}^{\infty} \sum_{p=-\infty}^{\infty} J_n(\beta) J_{n+p}(\beta) \delta(\omega - p\omega_{sw}) \\
&= \sum_{n=-\infty}^{\infty} J_n(\beta) \cdot J_n(\beta) + \sum_{p=1}^{\infty} \sum_{n=-\infty}^{\infty} J_n(\beta) \cdot J_{n+p}(\beta) [\delta(\omega - p\omega_{sw}) + \delta(\omega + p\omega_{sw})]
\end{aligned} \tag{2.5}$$

Taking the inverse Fourier transform of Equation 2.5, the time dependent photo-current is given by

$$\begin{aligned}
i(t) &= \sum_{n=-\infty}^{\infty} J_n(\beta) J_n(\beta) + 2 \sum_{p=1}^{\infty} \sum_{n=-\infty}^{\infty} J_n(\beta) J_{n+p}(\beta) \cdot \cos(p\omega_{sw}t) \\
&= I_{DC} + \sum_{p=1}^{\infty} I_p \cos(p\omega_{sw}t)
\end{aligned} \tag{2.6}$$

where

$$I_{DC} = \sum_{n=-\infty}^{\infty} |J_n(\beta)|^2 \tag{2.7}$$

and

$$I_p = 2 \sum_{n=-\infty}^{\infty} J_n(\beta) J_{n+p}(\beta) \tag{2.8}$$

Using Graf's generalisation of Neumann's addition theorem [59], Equation 2.8 can be rewritten as

$$I_p = 2 \sum_{n=-\infty}^{\infty} J_n(\beta) J_{n+p}(\beta) = 2J_p(0) \tag{2.9}$$

For $p \neq 0$, Equation 2.9 is derived as $I_p = 2J_p(0) = 0$, which shows that the phase modulated signal only generates DC power in the photo-detector in the point "C" of the Figure 2.1(b).

Phase modulation with optical filter: To realise the PM-IM conversion and to generate RF harmonics in OFM scheme, one option that is commonly used is to add an optical filter between the phase modulator and photo-detector [32, 60], as shown in Figure 2.1(a). Based on the analysis above and assuming a Mach-Zehnder interferometer (MZI) as the optical filter with the transfer function of $h_{MZI}(t) = 1/2[\delta(t) + \delta(t - \tau)]$, where τ is the delay time difference in MZI branches, the transfer function

2. HIGH CAPACITY RADIO-OVER-FIBRE TRANSMISSION SYSTEMS

for the electrical field of the optical filter in the frequency domain is given by

$$H_{MZI}(\omega) = \frac{1}{2}(1 + e^{-j\omega\tau}) = \cos\left(\frac{1}{2}\omega\tau\right)e^{-\frac{1}{2}j\omega\tau} \quad (2.10)$$

Inserting Equation 2.10 into Equation 2.4, Equation 2.5 becomes

$$\begin{aligned} I(\omega) &= \sum_{n=-\infty}^{\infty} \sum_{p=-\infty}^{\infty} \{J_n(\beta)J_{n+p}(\beta)e^{\frac{1}{2}j(\omega_0+n\omega_{sw})\tau} \cdot e^{-\frac{1}{2}j(\omega_0+(n+p)\omega_{sw})\tau} \\ &\quad \cdot \cos\left[\frac{1}{2}(\omega_0+n\omega_{sw})\tau\right] \cdot \cos\left[\frac{1}{2}(\omega_0+(n+p)\omega_{sw})\tau\right]\} \delta(\omega - p\omega_{sw}) \\ &= \sum_{n=-\infty}^{\infty} \sum_{p=-\infty}^{\infty} e^{-\frac{1}{2}jp\omega_{sw}\tau} \{J_n(\beta) \cos\left[\frac{1}{2}(\omega_0+n\omega_{sw})\tau\right] \\ &\quad \cdot J_{n+p}(\beta) \cos\left[\frac{1}{2}(\omega_0+(n+p)\omega_{sw})\tau\right]\} \delta(\omega - p\omega_{sw}) \end{aligned} \quad (2.11)$$

Similarly, in the case of optical filtering and ignoring the MZM employed data modulation in Figure 2.1(a), using Equation 2.11 and after algebraic rewriting, Equation 2.8 becomes

$$I_p = \sum_{n=-\infty}^{\infty} J_n(\beta)J_{n-p}(\beta) \cos[\omega_0\tau + (n - \frac{1}{2}p)\omega_{sw}\tau] \quad (2.12)$$

Using Graf's generalisation of Neumann's theorem [59] and trigonometric formulas, the even and odd harmonics of Equation 2.12 can be written as

$$\begin{aligned} I_{2k} &= (-1)^k \cos(\omega_o\tau) \cdot J_{2k}(2\beta \sin(\theta/2)) \\ I_{2k-1} &= (-1)^k \sin(\omega_o\tau) \cdot J_{2k-1}(2\beta \sin(\theta/2)) \end{aligned} \quad (2.13)$$

where $\theta = \omega_{sw}\tau$. Equation 2.13 is in line with OFM studies based on time domain analysis [27], and gives a good insight in the generation of the harmonics. It is observed from Equation 2.13 that even and odd order harmonics of the sweep signal are generated, where the amplitude of each harmonic is given by the two equations. Therefore, a low frequency sweep signal is optically up-converted to a high frequency RF carrier without the use of any high frequency electronics¹, but is achieved by the inherent property of phase modulation and optical heterodyning coming from a single source.

2.1.2 Influence of phase noise

Phase noise $\phi_{noise}(t)$ in a carrier can be viewed as an uncertainty in either frequency or time, which can be expressed as [52]

$$\begin{aligned} m(t) &= \cos(\omega_c t + \phi_{noise}(t)) \\ &= \cos\{[\omega_c + \delta\omega_c(t)]t\} \\ &= \cos\{\omega_c[t + \delta t(t)]\} \end{aligned} \quad (2.14)$$

¹Generating microwave or even millimeter wave without using high frequency electronics can largely reduce the system cost.

where $m(t)$ here presents a general form of a sinusoidal signal with a radial frequency of ω_c and noise term of ϕ_{noise} . δ presents the uncertain deviation from the central frequency or time. From the analysis in Section 2.1.1, the photo-current can be seen as the heterodyning of two optical carriers, which can be rewritten as follows

$$i(t) = \sum_{p=-\infty}^{\infty} \sum_{n=-\infty}^{\infty} e_n(t) e_{n-p}^*(t) \quad (2.15)$$

where $e_n(t)$ is the electrical field of the n^{th} optical carrier given by [52]

$$e_n(t) = J_n(\beta) e^{j(\omega_0 + n\omega_{sw})t} \quad (2.16)$$

Laser phase noise: Considering only the phase noise of the laser $\phi_L(t)$, the heterodyning product $e_n(t) e_{n-p}^*(t)$ can be written as [52]

$$\begin{aligned} e_n(t) e_{n-p}^*(t) &= J_n(\beta) e^{j[\omega_0 t + \phi_L(t) + n\omega_{sw}t]} \cdot J_{n-p}(\beta) e^{-j[\omega_0 t + \phi_L(t) + (n-p)\omega_{sw}t]} \\ &= J_n(\beta) J_{n-p}(\beta) e^{jp\omega_{sw}t} \end{aligned} \quad (2.17)$$

which shows that the phase coherence between two optical carriers cancels out the laser phase noise after heterodyning.

Sweep signal phase noise: Now assuming the phase noise $\phi_{sw}(t)$ in the sweep sinusoidal signal, the p^{th} harmonic is the summation of the heterodyning products of the form [52]

$$\begin{aligned} e_n(t) e_{n-p}^*(t) &= J_n(\beta) e^{j[\omega_0 t + n(\omega_{sw}t + \phi_{sw}t)]} \cdot J_{n-p}(\beta) e^{-j[\omega_0 t + (n-p)(\omega_{sw}t + \phi_{sw}t)]} \\ &= J_n(\beta) J_{n-p}(\beta) e^{jp(\omega_{sw}t + \phi_{sw}t)} \end{aligned} \quad (2.18)$$

which shows that the contribution of the phase noise of the sinusoidal signal in the p^{th} harmonic is proportional to p .

$$\phi_p(t) = p\phi_{sw}(t) \quad (2.19)$$

Measurement results on phase noise: To verify the analysis of the phase noise, the setup of the measurement is the same as Figure 2.1(a) [52]. A DFB laser at 1550 nm was phase modulated by a sinusoidal sweep signal at 3.33 GHz. The phase modulator had a half wave voltage of $V_\pi = 2.5$ V. An MZI with a free spectral range (FSR) of 10 GHz was employed as the optical filter for PM-IM conversion, and an MZM for the data modulation. First, Figure 2.2(a) presents the measured phase noise of the sweep sinusoidal signal. In comparison, the phase noise of generated p^{th} harmonics is plotted in Figure 2.2(b) without any external data modulation, in which the linear relation (between the phase noise of the p^{th} harmonic and that of the sweep signal) is shown. The analysis in Equation 2.19 is thus verified by Figure 2.2(b). Moreover, 16-level quadrature amplitude modulation (16-QAM) data were modulated on

2. HIGH CAPACITY RADIO-OVER-FIBRE TRANSMISSION SYSTEMS

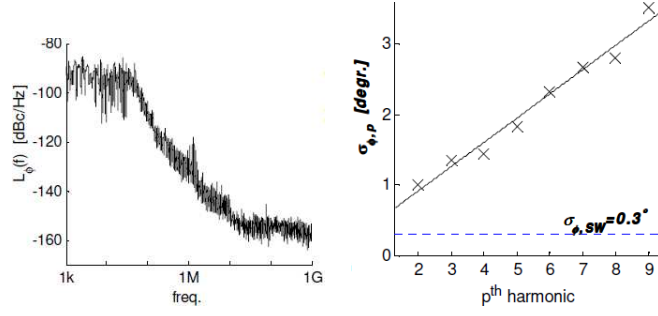
the generated harmonic with a sub-carrier frequency of 270 MHz and a data rate of 10 MSym/s by an external MZM. With OFM techniques, the data was up-converted to higher harmonics and measurements were taken at zero (where data was directly carried by the optical carrier) to 8th harmonics. Figure 2.2(c) and 2.2(d) illustrate the demodulated constellations. For $p = 8$, it is clearly seen that the constellation diagram is distorted by phase rotation from its original points. Error vector magnitude (EVM) is used to characterise the quality of the RF signal. EVM expresses the difference between the expected complex voltage value of a demodulated symbol and the value of the actual received symbol.¹ Therefore, a larger EVM value corresponds to a worse signal quality. Figure 2.2(e) also gives more explanations that most of the EVM is contributed from the phase error, which is again dependent on the harmonics index [52].

2.2 Radio-over-Fibre Distribution using SCM and OFM

With the evolution of passive optical networks (PONs) technology in broadband access network, wavelength division multiplexed PONs (WDM-PONs) have been proposed by LG Ericsson, Alcatel-Lucent and others [61], in order to improve the efficiency of wavelength utilisation, to enhance the total transmission capacity of the network. Due to the selectivity of optical filters and limitations in the wavelength stability of semiconductor lasers, the minimum channel spacing is 50 GHz in the current WDM-PON architecture, which is inherent from commercial WDM long-haul systems.

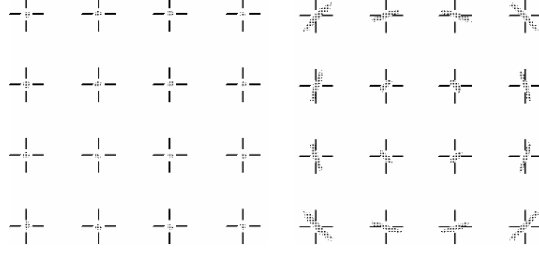
In contrast, sub-carrier multiplexing (SCM) is a technique where multiple signals are modulated on different sub-carriers and multiplexed in electrical or radio frequency (RF) domain and are transmitted with a single optical wavelength. Compared with the WDM-PON solution for access networks, the significant advantage of SCM for in-building networks is the fact that microwave devices are more mature and much more cost-effective than optical devices in order to achieve an improved capacity. The stability of RF oscillators and the frequency selectivity of an electrical filter are also much better than their optical counterparts. All these advantages make the SCM schemes more suitable for low-cost in-building networks. A typical application of SCM technology in fibre optic systems is analogue cable television (CATV) distribution [62]. One of the disadvantages of SCM application is that the system requires costly RF analogue electronics, RF-capable optical transceivers and highly linear components for advanced modulation formats. Nevertheless, in this section, to explore the emerging solutions of broadband in-building networks, the SCM scheme is proposed in combination with the OFM technique to provide high data rate RF services by employing low-frequency electronics. Moreover, to investigate the linearity

¹EVM values are calculated in linear percentage or in dB. To convert between each other: $EVM = 20 \log(\frac{|U_{err}|}{|U_{mod}|})dB$ and $EVM_{lin} = \frac{|U_{err}|}{|U_{mod}|} \times 100\%$, where U_{err} and U_{mod} are error and modulated signals respectively.



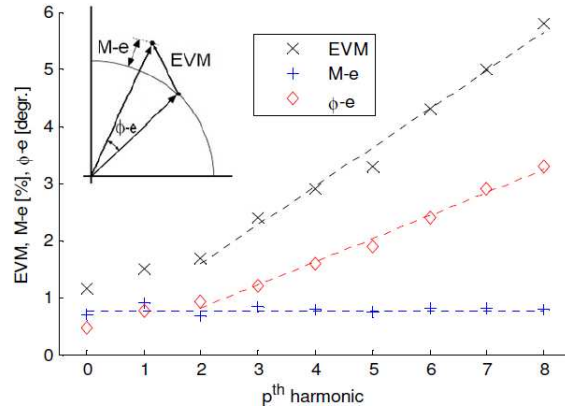
(a) PN-PSD of the sweep signal

(b) phase noise versus p



(c) constellation at $p = 0$

(d) constellation at $p = 8$



(e) magnitude and phase error as functions of p

Figure 2.2: (a) Phase noise power spectral density (PN-PSD) of the sweep sinusoidal signal, (b) Measured phase error as function of p^{th} harmonics, with reference of PN-PSD from the sweep signal, (c) constellation diagram of 16-QAM 10 MSym/s data at 270 MHz, (d) constellation diagram of same signal of 16-QAM 10 MSym/s data at 32.27 GHz and (e) Measured EVM, Magnitude-error (M-e) and phase-error (ϕ -e) as functions of p^{th} harmonic [52].

2. HIGH CAPACITY RADIO-OVER-FIBRE TRANSMISSION SYSTEMS

requirement of such system, a comparison between modulation formats will be addressed in the following section.

2.2.1 Broadcast architecture: system design and experiment

Based on the schematic analysis in Section 2.1 and Figure 2.1(a), the system design of an RoF link using SCM and OFM schemes is shown in Figure 2.3 [51, 63]. In the OFM transmitter, the harmonics are generated according to the OFM principle, which after photo-detection can be mathematically expressed by Equation 2.13. An MZM is employed to amplitude modulate the data signal, which is a sub-carrier multiplexed signal with sub-carrier frequencies f_{sc1} , f_{sc2} , etc. After transmission and photo-detecting, the SCM data signal is double-side-band modulated to each of the p^{th} OFM harmonics, resulting in the up-converted signal at desired radio frequency f_{RF1} , f_{RF2} , etc. Assuming the sweep signal having a radial frequency of ω_{sw} , the up-converted signal at f_{RF1} takes the form of

$$f_{RF1} = 2\pi \times p \times \omega_{sw} \pm f_{sc1} \quad (2.20)$$

where p is the order of the OFM harmonics. Electrical band-pass filters are then used to select the desired RF signal, and the signal is amplified and directly radiate through antenna. Due to the principle of OFM, note that the whole range of subcarriers needs to fit between the OFM harmonics, so the maximum subcarrier frequency should be given by $f_{sc,x} \leq \frac{f_{sweep}}{2}$ [56], where x is the index of sub-carriers.

The experimental setup is shown in Figure 2.4(a). A laser source of 1302 nm wavelength (model: NTT NLK5B5EBKA) was phase modulated by a sweep signal with frequency $f_{sw} = 6$ GHz. The phase modulated signal was then intensity modulated by an MZM. The electrical SCM data used to drive the MZM was generated by a vector signal generator (VSG) with a central frequency of f_{sc} of 300 MHz. The output signal was passed through an integrated MZI filter¹ with an FSR = 10 GHz, then was transported over a 4.4 km MMF link, and finally was detected by a photodiode with a MMF pigtail (NewFocus 1434-50). The MMF had a core diameter of 50 μm and a graded-index profile². The output electrical data signal was up-converted from f_{sc} to f_{RF} , the frequency of which was given by Equation 2.20, as explained above. The output of the photodiode was amplified and sent to a vector signal analyser (VSA) for evaluation. Figure 2.4(b) shows the right-hand sideband of the RF spectrum obtained at the output of the photodiode after fibre transmission. The central frequency of the RF data is up-converted to 18.3 GHz (corresponding to $p = 3$, and right-hand sideband signal). The sub-carriers are modulated with 64-level quadrature amplitude modulation (64-QAM) with symbol rate of

¹This was a home-made device, fabricated on the wafer layout in $\text{Si}_3\text{N}_4/\text{SiO}_2$. The same kind of device are employed for all the MZI filters mentioned in this thesis. Details of the device design and fabrication can be found in [64].

²fibre spool labeled F040 in laboratory PT11.11

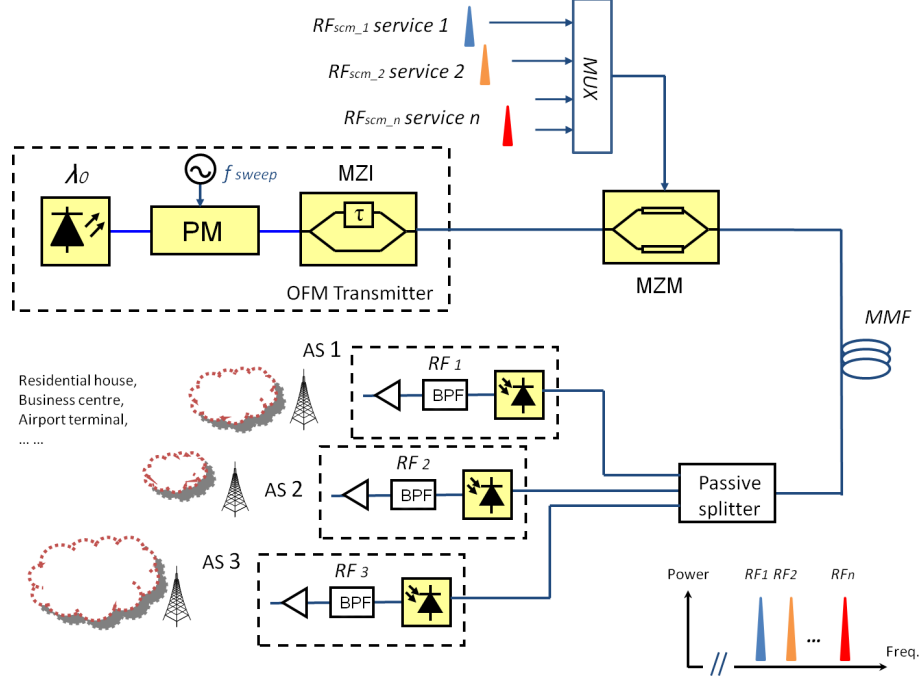


Figure 2.3: Schematic diagram of SCM transmission system based on OFM.

3.6 MSym/s corresponding to 21.6 Mbit/s. The whole SCM signal contains 5 sub-carriers with a total bit rate of 108 Mbit/s. Note that the noise level shown in Figure 2.4(b) (-85 dBm/Hz) is significantly above the thermal noise level (-110 dBm/Hz). This is due to the background noise from the measurement equipment (R&S FSQ40). In practice, this might be a problem for the noise level requirement in receiver band for full-duplex wireless standards. However, this problem can be solved by choosing a low-noise photodetector and low-noise amplifier [65].

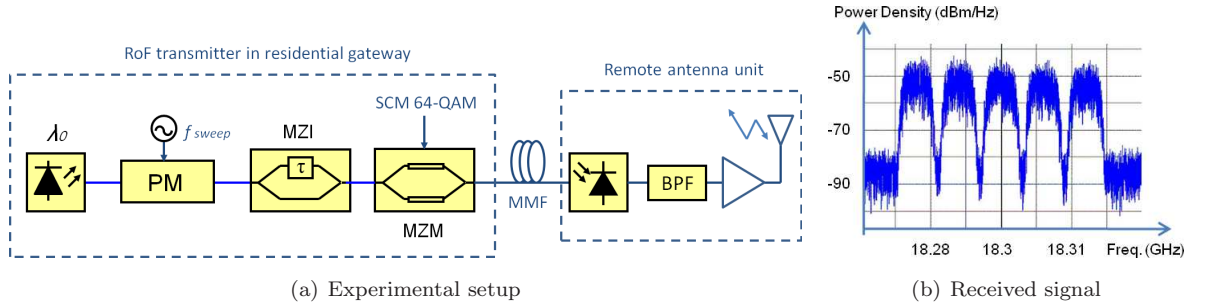


Figure 2.4: (a) Experimental setup for SCM transmission over MMF using OFM, (b) Spectrum of the received signal at 18.3 GHz after 4.4 km MMF transmission.

2.2.2 Parameters and trade-off

To investigate the performance of this multi-carrier system, the EVM value of the received RF signal is measured at 18.3 GHz by evaluating its demodulated 64-QAM constellation for different numbers of sub-carriers. In Figure 2.5(a), for a fixed total symbol rate of 18 MSym/s and 9 MSym/s, the EVM values of the received RF QAM data signal are shown for 1, 3, 5 and 10 sub-carriers¹. In this investigation, the SCM carrier spacings are all set to be 1.2 times the signal bandwidth for each carrier, enabling sufficient guard bands between sub-carriers. When the number of carriers increases from 1 to 3 while keeping the data rate constant (at 18 MSym/s \times 6 bit/Sym = 108 Mbit/s, and 9 MSym/s \times 6 bit/Sym = 54 Mbit/s), the EVM value decreases with more than 0.5% for 9 MSym/s total symbol rate and more than 1% for 18 MSym/s total symbol rate, indicating an improvement of the system performance for multi-carrier system when compared to the single carrier system. This EVM improvement is due to the decreased symbol rate per carrier in the multi-carrier system for a fixed data rate. As shown in Figure 2.5(a), when the number of carriers increases beyond 3, the EVM for the 18 MSym/s symbol rate system keeps increasing, whilst a decrease in EVM for 10 sub-carriers is observed in the 9 MSym/s curve. To explain this inconsistency of the two curves when the number of carriers equals to 10, the number of carriers and symbol rate per carrier are investigated in more detail.

Figure 2.5(b) shows the EVM value as a function of the number of carriers for the fixed 18 MSym/s total symbol rate in the back-to-back system. As seen in Figure 2.5(b), when multiple sub-carriers are employed the system performance is largely improved due to the reduced symbol rate per carrier. For the fixed total symbol rate, a fluctuation of EVM value versus the number of carriers can be seen. Since a larger number of carriers in the RF signal corresponds to a smaller symbol rate per carrier for the same total symbol rate, a trade-off between the number of carriers and the symbol rate per carrier can optimise the system performance. Still, it is worthwhile to notice that although there are some variations of the EVM, the performance of the single carrier QAM system is worse than the multi-carrier systems when the number of carriers is larger than 2. To assess the effect of both number of carriers and symbol rate per carrier separately, the results are presented in Figure 2.5(c). For each number of carriers, EVM values are plotted as a function of symbol rate per carrier. The system performance becomes worse if the symbol rate per carrier increases. In the mean time, for a certain symbol rate per carrier, the EVM is smaller when the number of carriers decreases due to the less inter-channel interaction in the multi-carrier systems. Such interaction is due to the intermodulation products caused by nonlinearity in the

¹In the following text of this section, number of sub-carriers are also denoted as number of carriers due to simplicity reason.

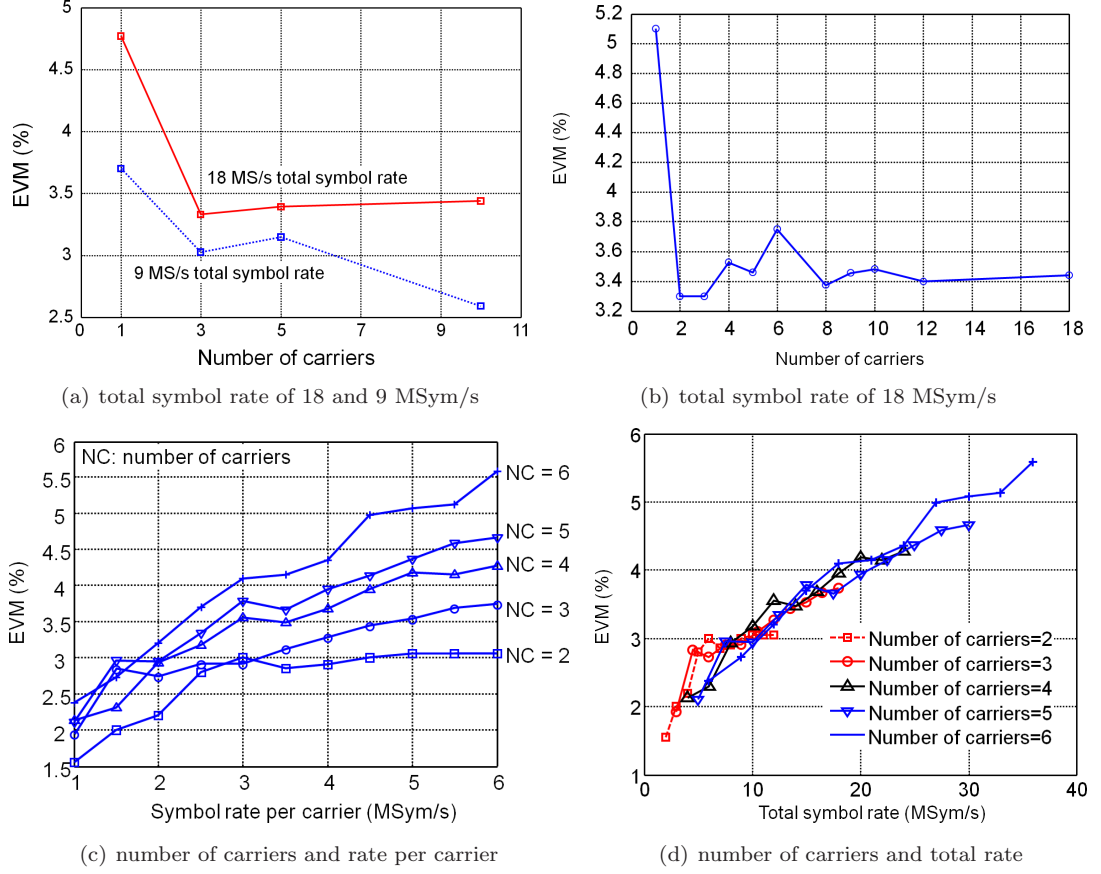


Figure 2.5: (a) EVM performance of SCM RoF system after 4.4 km MMF, for total symbol rate of 18 and 9 MSym/s, (b) EVM performance of SCM RoF system, for total symbol rate of 18 MSym/s, (c) The effect of number of carriers and symbol rate per carrier, (d) The effect of number of carriers and total symbol rate.

system. In the future investigations, adjacent channel power ratio (ACPR) or adjacent channel leakage ratio (ACLR), can be studied to characterise the inter-modulation distortion in the system [65, 66].

As a concluding investigation, the EVM value is shown in Figure 2.5(d) as a function of total symbol rate (i.e. number of carriers times symbol rate per carrier) in the RoF system for different number of carriers. It is seen that the EVM value for a certain total symbol rate does not depend on the number of carriers in the system, showing the trade-off between the number of carriers and symbol rates per carrier. When the number of carriers increases, the symbol rate and the signal bandwidth carried by each individual carriers reduce, whereas the inter-modulation between carriers are enhanced. Therefore, the trade-off between the reduced symbol rate per carrier and enhanced inter-modulation distortion leads to a linear relation between the EVM values and the total symbol rates shown in the figure. This means

2. HIGH CAPACITY RADIO-OVER-FIBRE TRANSMISSION SYSTEMS

the choice of the number of carriers is quite flexible for such SCM RoF systems.

The conclusion drawn above is verified by the measurement only with the number of carrier is around or below 10 due to the limitation of the test equipment. For an SCM system with a much larger number of carriers, the linear relation is predicted to be the same in the same system setup. However, for a multi-carrier system such as orthogonal frequency division multiplexing (OFDM), such relation might not hold because of the frequency orthogonality between neighboring carriers. Further discussion about OFDM will be addressed in the next section. It is also worthwhile to note that in this experiment the total symbol rate exceeds 35 MSym/s (210 Mbit/s) while the EVM is below 6%. In the IEEE 802.11a standards an EVM value is required of 7.94% for 64-QAM of 2/3 code rates.¹

2.3 OFM Transmitter Nonlinearity

2.3.1 Orthogonal frequency division multiplexing

In SCM systems, the sub-carriers are spaced far apart in the frequency domain in such a way that signals can be separately filtered by conventional filters and separately demodulated. Therefore, guard bands have to be inserted between different carriers leading to a lower spectral efficiency. Moreover, because of the existence of system nonlinearity and inter-modulation distortion, in dispersive medium and multi-path fading environment such as optical fibre and free space, the dispersion effect leads to a significant degradation of the signal quality due to interference from neighboring carriers [67]. In contrast to SCM signal, the carriers in the OFDM signal are arranged so that sidebands of the individual carriers overlap but due to the orthogonality the signals can still be received without adjacent carrier interference, giving rise to a higher signal spectral efficiency [68]. In order to achieve this, the carriers of such signals must be mathematically orthogonal, as shown in Figure 2.6. Suppose a set of signals Ψ , where Ψ_p is the p^{th} element in the set. The signals are orthogonal if

$$\int_a^b \Psi_p(t) \Psi_q^*(t) dt = \begin{cases} K, & \text{if } p = q \\ 0, & \text{if } p \neq q \end{cases} \quad (2.21)$$

where the $*$ indicates the complex conjugate and interval $[a, b]$ is a symbol period. A very simple example of the frequency orthogonality is that the series $\sin(mx)$ for $m = 1, 2, \dots$ is orthogonal over the interval $-\pi$ to π [69].

Mathematically, each carrier $s_{c,i}(t)$ ($i = 0, \dots, N - 1$) of the OFDM can be expressed by

$$s_c(t) = A_c(t) e^{j[\omega_c t + \phi_c(t)]} \quad (2.22)$$

¹In this thesis, only EVM values are presented to evaluate the quality of RF signals. In future work, more requirements such as noise level, code domain error (CDE), ACPR values are strongly recommended to be considered.

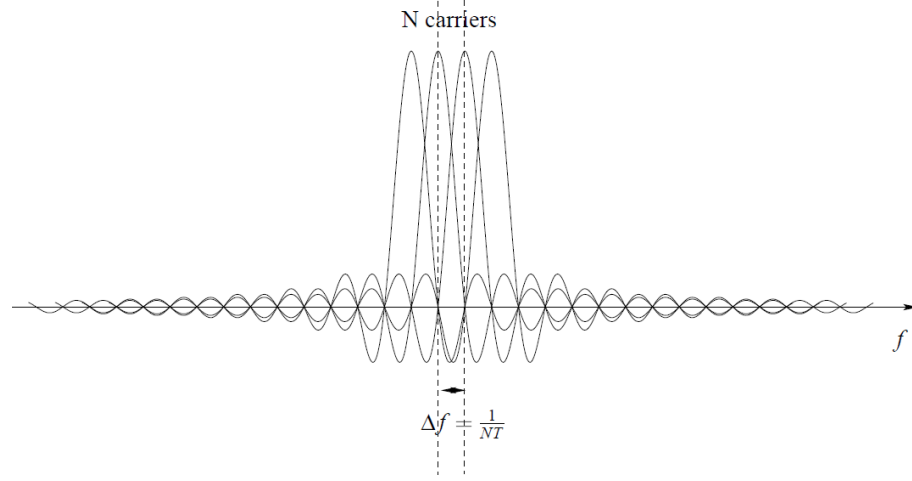


Figure 2.6: Frequency representation of OFDM.

where both the amplitude and the phase of the carrier, $A_c(t)$ and $\phi_c(t)$ are constant over the symbol duration τ . Thus, the OFDM signal $s_s(t)$ consisting of many carriers can be represented by [70]

$$s_s(t) = \frac{1}{N} \sum_{i=0}^{N-1} s_{c,i}(t) = \frac{1}{N} \sum_{n=0}^{N-1} A_N(t) e^{j[\omega_n t + \phi_n(t)]} \quad (2.23)$$

where $\omega_n = \omega_0 + n\Delta\omega$, N is the number of carriers of the OFDM signal and $\phi_n(t)$ is phase of the n^{th} carrier. Consider the waveforms of the each frequency component of the signal over one symbol duration; the amplitude and the phase of these components do not change. Assuming the signal is sampled using a sampling frequency of $\frac{1}{T}$, the resulting signal can be written as [70]

$$s_s(kT) = \frac{1}{N} \sum_{n=0}^{N-1} A_N e^{j[(\omega_0 + n\Delta\omega)kT + \phi_n]} \quad (2.24)$$

It is convenient to sample over the period of one symbol, therefore we have $\tau = NT$. Equation 2.24 can be simplified by omitting the base carrier frequency ω_0 :

$$s_s(kT) = \frac{1}{N} \sum_{n=0}^{N-1} A_N e^{j\phi_n} e^{j(n\Delta\omega)kT} \quad (2.25)$$

Comparing Equation 2.25 with the general form of inverse Fourier transform (IFFT)

$$g(kT) = \frac{1}{N} \sum_{n=0}^{N-1} G\left(\frac{n}{NT}\right) e^{j2\pi nk/N} \quad (2.26)$$

Note that $G(\frac{n}{NT}) = A_N \cdot e^{j\phi_n}$, so $G(\frac{n}{NT})$ is a complex number. The function $A_N e^{j\phi_n}$ in Equation 2.25 can be seen as a signal in the sampled frequency domain and $s(kT)$ is the time domain representation.

2. HIGH CAPACITY RADIO-OVER-FIBRE TRANSMISSION SYSTEMS

Equation 2.25 and 2.26 are equivalent if [70]

$$\Delta f = \frac{\Delta\omega}{2\pi} = \frac{1}{NT} = \frac{1}{\tau} \quad (2.27)$$

Equation 2.27 forms the condition that is required for orthogonality as shown in Figure 2.6. Therefore, the orthogonality can be obtained by using IFFT procedure.

Figure 2.7 illustrates the process of a typical Fourier transform (FFT) based OFDM system. The incoming serial data is first converted from serial to parallel and grouped into x bits each to form a complex encoded data in a vector format, e.g. I-Q modulated. The number x determines the signal constellation of the corresponding subcarrier, such as 16- or 32-QAM. The complex numbers are modulated in the baseband by the IFFT and converted back to serial data for transmission. A cyclic prefix is inserted between symbols to avoid inter-symbol interference (ISI) caused by multi-path distortion. The discrete symbols are converted to analogue and low-pass filtered for RF up-conversion to the RF carrier. The receiver performs the inverse process of the transmitter. One-tap equaliser is used to correct channel distortion. The tap-coefficients of the filter are calculated based on the channel information [70].

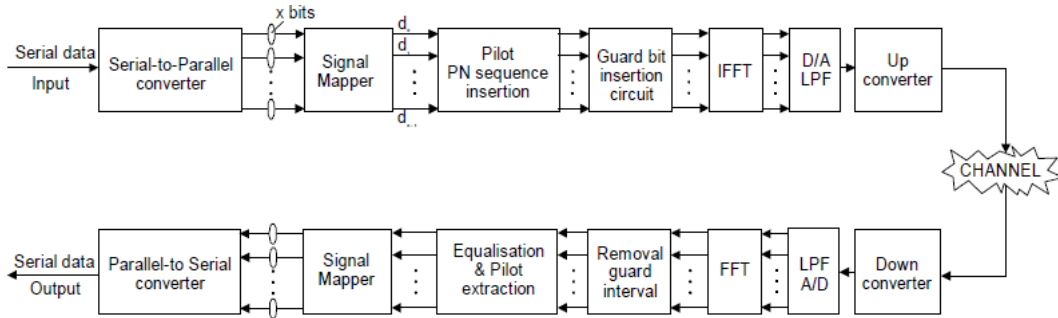


Figure 2.7: FFT-based OFDM modulation and demodulation.

2.3.2 Effects of MZM nonlinearity on single-carrier QAM and OFDM-QAM signals

Based on the OFM RoF system discussed in Section 2.1 and 2.2, an investigation about the effects of the MZM nonlinearity on QAM and OFDM signals is presented in this section [53]. In the fibre-optic system employing an MZM as an external modulator, when the power of the driving signal of the MZM (i.e. the data signal) increases, the nonlinear transfer function of MZM generates higher order nonlinearities in the spectrum, while distorting the signal and degrading the system performance. Stronger the nonlinear intermodulation products, more severe the signal is distorted. The effect of the MZM nonlinearity in

the RoF system has been investigated in [71–73]. In this section, the effect of the MZM nonlinearity in the OFM transmitter is investigated, by employing an experimental comparative study. The nonlinear transfer function of the MZM is given by [74]

$$\frac{P_{out}}{P_{in}} = \cos^2\left[\frac{\pi(v_1 - v_2)}{2V_\pi}\right] \quad (2.28)$$

where v_1 and v_2 are the driving signals in the upper and lower arm of MZM respectively. In the experimental investigation, the setup is the same as Figure 2.4(a), except for the FSR of the MZI in this experiment is 40 GHz. The MZI is responsible for the phase-to-intensity conversion and the FSR of the MZI can be chosen arbitrarily. In this work, a 40 GHz FSR is employed. In this experiment, no fibre transmission was included and the frequency of the sweep signal was 6.4 GHz and the data modulated by the MZM was single-carrier 16-QAM signal or OFDM 16-QAM signal with the same data rate of 36 Mbit/s and the same sub-carrier frequency of 1 GHz. Moreover, in this experiment, the received optical power remained the same level (−2 dBm) to ensure that the photo-detector was not saturated and the nonlinearity caused by the receiver amplifier was not severe.

First, Figure 2.8 shows the experimental results of the signal power spectrum after the photo-detection. It presents the details of the spectrum between 14 and 38 GHz, showing the 3rd, 4th and 5th harmonics of the OFM, corresponding to 19.2, 25.6 and 32 GHz respectively. The power of the driving signal of the MZM (16-QAM) is set to 7.5 dBm, which is strong enough to generate noticeable second order nonlinearities¹, as highlighted by the ellipses in Figure 2.8. The data power of 7.5 dBm corresponds to a peak-to-peak voltage of 1.4 V, and the V_π of the MZM is measured to be 2.5 V. The MZM is biased at its half quadrature point where $V_{bias} = \frac{1}{2}V_\pi$.

Secondly, to investigate such high order nonlinearities illustrated in Figure 2.8, the comparison of nonlinearity strength between two modulation formats is shown: the single-carrier QAM and the 52-subcarrier OFDM (with the same bit rate of 36 Mbit/s and same sub-carrier frequency 1 GHz), as shown in Figure 2.9. The results are taken at the 4th OFM harmonic, corresponding to 25.6 GHz (while the data is measured at 26.6 GHz due to 1 GHz sub-carrier). It is seen that with an increasing power of the driving signal, stronger nonlinearities are observed for both QAM and OFDM signals. However, nonlinearity strengths for OFDM are larger than those for QAM at a larger driving signal because of the multiple carriers in OFDM generating more inter-modulation products. A 5 dB difference of the 2nd order nonlinearity between QAM and OFDM is recorded at the driving power of 9.5 dBm. Moreover, the

¹The highlighted high order nonlinearities are denoted in this section as 2nd order nonlinearities. In theory, they are mainly contributed from the 3rd order intermodulation product between the carrier and the signal. However since this thesis does not investigate in terms of intermodulation products, they are simply denoted by 2nd as they are most close to the signal in frequency domain. Higher order nonlinearity will be denoted as 3rd, 4th, etc. in this thesis.

2. HIGH CAPACITY RADIO-OVER-FIBRE TRANSMISSION SYSTEMS

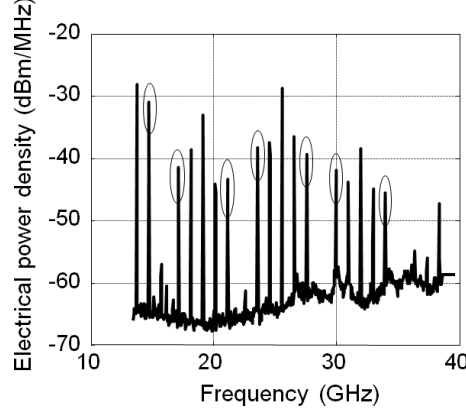


Figure 2.8: Measured spectrum of output signal from the transmitter, with 6.4 GHz sweep frequency, and 16-QAM driving signal of 7.5 dBm. Second order nonlinearity of the QAM signal is highlighted by ellipses.

3^{rd} order nonlinearity appears for the OFDM signal when the driving power is larger than 6 dBm, while no 3^{rd} order nonlinearity is observed for QAM signal in the whole measurement. This is again due to the multiple carriers generating more intermodulations in OFDM. In Figure 2.9, note that the 3^{rd} order intermodulation products grow with a steeper slope than the 2^{nd} order ones, due to their higher order.

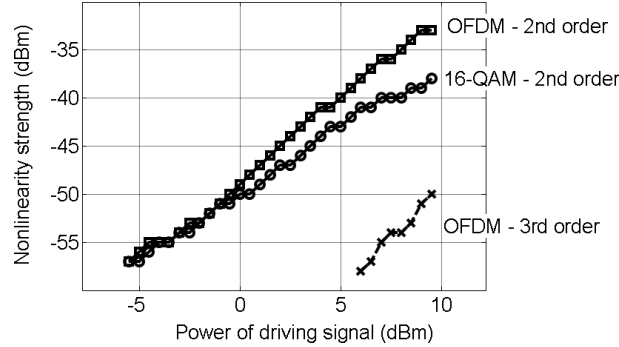


Figure 2.9: Measured 2^{nd} and 3^{rd} order nonlinearity strength at different driving signal powers, for QAM and OFDM signal.

Finally, the impact of MZM nonlinearity is evaluated in terms of the data quality carried by the 4^{th} harmonic, by measuring the EVM of the QAM and OFDM data at 26.6 GHz, for the different power levels of the data. A comparison between the QAM and OFDM signal is shown in Figure 2.10. The square markers curve represents the measured EVM values for the OFDM signal, compared with the circled markers for the QAM signal. Simulation results for this measurement are also shown in dashed

and dotted curves for QAM and OFDM, respectively. The simulation gives a clear indication of the impact of the MZM nonlinearity on the system performance. The simulated EVM for a lower driving power is also smaller due to the fact that the noise effect is not modeled so that the signal-to-noise ratio (SNR) is infinite in the simulation. Nevertheless, an optimum driving power can be found for the RoF transmitter for both QAM and OFDM signals. In this measurement, the optimum is observed to be around 1 dBm. The EVM penalty remains low before the driving power increases beyond 4 dBm. When the driving power is larger than 5 dBm, the dramatic increase of EVM shows a larger degradation of the system performance for the OFDM signal, compared with QAM, which is in line with the simulation results. For the same 1% EVM penalty from the nonlinearity effect, the tolerance of the power of OFDM driving signals is 2 dB less compared with QAM signals, indicating a more strictly confined electrical power budget. This is because of the intermodulation products from the harmonic carriers to the sub-carriers of OFDM as well as the intermodulation products between OFDM sub-carriers. Moreover, the larger peak-to-average power ratio (PAPR) of the OFDM signal also makes the nonlinear effect of MZM more severe for OFDM signal due to the larger peak amplitude of the OFDM signal, compared with the single-carrier QAM signal. On the left side of the optimum driving power, larger EVMs are observed due to a smaller SNR in both the QAM and OFDM cases. The increase of the EVM is caused by the decrease of the SNR in both cases.

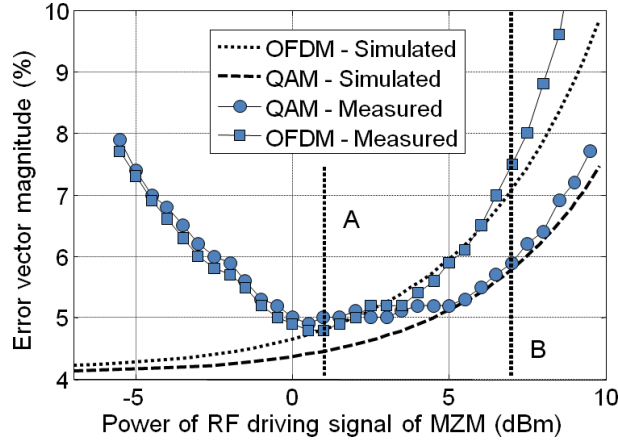


Figure 2.10: Simulated and measured EVM versus powers of the driving signals, for both OFDM and QAM signal. Dot line A and B indicate the driving power of 1 and 7 dBm, respectively. The EVM values are measured at 26.6 GHz (4^{th} harmonic).

In addition, to illustrate the nonlinearity impact, the sets of comparison of the constellations are presented for the QAM signal in Figure 2.11(a), 2.11(b) and 2.11(c) and OFDM in Figure 2.11(d),

2. HIGH CAPACITY RADIO-OVER-FIBRE TRANSMISSION SYSTEMS

2.11(e) and 2.11(f). The constellations of the electrical back-to-back (B2B) signals, which are directly detected from the signal generator, are shown in Figure 2.11. For comparison, the received signal at the output of the RoF transmitter for a 1 dBm (at power A as shown in Figure 2.10) and 7 dBm (at power B in Figure 2.10) driving power is also presented. It can be seen that the signal constellations are severely distorted by the MZM nonlinearity at the larger driving power (7 dBm) in the transmitter.

In the OFDM format, the constellation diagrams consist of two extra points on the horizontal axis. They present the pilot carriers and do not have phase components. Comparing Figure 2.11(c) and 2.11(f), note that the constellations for single-carrier QAM are more distorted by the phase errors than the amplitude errors. In contrast, the constellations in OFDM signal are distorted both in phase and amplitude. This is due to the fact that nonlinear intermodulation between the OFDM carriers have degraded the orthogonality of the carriers thus leading to demodulation errors both in phase and amplitude. A similar phenomenon and more detailed explanation will be presented in Section 3.3.

In this experiment, the OFDM signal from the standard WiFi signal with a number of carriers of 52 is used. Increasing this number will lead to a stronger effect of nonlinear inter-modulation and degrade the system performance more severely. Nevertheless, an OFDM signal with much less number of carriers, e.g. 8 or 16, will be more distorted from the effect of fibre dispersion, which is similar than the case of the SCM format. Therefore, there is an optimum number of carriers in OFDM in view of system performance degradation due to the fibre dispersion and due to the nonlinearities. This optimum number of carriers depends on the trade-off between dispersion-induced degradation and the nonlinearity-induced degradation.

2.4 Summary

This chapter mainly reported on the theoretical and experimental studies on RF microwave generation and the corresponding radio-over-MMF system employing the OFM scheme. Both the transmission demonstration and investigation on transmitter nonlinearities are presented in this chapter.

Optical frequency multiplication is a method to generate RF harmonics by the effect of the heterodyning of a single source. The analysis in the frequency domain has shown that in contrast with Figure 2.1(b), due to the presence of an optical filter, the Bessel harmonics generated by the phase modulation results in several beating products which are not equal to zero, therefore leading to RF harmonics. The analysis presented in the frequency domain is in line with the one presented in time domain. A linear relation between the phase noise of the generated harmonics and the phase noise of local oscillator, depending on the order of harmonics, has also been analysed mathematically and confirmed experimentally.

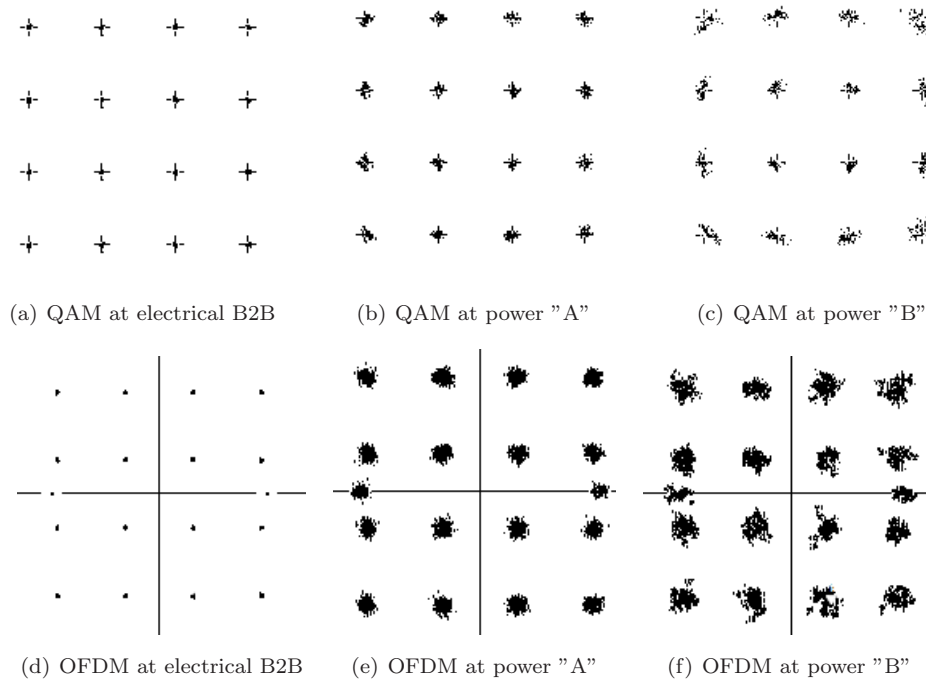


Figure 2.11: Constellation diagram for QAM and OFDM signals; "A" and "B" correspond to power levels equal to 1 and 7 dBm respectively as shown in Figure 2.10. (a): back-to-back connection between signal generator and detector for 16-QAM at 1 GHz, with EVM of 0.6%; (b): 16 QAM at 26.6 GHz for 1 dBm power; (c): 16 QAM at 26.6 GHz for 7 dBm power ; (d): back-to-back for OFDM at 1 GHz, with EVM of 0.8%; (e): OFDM at 26.6 GHz for 1 dBm power and (f): OFDM at 26.6 GHz for 7 dBm power.

2. HIGH CAPACITY RADIO-OVER-FIBRE TRANSMISSION SYSTEMS

Moreover, a radio-over-MMF distribution system employing the SCM and the OFM schemes has been studied. In Section 2.2.1, an improved system capacity with more than 210 Mbit/s has been demonstrated at 18.3 GHz over 4.4 km 50 μm core diameter silica graded-index MMF with EVM value less than 6%. The performance of the multi-carrier system has been shown to be better than that of the single carrier system. The trade-off between the number of carriers and the symbol rate per carrier in the multi-carrier RoF system have also been analysed, leading to a conclusion that the performance of the multi-carrier RoF system does not depend on the number of carriers, when the total symbol rate is considered. The robustness of the OFM method against laser phase noise and the fibre dispersion has been verified in Section 2.1.2 and 2.2.1 respectively.

Furthermore, in Section 2.3, through both the theoretical simulation and the experimental investigation, the nonlinearity of an MZM in the RoF transmitter employing the OFM scheme has been comparatively studied, for the single-carrier QAM and the OFDM signal at 26.6 GHz. It has been shown that for both modulation formats, optimum values for the power of the driving signal can be found. These optimum values correspond to the minimum transmitter nonlinearity and to the largest possible value of SNR. However, the maximum power level of the OFDM driving signal is 2 dB smaller than the QAM driving signal for a 1% EVM penalty. This discrepancy is caused by the intermodulation among the OFDM subcarriers, which become susceptible to high order nonlinearities. Because of the smaller tolerance of the OFDM to the nonlinearity effects, a more careful choice of the driving signal power is necessary when designing the RoF link suitable for the high capacity OFDM wireless in-building networks. Consequently, the linearisation option of the MZM has been developed and commercial available on the linearity of the MZM modules today due to the requirement of hybrid fibre-coaxial (HFC) systems. Furthermore, in the trade-off between the effect of fibre dispersion and the effect of nonlinearities, the number of carriers for the OFDM should also be optimised in order to have the best system performance.

Chapter 3

Ultra-Wideband Wireless Service over POF Systems

3.1 Ultra-Wideband Signal and Multi-Band OFDM

Ultra-wideband (UWB) is a wireless technology designed to exchange high speed data within short ranges while using little power [78]. Typically, radio technologies focus on simultaneously transmitting many separate signals over long distances. Each signal occupies a narrow frequency band located around a high-frequency carrier. These frequency bands are allocated by governments throughout the world to specific service providers. UWB, on the other hand, employs an entirely different technique than typical radio technologies. It broadcasts over short distances using a broad spectrum. Instead of concentrating a powerful signal in a narrow band, the signal is spread over a very wide band at very low power levels with high data rates. Figure 3.1 shows frequency spectra of traditional radio technologies and a spectrum of a UWB signal that overlays other spectra [79]. UWB operates at or below levels currently allowed for the unintentional radio frequency energy radiated by many electronic devices such as game players, and even PCs. UWB radio transmission can legally operate in the range from 3.1 GHz up to 10.6 GHz, at a limited transmit power density of -41.3 dBm/MHz. A bandwidth larger than 500 MHz or 20% of the central frequency is required for -10 dB point for UWB signals [78].

3.1.1 Multi-band OFDM UWB versus impulse radio UWB

For a UWB system, information on each of the sub-bands can be transmitted using either single-carrier (impulse radio) or multi-band techniques. Single-carrier UWB systems transmit information by modulating the phase of a very narrow pulse which has a broad spectrum. The main advantage of this type of

This chapter is based on the results published in [75], [76] and [77].

3. ULTRA-WIDEBAND WIRELESS SERVICE OVER POF SYSTEMS

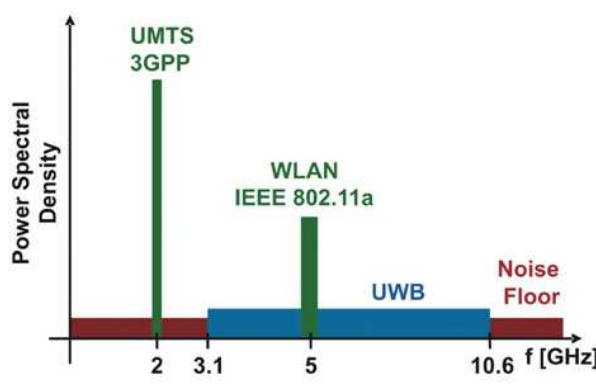


Figure 3.1: Frequency spectra of traditional radio and UWB technologies [79]

system is that the transmitter has a very simple design because no up and down conversion is required in the impulse radio. However, there are several practical issues with implementing the impulse radio. Due to the short pulses, accurate synchronisation and channel estimation is very difficult. Designing wide-band RF components is still a big challenge today and for digital implementation of high sampling rate analogue-to-digital conversion is very hard to achieve [80, 81].

In the other flavor of the UWB system, i.e. multi-band UWB systems, multi-band orthogonal frequency division multiplexing (MB-OFDM) techniques are used to transmit the information on each of the sub-bands. OFDM has several nice properties, including high spectral efficiency, inherent resilience to RF interference and the robustness to multi-path fading. It is also well understood and has been proven in other commercial technologies (e.g. IEEE 802.11a/g). The main advantage is that it is able to deal with the sub-band signal at the receiver without having to sacrifice the data rate. The drawback of this type of system is that the transmitter is more complex because it requires an inverse Fourier fast transform (IFFT) and the receiver requires an FFT. Additionally, the peak-to-average power ratio may be higher than that of the pulse-based UWB approaches [82].

3.1.2 Industrial standard on multi-band OFDM

Providing a data rate of up to 480 Mbit/s, MB-OFDM has been selected as an International Organization for Standardization (ISO) published radio standard for high speed UWB wireless connectivity that offers an unsurpassed combination of high data throughput rates and low energy consumption [83]. With regulatory approval in major markets worldwide (more than 350 partners in WiMedia Alliance), this technology has gained broad industry momentum as evidenced by its selection for Wireless USB and

3.1 Ultra-Wideband Signal and Multi-Band OFDM

high-speed Bluetooth [84]. Therefore, further in this thesis, only the MB-OFDM type of the UWB signals is considered.

According to ECMA-368/369 standard (approved by WiMedia Alliance) [85], the spectrum of MB-OFDM UWB signal is divided into 14 bands, each with a bandwidth of 528 MHz, as illustrated in Figure 3.2 with the specific spectral mask [85]. The first 12 bands are then grouped into four band groups each consisting of three bands. The last two bands are grouped into a fifth band group. A sixth band group is also defined within the spectrum of the first four, consistent with usage within worldwide regulatory agreements. A total of 110 sub-carriers (100 data carriers and 10 guard carriers) are used per band. In addition, 12 pilot subcarriers allow for coherent detection. Frequency-domain spreading, time-domain spreading, and forward error correction (FEC) coding are provided for optimum performance under a variety of channel conditions.

The coded data is spread using a time-frequency code (TFC). The standard specifies two types of time-frequency codes. One is the time-frequency interleaving (TFI) where the coded information is interleaved over three bands. For instance, during the first defined time slot information is transmitted in the first frequency sub-band and during the second time slot information is transmitted in the second frequency sub-band. The other type of the TFC is the fixed frequency interleaving (FFI) where the coded information is transmitted on a single band through the whole time.

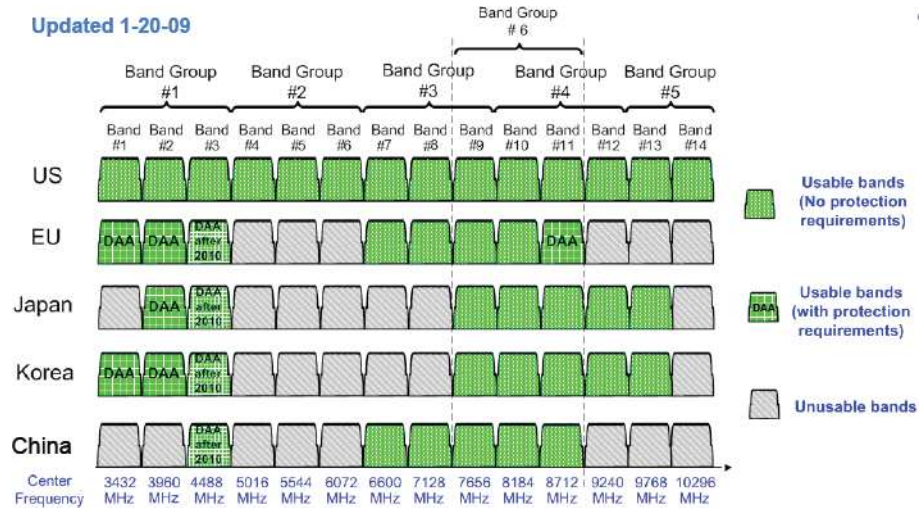


Figure 3.2: Worldwide MB-OFDM UWB spectrum regulatory status 2009, source: WiMedia Alliance

3.1.3 UWB-over-POF system

In Section 1.2, the property of the plastic optical fibre (POF) have been discussed and its application in in-home networks has been shown in Figure 1.2. In future in-home networks, RoF technologies enable us to deliver UWB signals over optical fibre to an extended coverage of UWB services, e.g. from 5 m to 100 m. Particularly, POF is more suitable than single-mode and multi-mode silica fibres thanks to "do-it-yourself" installation, easy maintenance and smaller bending radius (< 20 mm) [45]. The commercialisation of low power consumption and broadband transceivers at visible wavelength also opens large possibilities to the low-cost solutions for broadband in-building networks over POF.

UWB RoF transmission systems have been successfully shown recently using single-mode fibre [86], multi-mode fibre [87–89] and up to $62\text{ }\mu\text{m}$ core diameter perfluorinated (PF) POF [90, 91]¹. In comparison to the previous studies, the aim of this chapter is to demonstrate the feasibility of UWB RoF system for in-building application using the very large core diameter polymethylmetacrylate (PMMA) POF in combination with a visible eye-safe light source and to show a bi-directional UWB over POF system employing $50\text{ }\mu\text{m}$ core diameter PF graded-index (GI) POF. This chapter is organised as follows: Section 3.2 will discuss the feasibility of transmitting a more than 2 Gbit/s UWB signal over 1 mm core diameter PMMA GI-POF using off-line signal processing and discrete multi-tone modulation. After that, Section 3.3 will demonstrate the WiMedia-compliant UWB RoF system over PMMA POF, providing 200 Mbit/s data rate based on off-the-shelf real-time WiMedia UWB transceivers. Finally, the demonstration of full-duplex bi-directional transmission will also be presented by employing $50\text{ }\mu\text{m}$ core diameter PF GI-POF.

3.2 High Capacity Gbit/s UWB Transmission over PMMA POF

In recent years, Gbit/s transmission based on a low-cost transmitter has been demonstrated over 100 m PMMA step-index (SI) POF using sub-carrier multiplexing [92]; more than 10 Gbit/s transmission over PMMA GI-POF has also been shown using a high output power laser diode [93]. Given the bandwidth of the PMMA GI-POFs that has been reported in [94] (approximately 3 GHz for 50 m exclusive the bandwidth limitation of receiver), a feasibility study on high-speed transmission of baseband UWB transmission over 50 m long 1 mm core diameter PMMA GI-POF is presented in this section, using an eye-safe broadband red vertical cavity surface emitting laser (VCSEL) diode at 667 nm wavelength. The discrete multi-tone modulation (DMT) is employed with the fixed 16-level quadrature amplitude modulation (16-QAM) per tone according to the wireless-USB standard. Due to the absence of any optical

¹There are many other published work on UWB RoF from an EU project *UROOF*.

processings and the use of the low output power of the VCSEL, a promising low-cost solution for high capacity and robust UWB-over-POF systems will be predicted [75].

3.2.1 Baseband OFDM: discrete multi-tone modulation

As a baseband version of the OFDM format, DMT modulation format has been widely used in asymmetrical digital subscribers line (ADSL) systems and power-line communication systems. In DMT modulation, a high-speed serial data stream is divided into multiple parallel low-speed streams and modulated onto subcarriers of different frequencies for transmission [95].

Usually, each subcarrier stream is mapped onto complex values C_n according to an M-ary quadrature amplitude modulation (M-QAM) constellation mapping, where $n = 1, 2, \dots, N - 1$ denotes the subcarrier number and $N - 1$ is the total number of data-carrying subcarriers used for transmission. (The N^{th} carrier is set as null.) By using the inverse discrete Fourier transform (DFT) to modulate C_n onto different subcarrier frequencies, the resulting subcarriers are mutually orthogonal. In practice, the fast Fourier transform (FFT) algorithm is used to efficiently implement the DFT function. Furthermore, when the $N - 1$ information symbols $C_n (n = 1, 2, \dots, N - 1)$ are used as input values for a $2N$ -point inverse FFT (IFFT), where $C_0 = C_N = 0$ and Hermitian symmetry property [96, 97]:

$$C_{2N-n} = C_n^* \quad (3.1)$$

is satisfied, the resulting output multicarrier DMT time-domain sequence s_k can be written as [97]

$$s_k = \frac{1}{\sqrt{2N}} \sum_{n=0}^{2N-1} C_n \exp(j2\pi k \frac{n}{2N}), k = 0, 1, \dots, 2N - 1. \quad (3.2)$$

The resulting s_k is a real-valued, baseband multicarrier signal consisting of sample points. The resilience of DMT in a dispersive channel is the result of parallel transmission and the cyclic prefix. Due to the parallel transmission of the data, the symbol period is much longer than in the case of standard serial transmission. Therefore, intersymbol interference (ISI) affects only a small fraction of a symbol period. By use of a cyclic prefix, this ISI can be easily eliminated and orthogonality among the subcarriers is ensured [98]. At the receiver, demodulation of the DMT sequence is then accomplished by using a $2N$ -point FFT, resulting in [97]

$$\hat{C}_n = \sum_{k=0}^{2N-1} \hat{s}_k \exp(-j2\pi k \frac{n}{2N}), n = 0, 1, \dots, 2N - 1. \quad (3.3)$$

With a one-tap equaliser, the magnitude and phase shift of each subcarrier (as a result of channel impulse response) can be corrected and the information symbols \hat{C}_n recovered after demodulation with

3. ULTRA-WIDEBAND WIRELESS SERVICE OVER POF SYSTEMS

the FFT [97]. In the DMT format, it is also possible to allocate the number of bits per subcarrier according to its corresponding signal-to-noise ratio (SNR), typically known as the bit-loading algorithm [99]. Details of the bit-loading algorithm will be discussed in Chapter 5 where it is employed.

3.2.2 Experimental setup and results

In the experiment of high capacity UWB over POF, due to the required format for MB-OFDM signal according to the UWB standard, a fixed bit-loading algorithm was utilised to ensure all the 122 sub-carriers have the same bit allocation, which was 4 bits for 16-QAM. The use of the DMT format enabled us to transport a down-converted intermediate frequency (IF) UWB radio signal received from air over a bandwidth-limited POF. In combination with down-conversion before fibre transmission and up-conversion after fibre transmission, either optically or electrically, RF UWB signals can eventually be delivered between the home gateway and the end users, and among multiple end users. In this investigation, the IF UWB transmission over POF is focussed and no up- or down-conversion is realised in this section [75].

The experimental setup of the UWB signal transmission over POF is shown in Figure 3.3. A 667 nm wavelength VCSEL from Firecomms (RVM665T) was modulated by the output of an arbitrary waveform generator (AWG) sampling at 2.1 GSamples/s. The VCSEL was designed to have a bandwidth of 3 GHz. The bias current of the VCSEL was set to 6 mA, resulting in a peak-to-peak driving current of maximum 12 mA. The optical power of the VCSEL launched into the POF was measured as -2 dBm. After transmitting the directly modulated signal over 50 metres of 1 mm core diameter PMMA GI-POF, a -17 dBm optical power was received due to the 17 nm deviation of the VCSEL wavelength from the POF minimum loss wavelength. An avalanche photodiode (APD) receiver, which had an active area of $230\text{ }\mu\text{m}$ and a -3 dB bandwidth of 1.3 GHz, was used to detect the signal. The APD was from Silicon Sensor (230-8) and equipped with two stages of amplifiers (HP IVA-14228). 130 V supply voltage was required for the operation of the APD receiver. An optical lens (C230220P-B)¹ was also mounted before the APD to collect more optical power received by the APD, hence decreasing the coupling loss (and increasing the coupling efficiency) from the POF to the APD receiver.

The bandwidth of the investigated system is limited by the APD detector and the POF, which can be seen from the frequency response of the system in Figure 3.4(a). However, for the transmission of one sub-band of UWB signal, the transceiver and the POF have bandwidth up to more than 528 MHz. As also indicated in Figure 3.3, the DMT (de)modulation to generate and evaluate the UWB signal is

¹One side of the aspheric lens with a numerical aperture of 0.55 is used to collimate the light emitted from 1 mm POF, while the other side of the lens with numerical aperture of 0.25 to focus the light to the APD receiver.

3.2 High Capacity Gbit/s UWB Transmission over PMMA POF

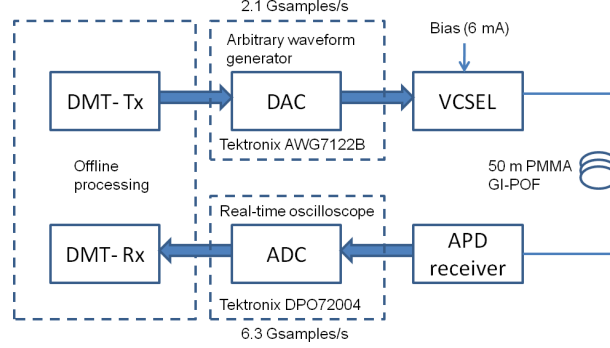


Figure 3.3: Experimental setup of the UWB over POF employing DMT.

executed off-line. In this experiment, 256 sub-carriers are used as Fourier transform size, ranging from 0 to 1.05 GHz. According to the ECMA-368 standard, only the first 122 sub-carriers are modulated by data and the rest (123 to 256) sub-carriers are left to be null. 256 carriers is chosen since it is an integer number of the power to 2. Another reason of choosing 256 is by leaving 123th to 256th sub-carriers as null carriers a guard band is introduced between the the useful data and the transmitter aliasing effect thus enables an easier investigation of the signal spectrum. In Figure 3.4(b)(up) the bit allocation of the 256 sub-carriers is shown. It is seen that up to 122 sub-carriers, 4 bits are assigned for each sub-carrier and no information is carried beyond these 122 sub-carriers. The resulting SNR is plotted in Figure 3.4(b)(down). The relatively flat SNR is due to the flat frequency response of the POF system and the uniformly distributed bit allocation.

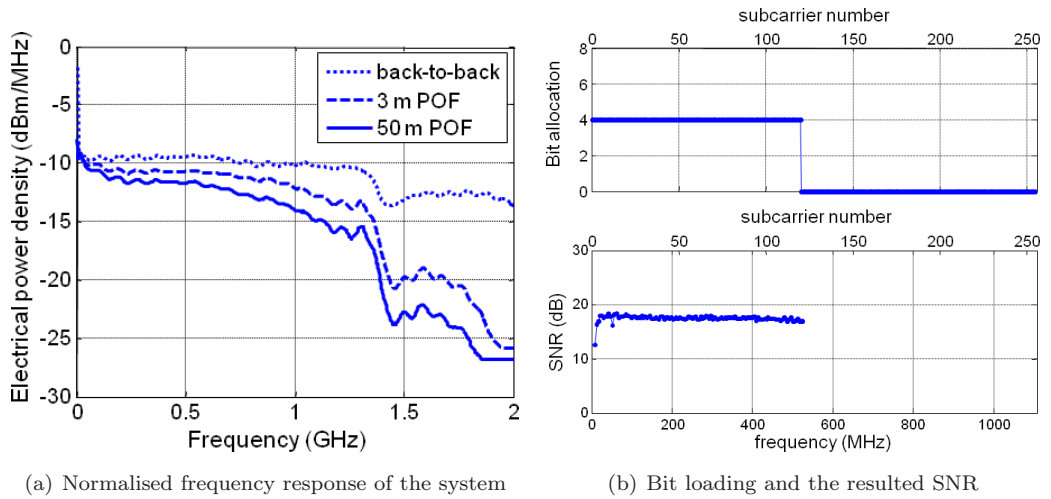


Figure 3.4: (a) Normalised frequency response of the system and (b) Up: bit allocation for 2.1 gross bit rate; Down: SNR after 50 m transmission over GI-POF.

3. ULTRA-WIDEBAND WIRELESS SERVICE OVER POF SYSTEMS

Figure 3.5(a) presents the bit error ratio (BER) value as a function of the index of sub-carriers of the received signal. The gross bit rate is 2.1 Gbit/s (corresponding to 1.9 Gbit/s excluding overhead). It is seen from Figure 3.5(a) that the BER value varies from 5×10^{-4} to 2×10^{-2} over 122 carriers. The average BER is 6×10^{-4} . In the DMT scheme, the signal is not demodulated per carrier, which provides the benefit that even if some carriers have a BER larger than 10^{-3} , the signal quality is still below the forward-error-correction (FEC) limit for error-free operation. The FEC limit for error free is 10^{-3} which forms the target average BER value in this experiment. Excellent performance of the transmitted signals can be observed. As an example, the overlapped constellations of the demodulated 10^{th} to 20^{th} sub-carrier are presented in Figure 3.5(b). These sub-carriers have 4-bit allocation (see Figure 3.4(b)), which gives a 16-QAM constellation. Finally, the electrical spectrum of the received UWB signal is presented in Figure 3.6. The spectral width of the signal is exact 528 MHz, with the power spectrum density below -41.3 dBm/MHz, as shown in the figure. It should be noted that the noise density level of the received signal is around -70 dBm/MHz. This is due to the background noise of the APD receiver. Applying a low-pass filter or replacing the APD receiver by a low-noise PIN receiver would significantly reduce the noise level to the thermal noise level (-110 dBm/Hz).

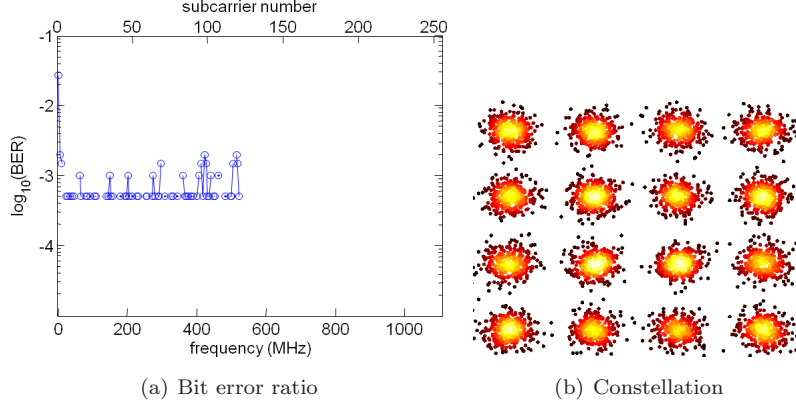


Figure 3.5: (a) BER for different carrier index and frequency after 50 m transmission, with average BER of 6×10^{-4} . and (b) Constellation diagrams of the demodulated signal at sub-carrier indices between 10 and 20.

3.3 WiMedia-compliance UWB Transmission over PMMA POF

Based on the discussion in Section 3.1 and the results shown in Section 3.2, in this section a more realistic low-cost approach using a commercially available UWB transceiver and on the real-time signal processing is focussed. The transceiver can be used only for sending/receiving UWB signals that comply with the

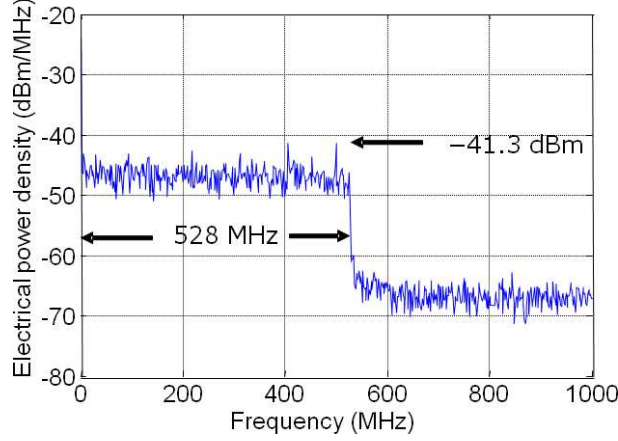


Figure 3.6: Received electrical spectrum of the UWB signal after 50 m POF.

WiMedia standards. The key question in this section is: can PMMA POF be used as a transmission medium for WiMedia-compliant UWB signals as illustrated in Figure 1.2 for future in-home networks which employ pico-cell communication standards such as MB-OFDM UWB?

3.3.1 Principle of operation

The very large core diameter of the PMMA POF provides an easy operation and cost-efficient solution for in-building UWB-over-POF systems. However, the large core diameter of the GI-POF (1 mm) and the resulting fibre modal dispersion limits the operational bandwidth of the fibre to a typical -3 dB bandwidth of 3 GHz for a 50 m long PMMA GI-POF. Meanwhile, the optical transceivers suitable for PMMA POF normally operate at the visible light wavelength around 650 nm. The available modulation bandwidth of such transceivers is also 3 GHz or even lower. Therefore, to deliver UWB signals with large core POF systems with critical bandwidth limitations, the UWB signals have to be firstly down-converted from the radio frequency (RF) (i.e. from 3.1 to 10.6 GHz) to an intermediate frequency (IF). The transmitted light is then modulated by the IF UWB signal and transmitted over POF. The signal is then received by a home communication controller or a residential gateway to be processed and eventually to be switched to other destinations. Then, the signal is put again in the optical domain and is launched into another span of POF. At the end of the transmission, a frequency up-conversion is used to bring the UWB signal to its original frequency band for radiating from the remote UWB antenna [76].

Based on this principle of operation, the experimental setup to achieve UWB-over-POF is depicted in Figure 3.7. A UWB transceiver¹ (Wisair prototype) was used to generate the UWB data with the bit rate

¹In the following chapters, the same Wisair transceiver is used to generate the UWB MB-OFDM signal.

3. ULTRA-WIDEBAND WIRELESS SERVICE OVER POF SYSTEMS

of 200 Mbit/s at the time-frequency code 7 (TFC 7), which meant that the transmitter only sends one sub-band data at the central frequency of 4.48 GHz (band group 1, sub-band 3). Other FFI TFCs were also possible for the system because only one frequency band was employed in FFI. In contrast, the TFI cases where frequency bands were interleaved were not suitable for this principle of operation due to the limited bandwidth of the 1 mm core diameter POF system.¹ In Figure 3.7, after an electrical mixer, the UWB signal with a signal bandwidth of 528 MHz was down converted to a central frequency of 380 MHz and filtered by a low-pass filter with a -3 dB bandwidth of 800 MHz to eliminate the unwanted high frequency components. The signal was then used to intensity-modulate (IM) the VCSEL together with a bias DC voltage of 4 mA. The -3 dB bandwidth of the VCSEL (model: RVM665T) was 3 GHz given by the data-sheet and the wavelength is 667 nm. The transmitted signal was launched into the POF with an optical power less than 0 dBm. After transmitting the signal over 1 mm core diameter POF with the length of maximum 50 metres, a PIN photodetector (model: Hamamatsu s5052)² with an active area diameter of 800 μm equipped with four stages of trans-impedance amplifiers (TIA) (one MMIC GALI-51 and three MMIC GALI-6) was used to directly detect (DD) the signal. The PIN photodetector had a -3 dB bandwidth of 800 MHz. The responsivity of the PIN diode was 0.4 A/W. The received and amplified signal was then sent to a real-time scope for off-line up-conversion, filtering and performance evaluation. The frequency response of the system shown in the inset of Figure 3.7 points out that the available overall -3 dB bandwidth of this IM-DD system was around 800 MHz.

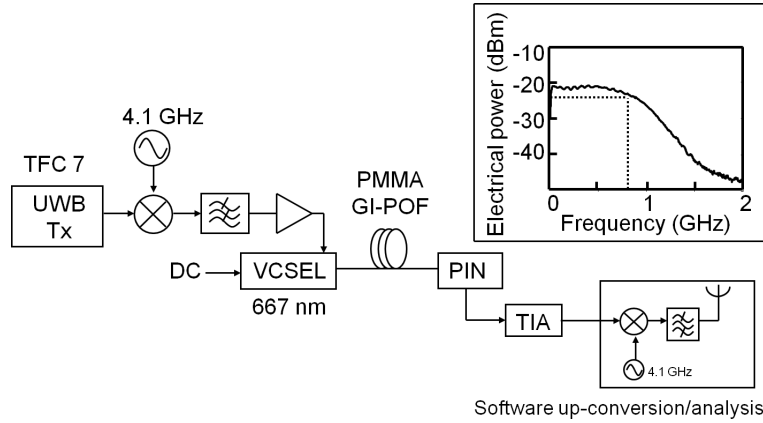


Figure 3.7: Experimental setup for 200 Mbit/s WiMedia-compliant UWB-over-POF system

¹In TFI cases, generated signals occupy at least two sub-bands, the bandwidth of which are more than 1 GHz.

²s5052 detector is internally equipped with a lens with the diameter of 3 mm whereas the photodetector itself has a diameter of 800 μm .

3.3.2 Experimental results

Figure 3.8(a) shows the power spectral density of the received signal after 50 m transmission over 1 mm core GI-POF. The compliance of the received signal with the spectral mask defined by the ECMA-368 standard has been illustrated. Figure 3.8(b) shows the corresponding spectrogram of the received signal. In this case, the FFI scheme is used where only one frequency is employed for data transmission. As a consequence, it is shown in Figure 3.8(b) that only one sub-band centered at 4.48 GHz is transmitted over the measuring time period. In Figure 3.9(a), the measured error vector magnitude (EVM) of the received signal is shown as a function of the indices of the sub-carriers, varying from -12 to -20 dB. According to the standard, the MB-OFDM signal is coded in the QPSK format. The overall EVM of the received signal after 50 m transmission is -16.21 dB (15.5 %). As shown in Figure 3.9(c), the overall performance of the transmission system well complies with the standard requirement (-16 dB). The constellation of the received signal after 50 m transmission is illustrated in Figure 3.9(b). In the worst case of our longest POF transmission (50 m), the constellation points are still clearly separated.

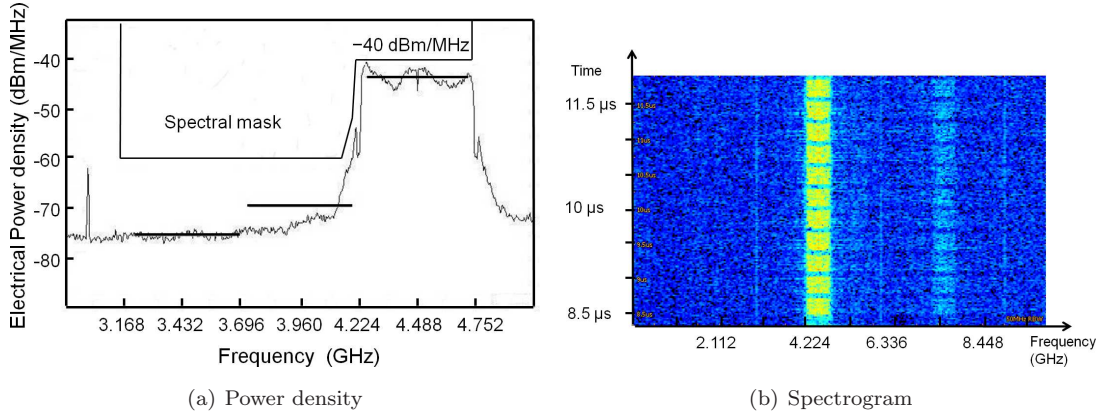


Figure 3.8: (a) Power spectral density of the received MB-OFDM UWB signal at 4.48 GHz (after up-conversion) for 50 m transmission and (b) Spectrogram of the corresponding signal.

Moreover, the measurement results are presented for different transmission lengths of 3, 15, 25, 35 and 50 metres respectively, as shown in Figure 3.9(c). The EVM value for electrical back-to-back test is measured as -22.76 dB. This value is used as the reference for the penalty evaluation. As shown in Figure 3.9(c), the optical-to-electrical and electrical-to-optical conversion gives a system penalty of less than 2 dB. This sufficiently low penalty is obtained due to the gain of the amplifiers at transmitter and receiver sides. Moreover, as indicated in Figure 3.9(c), the POF transmission adds a penalty from 0.5 to 5 dB depending on the length of transmission. The overall system penalty is less than 7 dB for up to 50 m POF transmission. Apart from the EVM requirement, there are also many other standard requirements

3. ULTRA-WIDEBAND WIRELESS SERVICE OVER POF SYSTEMS

for the signal to fully compliant with, such as frequency tolerance, preamble sync, ACPR, spectral mask and etc. In this experiments, all the measurement points shown in Figure 3.9(c) comply with the all specification required for MB-OFDM UWB signals. See Appendix B for an example.

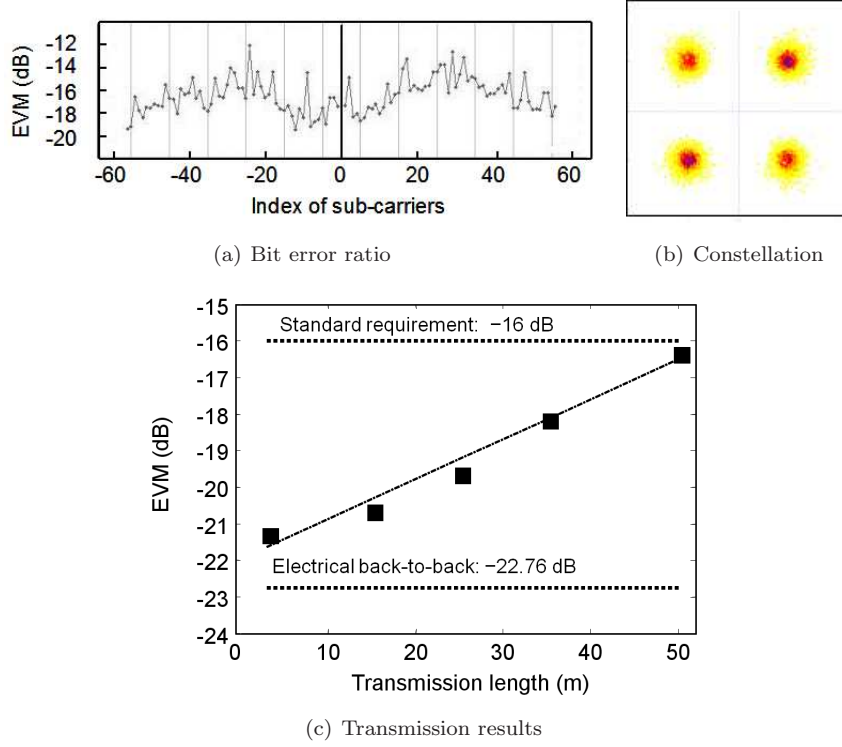


Figure 3.9: (a) EVM values as a function of the indices of sub-carriers for the MB-OFDM signal, after 50 m transmission, (b) Constellation diagram of the received MB-OFDM signal after 50-m transmission and (c) EVM values for different transmission lengths of 1 mm PMMA GI-POF.

In this experiment, the local oscillator (LO) employed for up-conversion is a state-of-the-art equipment (signal generator R&S SMR20) with a very small phase noise (-90 dB at 10 KHz). It has been observed in a recent study¹ that the system performance and the signal quality does not degrade when an off-the-shelf voltage controlled oscillator (VCO) (MITEQ 1548890/ETCO, model: 03400-04100-15P) with a large phase noise² is employed. This is due to the robustness of the MB-OFDM format with respect to the phase noise. In OFDM format, phase noise effects in an OFDM system can be separated into two categories: phase noise maintained within one subcarrier spacing (also known as common phase error), and phase noise that extends across subcarrier spacings. Phase noise within one subcarrier spacing can be eliminated by the use of pilot sub-carriers, while the phase noise extending across subcarrier spacings

¹Results are not published yet. For reference, contact Yan Shi for private communication.

² -66 dB at 10 KHz, -60 dB at 100 KHz and -100 dB at 1 MHz

leads to demodulation errors which cannot be corrected [100, 101]. In this experiment, the carrier spacing of the MB-OFDM signal is around 4 MHz (given by 528 MHz/128 carriers). Since the phase noise of the VCO is less than 1 MHz, the phase noise introduced by the LO maintains within the subcarrier spacing, thus hardly introduces any degradation of the signal quality. Therefore, the phase noise of the LO for such systems should remain in the order of KHz to prevent system degradation.

3.4 Bi-directional Transmission of WiMedia-compliance UWB over PF POF

Recently, several scenarios have been presented for UWB-over-fibre transmission including a bi-directional transmission system over the single-mode fibre [86]. However, for short-range in-building infrastructures, plastic optical fibres are more attractive than silica single/multi-mode fibres due to the reason discussed in Section 3.1. Hence, further developments in this direction have led to the demonstration of UWB signals transmission over 62 μm core diameter perfluorinated (PF) GI-POF [91]. Moreover, an in-building/home network architecture using directly modulated lasers and direct detection transmission system over a single fibre is an attractive solution for easy implementation. In such cases, the in-home installer does not require knowledge of uplink/downlink fibre as in the case of dual fibre installations. Therefore, full duplex and bi-directional transmission of UWB signals using PF GI-POF is our focus in this section.

3.4.1 Experimental setup

The experimental setup is shown in Figure 3.10 [77]. In this experiment, due to the relatively large bandwidth of the PF GI-POF (>10 GHz for 100 m), no down- and up-conversion is needed as in previous section. The UWB signal generated at the residential gateway (RG) used an off-the-shelf UWB transceiver (Wisair prototype). For the downlink, the UWB data was at the time-frequency code 5 (TFC 5), meaning that the transmitter only sends one sub-band data at the centre frequency of 3.432 GHz corresponding to band group 1, sub-band 1. After an electrical power amplifier, the signal was used to directly intensity-modulate a distributed feedback (DFB) laser (NTT NLK5B5EBKA) at 1302 nm wavelength with a bias current in the linear regime at 50 mA. This was chosen according to the peak-to-peak driving current in order to ensure full modulation of the DFB laser. The laser bandwidth (typically 10 GHz) was large enough for the transmission of UWB signals over 50 μm core diameter PF GI-POF.

The transmitted signal was launched via a multimode optical circulator (OC1) into the POF with an optical power of -2 dBm. After transmitting the signal over 50 μm POF of 100 m, a 21 μm diameter

3. ULTRA-WIDEBAND WIRELESS SERVICE OVER POF SYSTEMS

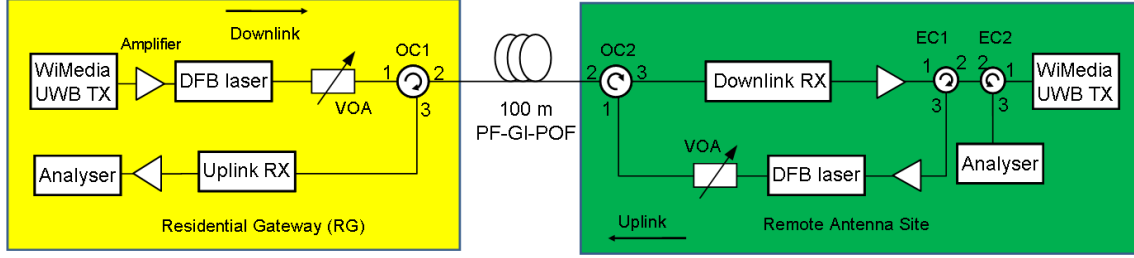


Figure 3.10: Concept and experimental diagram (Downlink: MB-OFDM UWB TFC 5, Uplink: TFC 7).

active area multimode-pigtailed photo-detector (NewFocus 1434-50) working at 1310 nm window with a sensitivity of 0.8 A/W was used to directly detect the signal. The received signal was electrically amplified before being sent via two electrical circulators to a real-time oscilloscope running at a sampling rate of 25 GSamples/s for accurate WiMedia compliance evaluation. Because of the low power density and wide bandwidth of the UWB signal (-41 dBm/MHz and 528 MHz), the gain of the electrical amplifiers had to be optimised in such a way that the signals were sufficiently amplified whilst the amplifiers were not saturated thus distorting the UWB signals. By optimising the gains of the amplifiers, the signal-to-noise ratio (SNR) of the signal was maximised, whilst the absolute signal power maintained as high as possible.

For bidirectional transmission, the electrical circulator (EC1) enabled the simultaneous transmission of the uplink UWB signal at TFC 7 generated by the UWB transceiver with a center frequency of 4.488 GHz chosen to minimise interference at the receiver. Injected at port 1 of the second electrical circulator (EC2), the uplink signal propagated through port 2 to electrical circulator 1 (EC1). At port 3 of EC1, the signal was electrically amplified and used to modulate the uplink DFB laser (a same model as downlink) running at the same wavelength of 1302 nm. Note that a fixed transmission rate of 200 Mbit/s was used for both directions. After transmission over the same 100 m POF link, the signal was received at the RG for evaluation.

3.4.2 Experimental results

The compliance of the received signals for both directions with the FCC spectral mask was measured. Figure 3.11 shows the power spectral density and spectrograms obtained using the real-time oscilloscope. Note in Figure 3.11(a), that the crosstalk in the downlink appears to be more severe due to the interference between uplink and downlink signals at the electrical circulator (EC2), namely because of the signal leakage from port 1 to 3 at EC2. However, EC2 is not compulsory for this setup; it is only used for monitoring purposes. In real implementation of the system, EC2 can be removed. From spectrogram measurements shown in Figure 3.11(b), the variation of the spectral density can be observed with time.

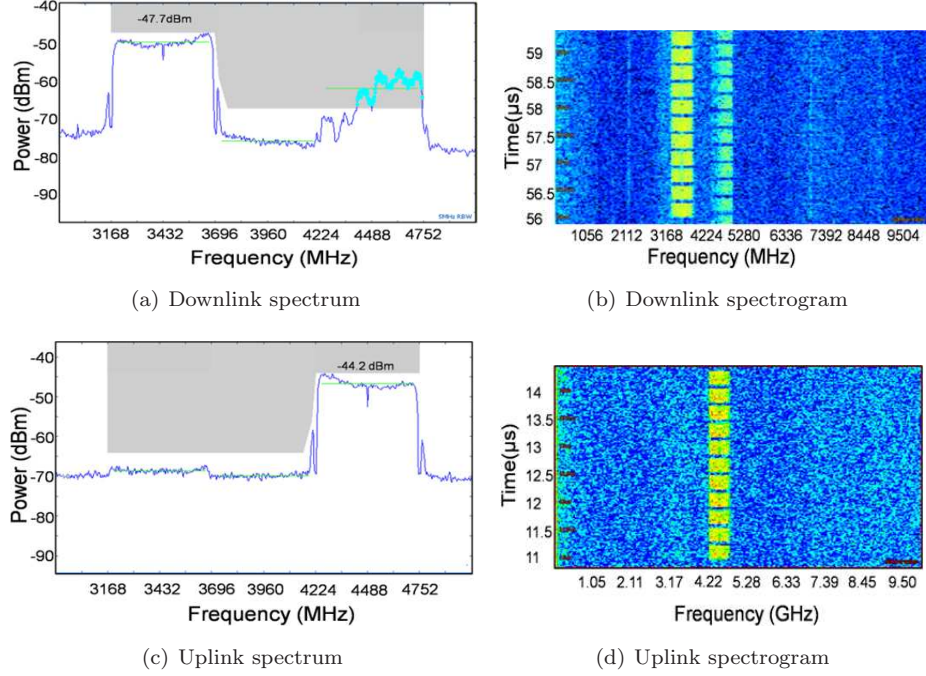


Figure 3.11: (a) Downlink power spectral density, (b) Downlink measurements spectrogram, (c) Uplink power spectral density, and (d) Uplink measurements spectrogram.

In Figure 3.11(a) and 3.11(b), the coexistence of the two bands centered at 3.432 and 4.488 GHz at the same time indicates crosstalk. Despite the detected crosstalk, the downlink signal passes the FCC spectral mask requirements for air transmission with a power density of -47.7 dBm/MHz. With both uplink and downlink signals transmitted simultaneously, Figure 3.12 shows the measured EVM values of the received UWB sub-band. In the best case, the EVM value for downlink back-to-back is 7.3% (-22.7 dB) for a received optical power of -3 dBm. After 100 m POF transmission, the penalty is negligible indicating excellent performance. For the worst case (i.e. at a received optical power of -8 dBm), the EVM for the back-to-back case is 9.4% (-20.9 dB). After 100 m transmission with the same received optical power, the measured EVM is 10.4% (-19.7 dB), indicating a penalty of 1.2 dB. For the worst-case in the uplink direction, the minimum received optical power is -7 dBm with an EVM of 11.8% (-18.6 dB). Note that compared to the corresponding back-to-back EVM of 9.2% (-20.7 dB) this indicates the penalty of 2.1 dB. Compared with the downlink measurement, the penalty with 100 m transmission is higher for the uplink. Due to the losses at the electrical circulators (EC1 and EC2), the SNR of the input signal for uplink is significantly low (less than 20 dB). Due to the low power density of the UWB signal, after electrical amplification the SNR of the input signal to the DFB laser for the uplink is still lower than that of the downlink, leading to a lower modulation swing for the uplink laser.

3. ULTRA-WIDEBAND WIRELESS SERVICE OVER POF SYSTEMS

Note that the standard EVM requirement for WiMedia compliance is 15.5% (−16 dB), and all measurement results obtained are well below this requirement. All the other standard requirements listed in Appendix B are also satisfied for all the measurement points, except for the spectral mask hits in the downlink measurement. However, employing a circulator with a larger isolation between ports for EC2 can eliminate the cross-talk. The demodulated signals for downlink and uplink are shown in Figure 3.13. The constellation diagrams of Figure 3.13(b) and Figure 3.13(d) show clear separation between the points of the demodulated QPSK signals. Both figures indicate good performance for either direction during simultaneous transmission.

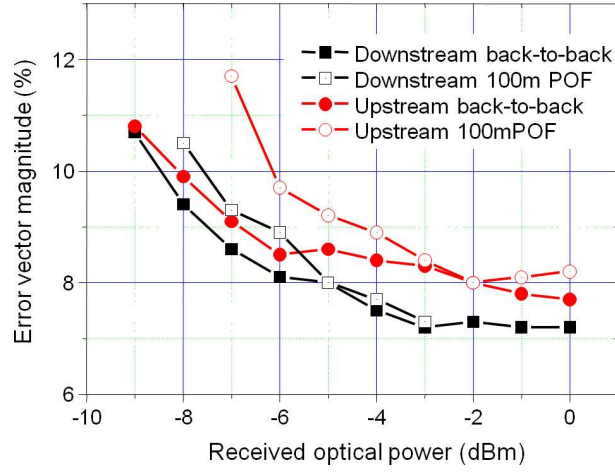


Figure 3.12: EVM performance measurement for upstream and downstream links after 100 m PF GI-POF transmission compared with back-to-back.

3.5 Summary

In this chapter, the emerging high-capacity short-range personal area network UWB standard with the format of MB-OFDM is discussed. The feasibility for delivering such signal formats over a POF infrastructure has been investigated by means of intensity modulation and direct detection. In Section 3.2 the spectral efficient DMT is employed with a uniform bit allocation using an AWG. This study is performed to find the maximum capacity of 528 MHz signal bandwidth. The feasibility of the UWB over 1 mm PMMA POF has been verified in Section 3.2. However, the signal format only complies with the WiMedia industry standard in the requirements of spectral width and sub-carrier numbers. All the other requirements such as modulation format, pilot sub-carrier, frame structure, relative power level, etc. are not considered in this section. An APD receiver is employed with a voltage supply of 130 V and more than

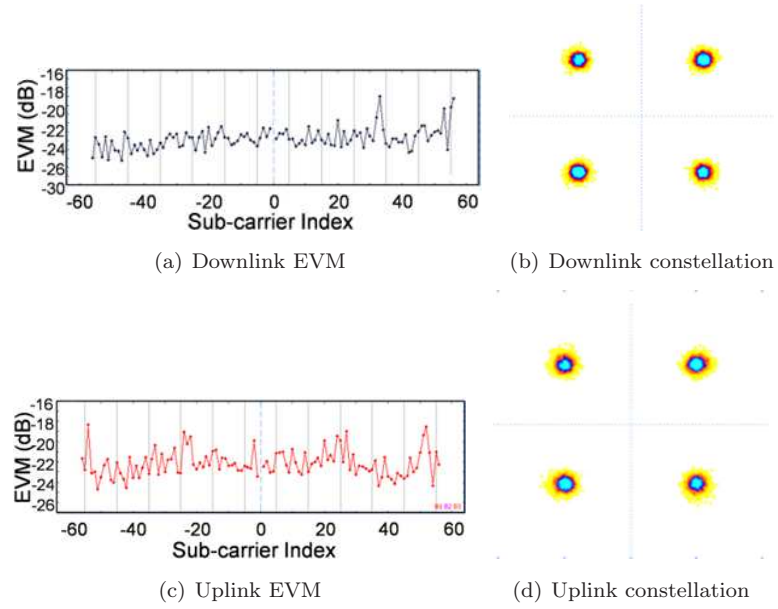


Figure 3.13: (a) EVM (dB) of demodulated MB-OFDM UWB sub-carriers for downlink transmission over 100 m POF, (b) constellation diagrams of demodulated MB-OFDM UWB sub-carriers for downlink transmission over 100 m POF, (c) EVM (dB) of demodulated MB-OFDM UWB sub-carriers for uplink transmission over 100 m POF, and (d) constellation diagrams of demodulated MB-OFDM UWB sub-carriers for uplink transmission over 100 m POF.

3. ULTRA-WIDEBAND WIRELESS SERVICE OVER POF SYSTEMS

2 Gbit/s data transmission over 50 m PMMA GI-POF has been achieved. Further study can be conducted by replacing the APD receiver with a PIN diode receiver. In Section 3.3 the WiMedia-compliant UWB over PMMA POF by employing low-cost transceivers is demonstrated. In this section, the UWB signals are fully compliant with the standard requirements, as shown in Appendix B. However, to accommodate UWB data of which the spectrum does not fit in the low-pass transmission characteristic of the POF link, an electrical spectral shift is utilised in the transmitter side. At the residential gateway, an up-conversion in software is also employed to analyse the data quality in this original frequency band. In such a configuration, the measured system penalty is still less than 7 dB for up to 50 m PMMA POF links. Finally, an experimental demonstration of UWB over 50 μm core diameter PF GI-POF is demonstrated. The proposed architecture realises the full-duplex bi-directional transmission of UWB signals over 100 m PF GI-POF. An overall system penalty of 1% and 1.8% has been measured for the downlink and the uplink respectively. The work presented in this chapter has indicated that a potential low-cost, large-scale UWB radio-over-fibre deployment for in-home personal area networks (PANs) employing either PMMA or PF POF is an attractive wireless access solution for future home networks.

Chapter 4

Optical Dynamic Routing in Radio-over-Fibre Links

In Chapter 2 and 3, the transmission of RF services over multimode silica or plastic fibres has been investigated by means of either intensity modulation/direct detection (IM/DD) or optical frequency multiplication. Next to the high capacity transmission of radio-over-fibre (RoF) systems, the flexible optical routing of the RoF signals should be developed as well for in-building networks, with which the network resources can be efficiently used. When users are moving around in buildings, the traffic loads on the remote antenna units may change. By dynamically routing one or more RoF signals from the residential gateway (RG) to an antenna unit, the capacity of the optical link connecting to this antenna unit can be adapted in order to meet these changes. This will enable flexible mobility management, dynamic capacity allocation, dynamic network dimensioning and efficient radio resource management. The routing of the traffic needs to be transparent for the signal format and its wavelength, in order to guarantee multi-standard operation [14]. Optical cross-connect switches have been developed for switching high-speed digital data streams in core and metropolitan networks. Handling analogue radio-over-fibre signals, however, puts additional requirements on the switch design, e.g. regarding the transparency and the linearity. Moreover, the switch needs to be able not only to provide point-to-point switching, but also should be capable of setting up point-to-multipoint connections, e.g. selective-casting between a small set of users. Furthermore, the switch needs to have control interfaces which allow steering of its settings by the RG. The RG is in charge of the wireless traffic routing, and its routing strategies can be executed via setting this optical routing switch. In this chapter, the routing of RF signals utilising wavelength conversion in a semiconductor optical amplifier (SOA) is discussed. Spatial routing is done with an arrayed waveguide

This chapter is based on the results published in [102] and [103].

4. OPTICAL DYNAMIC ROUTING IN RADIO-OVER-FIBRE LINKS

grading (AWG) whose passbands are aligned with the new wavelengths.

This chapter is organised as following. Section 4.1 introduces the principle of cross-gain wavelength conversion using an SOA including the basic theory of wavelength conversion and the system design for an in-building network using optical routing. Section 4.2 presents experimental studies on the system performance of an SOA-based RoF system with optical routing. The combination of electrical sub-carrier multiplexing (SCM) and SOA-based optical routing are proposed and experimentally verified for an in-building network. Finally, an inter-room cross-connect for ultra-wideband services employing an SMF infrastructure is proposed in Section 4.3.

4.1 Principle of Operation

4.1.1 Wavelength conversion techniques

The nonlinearity of SOAs can be used to create devices for all-optical signal processing such as wavelength converters [104]. An all-optical wavelength converter is a device that transfers information from one wavelength to another wavelength without entering the electrical domain. In particular, nonlinearities in SOAs applied to wavelength conversion are cross-gain modulation (XGM), cross-phase modulation (XPM) and four-wave mixing (FWM). Cross-gain modulation and cross-phase modulation rely on carrier density dynamics within the SOA, while FWM relies on carrier intra-band dynamics for the wavelength conversion range of interest for optical networks [105, 106].

The simplest technique for realisation of such functionality is the use of XGM in SOAs. In XGM, a signal at λ_1 (the pump) reduces the carrier density within the SOA by stimulated emission, thereby imposing a gain modulation on a second, independently tunable, CW input at λ_2 to the SOA (the probe), which becomes the wavelength converted output [107]. This technique requires only a single SOA and is effective only for intensity modulated formats. Because the target wavelength is input directly to the SOA, the signal-to-noise ratio (SNR) of the converted signal is excellent. However, the problem associated with XGM is the chirp generated by the phase modulation that necessarily accompanies gain modulation in an SOA, which limits the high bit rate transmission over dispersive optical links [108].

In the second technique, the phase modulation caused by the signal-induced carrier depletion by λ_1 in the SOA is used as advantage. Using this XPM to produce intensity modulation on the probe at λ_2 requires an interferometric configuration, in which one or two SOAs are placed inside a Mach-Zehnder interferometer. In such configuration, the chirp of the wavelength converted signal is controlled, so that transmission over dispersive fibre at high bit rate is possible [109]. However, same as XGM, XPM can only function for intensity-modulated formats [105].

Cross-gain and cross-phase modulation techniques operate only on intensity-modulated signals. In contrast, FWM technique using SOA allows a greater transparency because they can convert frequency and intensity-modulated signals. In FWM, the converted output wavelength is generated as a mixing product between the input signal wavelength and a CW pump wavelength. Because the interactions are based on optical fields, phase information is preserved and the coherent techniques can convert signals with phase and frequency modulation as well as intensity modulation. Thus, strict transparency is supported in FWM. However, the coherent interactions are based on nonlinear optical susceptibilities of various materials and the output wavelength is created by the mixing process. Therefore, the wavelength conversion efficiency is relatively low [105].

In comparison, FWM provides a more transparent wavelength conversion solution with respect to phase-modulated signal while XGM and XPM only deal with intensity modulated signal. In RoF systems with simplified remote antenna unit, the RF signal has to be intensity modulated in the RG and directly detected by the photo-receiver in the remote unit. Therefore, considering the low efficiency of the wavelength conversion, it is not necessary to employ FWM technique in RoF systems. Again, in RoF systems, the most effective solution is desired also in terms of complexity. XGM is preferred compared with XPM due to its simpler structure. Furthermore, wavelength conversion for RoF systems requires at least 7 GHz operation bandwidth (considering the most demanding application of RoF at 60 GHz band). This bandwidth can be utilised to have more than 40 Gbit/s data rates by using advanced modulation formats. Very complex wavelength conversion techniques such as XPM and FWM providing up to 640 Gbit/s data rate [109, 110] are not suitable for in-building networks. In the following sections, primarily due to its simplicity, the XGM is used for the optical routing in RoF links.

4.1.2 XGM effect on analogue RF signal in SOA

The simplest technique for realising wavelength conversion functionality is the use of XGM in SOAs. The principle of XGM is well known in digital optical communications employing non-return-to-zero (NRZ) coding formats [107].

Assume two fields, one of intensity P_1 with data modulation and the other of CW intensity P_2 , injected into an SOA. In a time frame of $t = t' - z/v_g$, where z is the wave propagation distant on the waveguide, v_g is the group velocity of the waveguide and t' is the next sample point in time, the equation describing the carrier density and photon density can be written as [111]

4. OPTICAL DYNAMIC ROUTING IN RADIO-OVER-FIBRE LINKS

$$\begin{aligned}\frac{dP_i}{dz} &= \Gamma a_i (N - N_i) P_i, \text{ for } i = 1, 2 \\ \frac{dN}{dt} &= -\frac{N}{\tau_s} - a_1 (N - N_1) \frac{P_1}{\hbar \omega_0 A_{eff}} - a_2 (N - N_2) \frac{P_2}{\hbar \omega_0 A_{eff}} + \frac{I}{eV}\end{aligned}\quad (4.1)$$

where $a_i = a(\omega_i)$ and $N_i = N(\omega_i)$ are the differential gain and the transparency carrier density at the frequency of the two fields, ω_i is angular frequency of the two fields, Γ is the waveguide confinement factor, A_{eff} is the effective area of the waveguide, $N(t)$ is the carrier density, \hbar is the normalised Planck constant, ω_0 is the optical angular frequency, I is the injected current, e is the electron charge, V is the active volume and τ_s is the spontaneous carrier lifetime. Equation 4.1 mathematically describes the carrier dynamics in the SOA.

Now assuming we have the input pump optical signal modulated by QAM signal with the form of

$$\begin{aligned}S(t) &= P(t)e^{i\omega_c t} + Q(t)e^{-i\omega_c t} \\ &= S_I(t) \cos(\omega_c t) + S_Q(t) \sin(\omega_c t)\end{aligned}\quad (4.2)$$

where ω_c is the carrier frequency of the QAM signal. By using the perturbation approach, the output signal of XGM takes the form of [111]

$$S_{CW}(z, t) = \Gamma \xi M_1(t) z e^{[\Gamma \xi (M_0 - N_t) - \alpha_{int}]z} \quad (4.3)$$

where M_0 is a constant, ξ is the differential gain, N_t is the transparency carrier density, α_{int} is the internal loss of the SOA and M_1 can be written as [111]

$$M_1(t) = \frac{\Gamma v_g \xi (M_0 - N_t)}{\sqrt{\omega^2 + K^2}} [S_I(t) \cos(\omega_0 t + \phi) + S_Q(t) \sin(\omega_0 t + \phi)] \quad (4.4)$$

where K is a constant and the phase shift ϕ in the wavelength converted QAM signal can be expressed by [111]

$$\tan(\phi) = \frac{-\omega_c}{\frac{1}{\tau_s} + \Gamma v_g \xi S_{CW}^0} \quad (4.5)$$

where S_{CW}^0 is the steady state solution of S_{CW} .

Due to the gain saturation of the SOA, the principle of XGM is shown in Figure 4.1(a) for the case of gain modulation by an RF signal. A CW signal at the desired output wavelength is modulated by the gain variation, so after the SOA it carries the same information as the intensity modulated input signal. In the XGM for digital data or NRZ signal, there are polarity conversions due to the gain saturation [107]. Nevertheless, in the XGM for analogue RoF signals the waveform of the input signals are preserved after

wavelength conversion, but imposed with a phase delay presented in Equation 4.5. Details of the analysis and derivation can be found in Appendix A and [111].

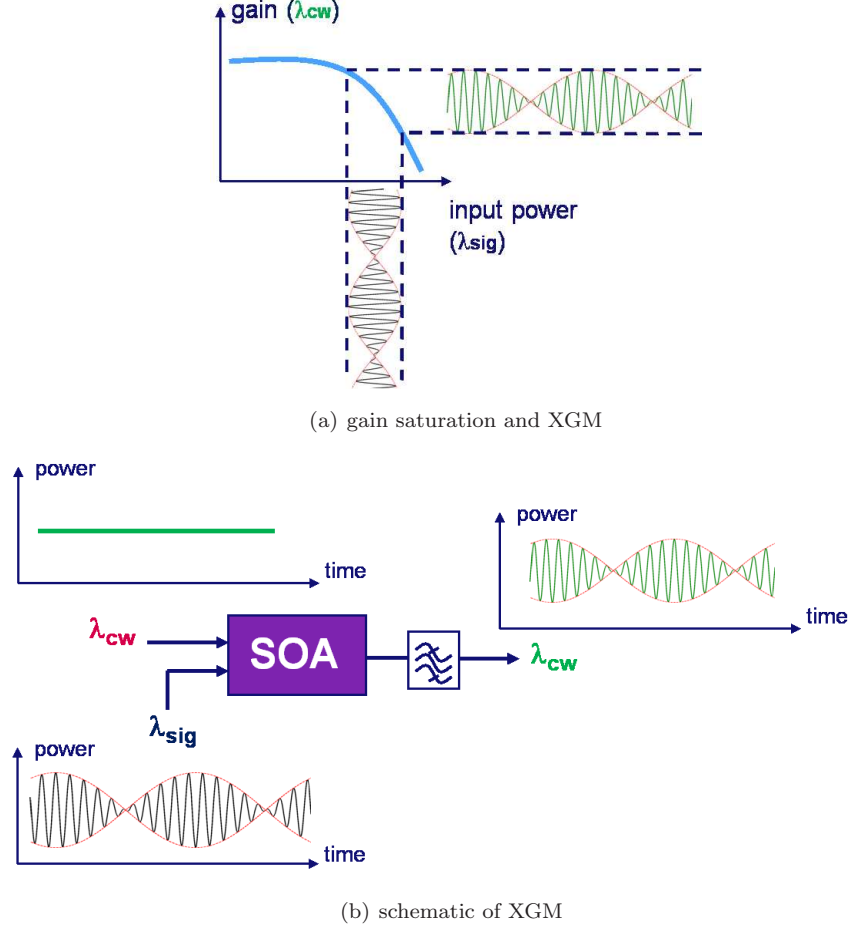


Figure 4.1: (a) Principle of gain saturation and XGM and (b) schematic of XGM wavelength conversion principle. The phase delay expressed by Equation 4.5 cannot be illustrated.

4.1.3 Optical routing using SOA

System design: Wavelength conversion based optical routing has been investigated extensively for long-haul optical communication systems [107, 112]. The all-optical routing architecture of radio signals using label processing technique to all-optically control the wavelength conversion has also been demonstrated [113]. The proposed architecture for the dynamic routing for in-building RoF systems is illustrated in Figure 4.2. In the inset schematic diagram, the building may be a residential area, an office building, an airport lounge, a shopping mall, a university building, etc. The residential gateway (RG)

4. OPTICAL DYNAMIC ROUTING IN RADIO-OVER-FIBRE LINKS

connects the in-building network to the outside access network, delivering one or more RF signals at different RF carriers with a certain optical wavelength (λ_1) over optical fibre, e.g. multi-mode fibre and routed to another wavelength (λ_2 to λ_5) by the routing device (denoted as "R" in Figure 4.2 inset), followed by another length of fibre transmission to different antenna side (AS), where the RF signals are radiated. Creating the possibility of inter-room wireless communications by means of the routing in "R", this architecture brings more flexibility in operating, maintaining and reconfiguring the network. The network configuration can also be adaptive to the desired network coverage area, by choosing the physical location of such routers in the networks. The realisation of the proposed routing system is presented in Figure 4.2. In this chapter, the optical frequency multiplication (OFM) method discussed in Chapter 2 is employed to generate a microwave carrier and to transport the wireless services over fibre links. The OFM transmitter is located at the RG while an SOA-based router is allocated within (or very close to) the building, as shown in Figure 4.2. XGM in an SOA is utilised to achieve the wavelength conversion at the router so that services can be transferred to other wavelengths. After the arrayed waveguide grating (AWG), the data carried by the desired wavelength is transported via the second span of the fibre to its desired destinations and radiated through an antenna. In the case of in-building network with larger geographic size such as airport buildings or industry campus, more than one router can be connected to the RG to further enhance the flexibility of the whole network.

Dynamic allocation: In the electrical domain, the data can be multiplexed by using the sub-carrier multiplexing (SCM) technique. As shown in the transmitter side of Figure 4.2, the RF signal imposed on the OFM transmitter in RG takes the format of SCM over a number of RF carriers. Each carrier presents a wireless service with a different central frequency. Different services at different radio frequencies should be chosen by different end users either according to the specific service demand or the central management at the RG. In the AS, a tunable electrical band-pass filter (BPF) can be used to select the desired signal in the SCM domain. Moreover, RF carriers with more than one service are grouped on an arbitrary wavelength in the optical domain, which can be assigned to a number of different end users. The identification of the end users in wavelength should be matched with the physical address of each user in a certain time period. In such configuration, by combining the technologies of electrical SCM and optical wavelength conversion, the dynamics of capacity allocation can be largely improved, therefore leading to an easier network control, monitoring and management.

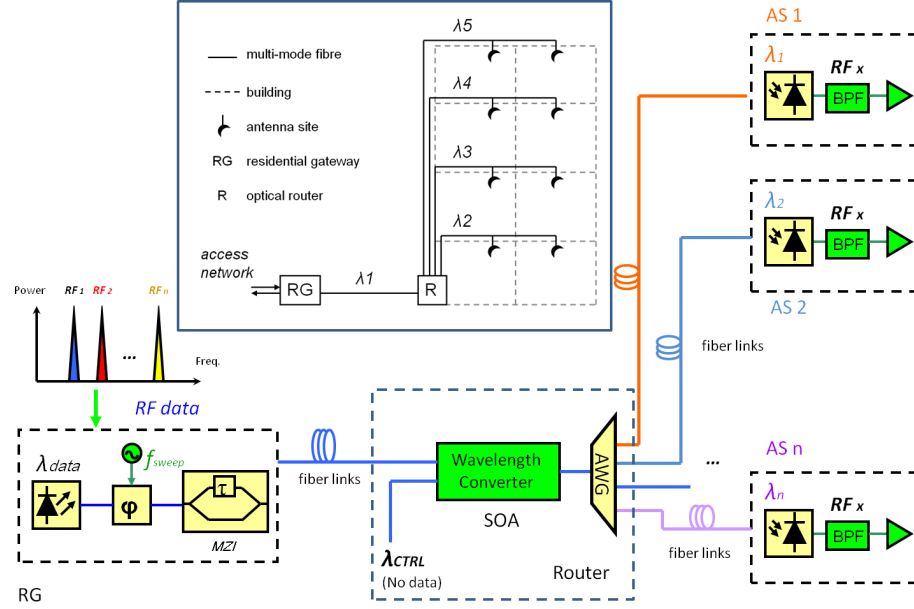


Figure 4.2: Optical routing in RoF systems for broadband in-building networks by employing SOA-based wavelength conversion and electrical sub-carrier multiplexing. MZI: Mach-Zehnder interferometer, SOA: semiconductor optical amplifier, AWG: arrayed waveguide grating, BPF: tunable band-pass filter.

4.2 Experimental Study

To realise the optical routing using SOA as proposed in Section 4.1, two experiments are presented in this section: the first one includes only optical routing [102] and the second one investigates the combination of both optical routing and electrical SCM scheme [103].

4.2.1 One-level dynamics with optical routing

Experimental setup: As shown in Figure 4.3, following the OFM method [102], a CW pump signal (with 8 dBm output power) at 1552 nm wavelength was phase modulated (PM) by an electrical sweep signal at 9 GHz. A WiFi-format OFDM signal with a carrier frequency of 300 MHz was then put onto the optical carrier by a Mach-Zehnder modulator (MZM). The electrical input of MZM was labeled "A". The OFDM signal had a 16-quadrature amplitude modulation (16-QAM) with a data rate of 36 Mbit/s and 52 frequency sub-carriers. After amplification in the optical amplifier¹, a Mach-Zehnder interferometer (MZI) with a free spectral range (FSR) of 40 GHz converted the phase modulated signal into the intensity modulated (IM). The PM-IM conversion by the MZI generated several harmonics in

¹In this experiment, an erbium-doped fibre amplifier (EDFA) with a gain of 20 dB was used for amplification. The output power of this EDFA in the setup was 5 dBm.

4. OPTICAL DYNAMIC ROUTING IN RADIO-OVER-FIBRE LINKS

the frequency domain, each of which was separated from the adjacent harmonic by the sweep frequency 9 GHz [28]. By using this effect, each harmonic frequency was a multiple of 9 GHz. The output of the OFM transmitter was labeled "B", and after 750 m MMF transmission "C". After optical amplification using the EDFA, an optical Gaussian band-pass filter with a bandwidth of 2 nm was employed to remove the amplified spontaneous emission (ASE) noise of the EDFA. After that, wavelength conversion employing an SOA was performed. The SOA was a Kamelian nonlinear SOA at 1550 nm band, biased at nonlinear region using 250 mA injection current. Another CW light (acting as probe) at 1535 nm was injected into the SOA. From the XGM effect in the SOA, the OFDM data at 1552 nm was copied to the target wavelength of 1535 nm, which was aligned to one of the pass-bands of the filter. The converted signal, labeled "D", was sent to the second MMF span of 200 m before being received. At the receiver side, a photo-detector with 25 GHz bandwidth (model: NewFocus 1434-50) was used, followed by an electrical band-pass filter at 18.3 GHz for detecting the 2nd harmonic frequency of 18 GHz plus the RF sub-carrier 300 MHz, labeled "E". The 750 m and 200 m MMF fibres used in this experiment were step-index silica 50 μm core diameter from Draka, labeled with 31.0007...220_2 and 31.0007...200 respectively in the laboratory.

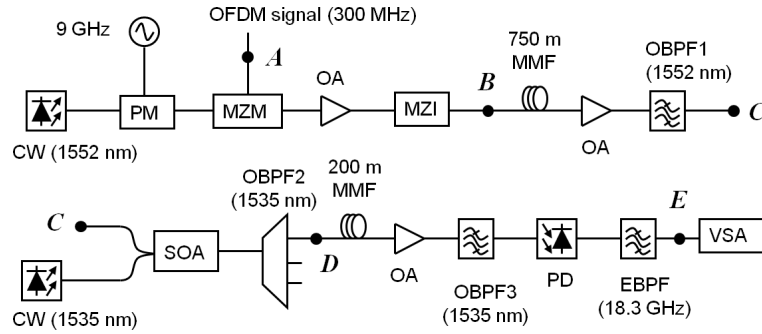


Figure 4.3: Experimental setup for one-level dynamics with optical routing; OBPF: optical band-pass filter; PD: photo-detector; EBPF: electrical band-pass filter; OA: optical amplifier.

Measurement results: First, the spectrum of the signal generated by the OFM transmitter is presented in Figure 4.4. Five harmonics are displayed in the plot, where the power of the second harmonic at 18 GHz is optimised by adjusting the alignment between the MZI and the laser wavelength [27]. The OFDM signal is carried by each of the harmonics on double side-bands. The inset plot shows the spectrum of OFDM signal centered at 18.3 GHz corresponding to the right-hand side-band. Second, the effect of parameters is investigated in the wavelength conversion in order to find an optimum system performance. The results in the averaged error vector magnitude (EVM) are taken at point "E". In Figure 4.5(a),

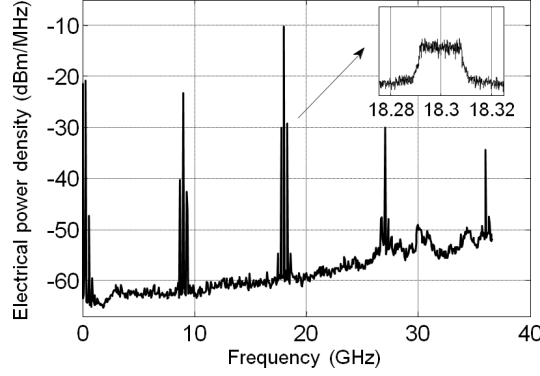


Figure 4.4: Spectrum of 16-QAM OFDM signal at point "B". Measurement point "B" is labeled in Figure 4.3.

EVM values are plotted versus the probe power, for three different pump powers. For each pump power, an optimum probe power can be found at the minimum EVM values. Results on the left hand side of the optimum value are worse when the power of the probe signal decreases. This is because the low optical signal-to-noise ratio (SNR) at the output of the SOA. The results on the right hand side of the optimum value are also worse with the increasing of the probe signal. This is because of the deep gain saturation of the SOA. When the input power to the SOA is too high that the SOA gain has been largely depleted hence hardly provides the XGM output. Moreover, it is also observed that to keep EVM low for larger pump powers, larger probe powers are needed. For instance, for 6 dBm pump power, 0 dBm probe power is necessary while for 3 dBm pump power, only -3 dBm probe power is needed to optimise the EVM value. When the pump power is larger, the gain of the SOA becomes smaller due to gain saturation, therefore to keep the same quality of the converted signal, the probe power has to be increased. This is the reason that the optimum probe power shifts to the larger value for larger pump powers. It is observed that the system can handle 8 dB probe power fluctuations within an EVM increase of less than 1%. Similarly, in Figure 4.5(b), EVM values are shown versus pump powers for different probe powers. It is observed again that to keep EVM low for larger probe powers, larger pump powers are needed. As an example, for 3 dBm probe power, 9 dBm pump power is necessary while for -3 dBm probe power, only 5 dBm pump power is needed for the same EVM.

The EVM value is presented at different measurement points ("A", "B", "C", "D" and "E"), as shown in Figure 4.5(c). The pump power and probe power are set to 6 and 0 dBm, respectively, according to Figure 4.5(a) and 4.5(b). It is seen that even though a 52 sub-carrier OFDM signal is transmitted over 950 m MMF and is converted to another wavelength in the link, the measured EVM value is only around 3%, with the total system penalty less than 3%. For comparison, in IEEE 802.11a standard,

4. OPTICAL DYNAMIC ROUTING IN RADIO-OVER-FIBRE LINKS

the required EVM is 11.2% for 16 QAM. This good system performance is partially due to the strong in-line amplifications in EDFAs to compensate the coupling loss from larger core multimode to smaller core single-mode fibre, so that the SNR of the received signal keeps relatively large. It is also seen from "B–C" and "D–E" in Figure 4.5(c) that the MMF gives negligible EVM penalty in the system, due to the robustness of the OFM technique to the modal dispersion [55]. The frequency up-conversion of the signal from 300 MHz to 18.3 GHz (point "A" to point "B") gives an EVM penalty of almost 2% and the wavelength conversion (point "C" to point "D") leads to a 1% EVM penalty. Figure 4.5(d) shows the constellation diagram of the demodulated 16 QAM signal at point "E". With 3% EVM value, the constellation points are very well separated. The two points on the horizontal line present the pilot tones of the WiFi-format OFDM signal. In Figure 4.6, the EVM versus the index of sub-carrier of the OFDM signals is shown, at three measurement points "A", "B" and "E", by using the same parameters as Figure 4.5(c) and 4.5(d). The number of carrier corresponding to the central frequency of signal is denoted as 0, and on both sides there are 26 carriers where the OFDM data is modulated.

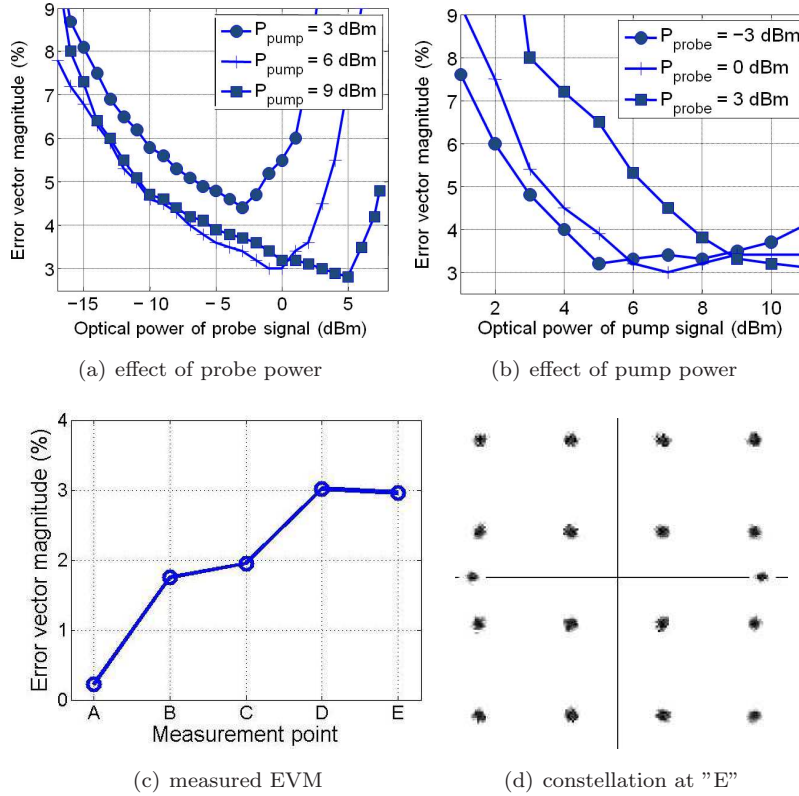


Figure 4.5: (a) EVM vs. probe power for different pump powers, (b) EVM vs. pump power for different probe powers, (c) EVM at different measurement points and (d) Constellation diagram at point "E". All the measurement points are labeled in Figure 4.3.

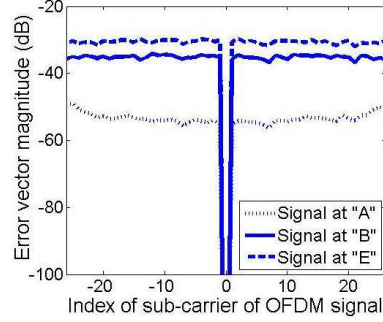


Figure 4.6: EVM vs. index of sub-carrier of OFDM signals. All the cited measurement points are labeled in Figure 4.3.

4.2.2 Two-level dynamics with optical routing and electrical SCM

In [63] the SCM scheme has been utilised to enable a high capacity RoF transmission link. This experiment demonstrates the full concept employing both SCM and optical routing by XGM in an SOA, which has been proposed in Section 4.1. Similarly with Figure 4.3, the experimental setup is illustrated in Figure 4.7. The major difference compared with Figure 4.3 is the RF signal imposed on the MZM. Instead of the OFDM signal, subcarrier-multiplexed RF carriers without orthogonality were employed so that each RF carrier can be (de-)modulated independently, relying only on the central frequency of the SCM signal. The central frequency of the SCM was 700 MHz, with more than 16 sub-carriers. Each of the sub-carriers was modulated by up to 3 MSym/s 16-QAM data. The sweep signal of the OFM scheme had a frequency of 4.8 GHz. After modulating the SCM signal onto the optical carrier by using the OFM scheme, the signal was labeled as "A" after amplification; while after the wavelength conversion by an SOA, the signal was labeled as "B" before feeding into the PD. For simplicity, there was no fibre transmission included in this experiment since the standard single mode fibre (SSMF) deployed for access and in-building networks did not add any significant dispersive penalties on the system but only attenuation. Another reason for not using MMF in this experiment was the mode compatible issue. In the Section 4.2.1, single-mode to multi-mode coupling occurred at the beginning of the MMF transmission. Without extra mode scrambling, only a few modes that propagated in the MMF were excited. Additionally, multi-mode to single-mode coupling also existed at the input of the wavelength converter. This introduced considerably large loss of the signal and the mode filtering effect which introduced instability of the system. Therefore, MMF was not used for this experiment and all the optical components in this experiment were in single-mode operation [103].

4. OPTICAL DYNAMIC ROUTING IN RADIO-OVER-FIBRE LINKS

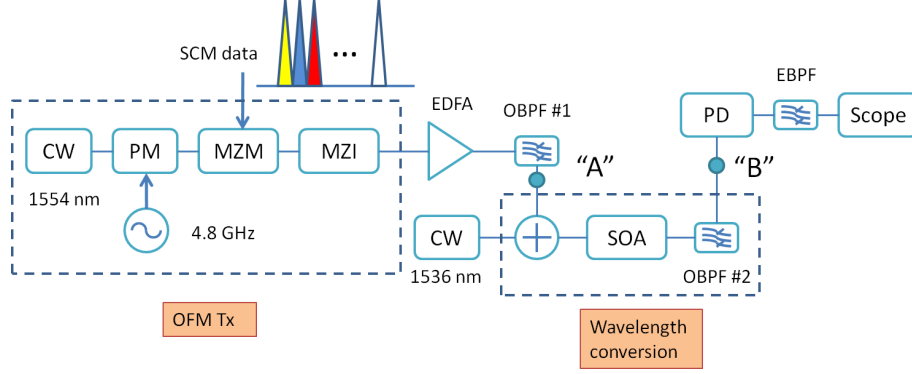


Figure 4.7: Experimental setup for two-level dynamics based on both SOA wavelength conversion and electrical SCM.

Figure 4.8(a) illustrates the signal measured in the optical spectrum analyser at point "A". Before the wavelength conversion, data is carried on the wavelength of 1554 nm. The two insets present the two spectra in more details. The left one is the CW signal (probe) and the right one is the modulated signal with a much wider spectral width (pump). In Figure 4.8(b), the spectra of the pump and probe signals are illustrated after the wavelength conversion and the filtering. The OFM data is copied from 1554 nm to 1536 nm and delivered to the desirable end user assigned by wavelength 1536 nm. Note that the harmonics in the optical spectrum shown in the zoomed inset of Figure 4.8(a) and 4.8(b) are not the SCM data. Instead, the harmonics appear due to the OFM technique employed to up-convert the low-frequency SCM to higher RF carriers. The 4.8 GHz separation of the harmonics is given by the sweep frequency used in the OFM transmitter. In the OFM approach, the 4th harmonic is optimised and the left side band of the signal carried by 4th harmonic is measured, corresponding to a central data frequency of 18.5 GHz. Nevertheless, due to the SCM method on the top of OFM 4th harmonic, each carrier has a different frequency varying from 18.47 to 18.53 GHz.

Figure 4.8(c) and 4.8(d) present the measured EVM values of the received signal after wavelength conversion in dB. The EVM values are averaged over the all sub-carriers. Different SCM formats are investigated for different symbol rates from 1 to 3 MSym/s over 16 sub-carriers, as shown in Figure 4.8(c) (corresponding to 64 to 192 Mbit/s total data rate). As a reference, the EVM values in optical back-to-back without wavelength conversion are also shown in Figure 4.8(c). In Figure 4.8(c), less than 2 dB penalty after XGM wavelength conversion is observed which is attributed to the SNR degradation of the investigated formats after wavelength conversion. For the data rate of 192 Mbit/s over 16 sub-carriers, EVM value of -24.7 dB (5.8%) is obtained at a received optical power of -3 dBm. The EVM value for

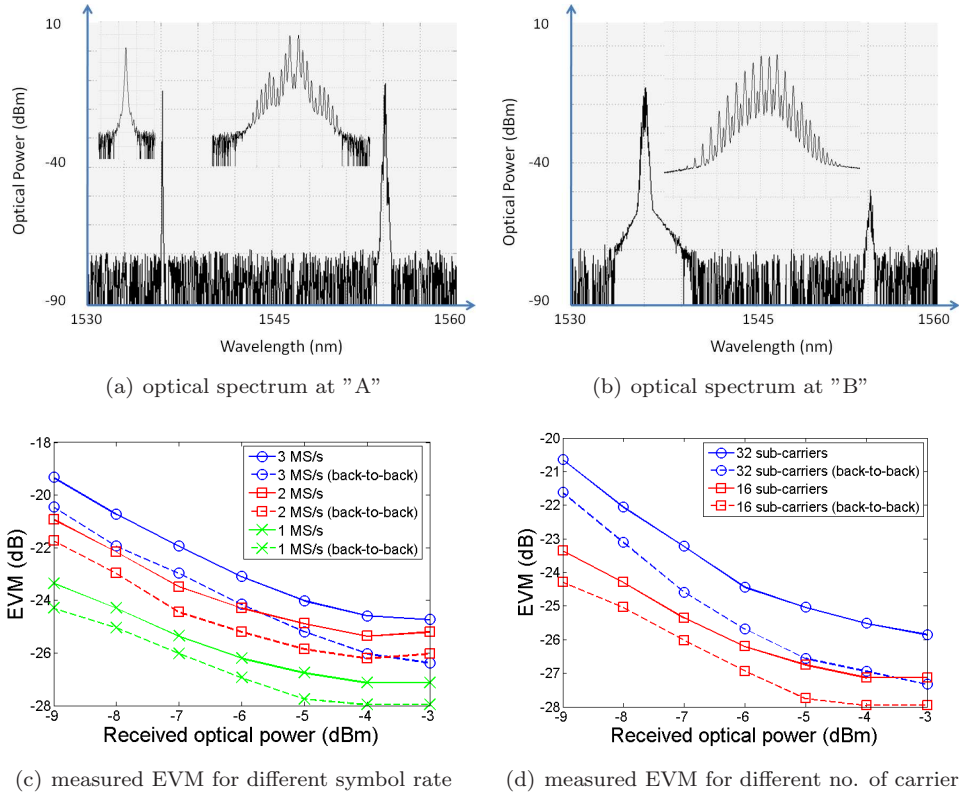


Figure 4.8: (a) spectrum of the signal at point "A" of Figure 4.7 with data modulated at 1554 nm, (b) optical spectrum of the signal at point "B" of Figure 4.7 with data modulation on 1536 nm, (c) EVM as a function of received optical power, with the symbol rate per carrier, for a fixed number of carriers and (d) EVM as a function of received optical power, with the number of carriers containing the same symbol rate per carrier. Back to back is the measurement without wavelength conversion.

4. OPTICAL DYNAMIC ROUTING IN RADIO-OVER-FIBRE LINKS

3 MSym/s SCM data in the electrical back-to-back case is measured to be -43 dB.¹ Therefore most of the EVM penalties in the system come from the OFM up-conversion of the SCM signal from 700 MHz to 18.5 GHz, which is in line with the results shown in Figure 4.5(c). The XGM in the SOA only adds an approximately 2 dB penalties as measured in Figure 4.8(c). In this experiment, the electrical driving signal remains below -2 dBm, resulting in a negligible nonlinearity penalty as discussed in Section 2.3. This investigation shows that the proposed architecture for routing the RF signals is very transparent for RF data formats. Moreover, the system performance are evaluated for different numbers of sub-carriers. A comparison is presented in Figure 4.8(d) between 32 and 16 sub-carriers for 1 MSym/s symbol rate per carrier. An approximately 2 dB penalty is achieved independent of the received optical power, meaning that the photo-receiver still operates in the linear region. It is also observed in Figure 4.8(d) that the measured wavelength conversion penalty is transparent for the number of carriers. Due to the relatively small bandwidth in RF domain compared with the wavelength conversion bandwidth in optical domain, increasing the number of carriers and the bandwidth of the signal do not lead to an extra penalty for wavelength conversion.

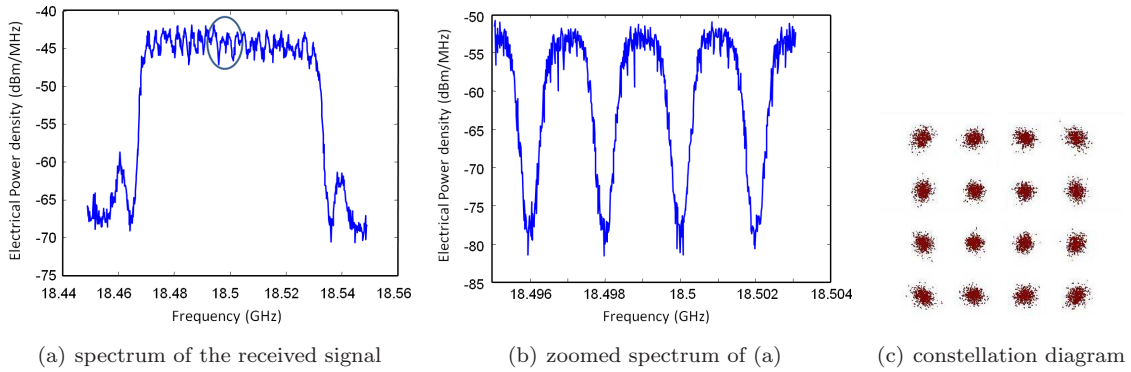


Figure 4.9: (a) The electrical spectrum of the received signal after wavelength conversion with a received optical power of -7 dBm, (b) the zoomed spectrum in the area highlighted by the circle in (a), and (c) the constellation diagram of the signal.

Finally, an example of the received electrical signal is shown after wavelength conversion at 18.5 GHz in Figure 4.9 (both electrical spectrum and constellation diagram). The signal takes the format of 16 sub-carriers centered at 18.5 GHz with 1 MSym/s on each carrier. The received optical power is -7 dBm. Figure 4.9(b) show the zoomed spectrum in the circled area which contains three full sub-carriers. The SNR of the received signal is approximately 30 dB. The clearly separated constellation points in Figure 4.9(c) show the good quality of the demodulated signals with an EVM value of -24 dB.

¹This is not shown in the figures.

4.3 Inter-room Communication via Optical Cross-connect

As illustrated in Figure 1.2, the optical backbone infrastructure should provide the functionality of intra- and inter-room connectivity. An example of such an optical backbone is shown in Figure 4.10(a) [14]. It illustrates two devices interacting within a room, or between two rooms, or multiple devices interacting across multiple rooms. The home gateway or home communication controller (HCC) contains the hardware and software facilities that establish the transparent RoF connections by low-cost optical cross-connects, taking care of the control protocols, and providing the gateway to the access network [14].

Based on such a network infrastructure, the experimental system illustrated in Figure 4.10(b) is proposed targeting at the inter-room communication of UWB services via a single-mode fibre (SMF) backbone¹. Four rooms are highlighted in the figure including a ultra-wideband transceiver, an electrical circulator, a CW laser and a photo-detector. Each room can be assigned two wavelengths for down-link and up-link respectively. In the first consideration of such systems, the dual-fibre scenario for up- and down-link is presented. Future work can be considered by using one fibre for a duplex system. In the present proposal shown in Figure 4.10(b), a wavelength pair for each room is fixed. For instance, λ_1 is assigned to room no. 1 for uplink and λ_2 for downlink. Suppose the radio antenna unit (RAU) in the room no. 1 (illustrated by the mobile unit of UWB devices) wants to communicate with another counterpart in room no. 2. The uplink data is modulated by the CW source at λ_1 and transported from room no. 1 to the AWG located in the HCC. The signal is guided to the XGM-based wavelength converter which is input by the pump signal at the desired wavelength (in this case λ_4). However, for the uplink of room no. 2, another SOA in the HCC is used to switch data in the reverse direction. In this proposal, UWB signals can also be replaced by other narrow-band RF signals and the optical infrastructure should be transparent for the signal format. Moreover, even impulse-radio UWB signal, which occupies the whole bandwidth from 3 GHz to 10 GHz, can be successfully wavelength converted due to the fast response time of XGM technique [114].

Although the proposed physical realisation of such inter-room cross-connect is rather simple, a higher level control on the protocol layer is required to prevent contention. In principle, it is an inter-room communication model which only allows two rooms interacting at a time. To extent the flexibility to multiple room interaction, time division multiplexing should be implemented in the proposed architecture. Otherwise the complexity of the physical implementation has to be increased, for example duplicating several SOA wavelength conversion modules in the home gateway. Another option is to employ optical add/drop multiplexing in the antenna side with a ring network configuration, which has been shown in [115].

¹SMF is chosen because of the single-mode operation of wavelength conversion devices, namely SOAs.

4. OPTICAL DYNAMIC ROUTING IN RADIO-OVER-FIBRE LINKS

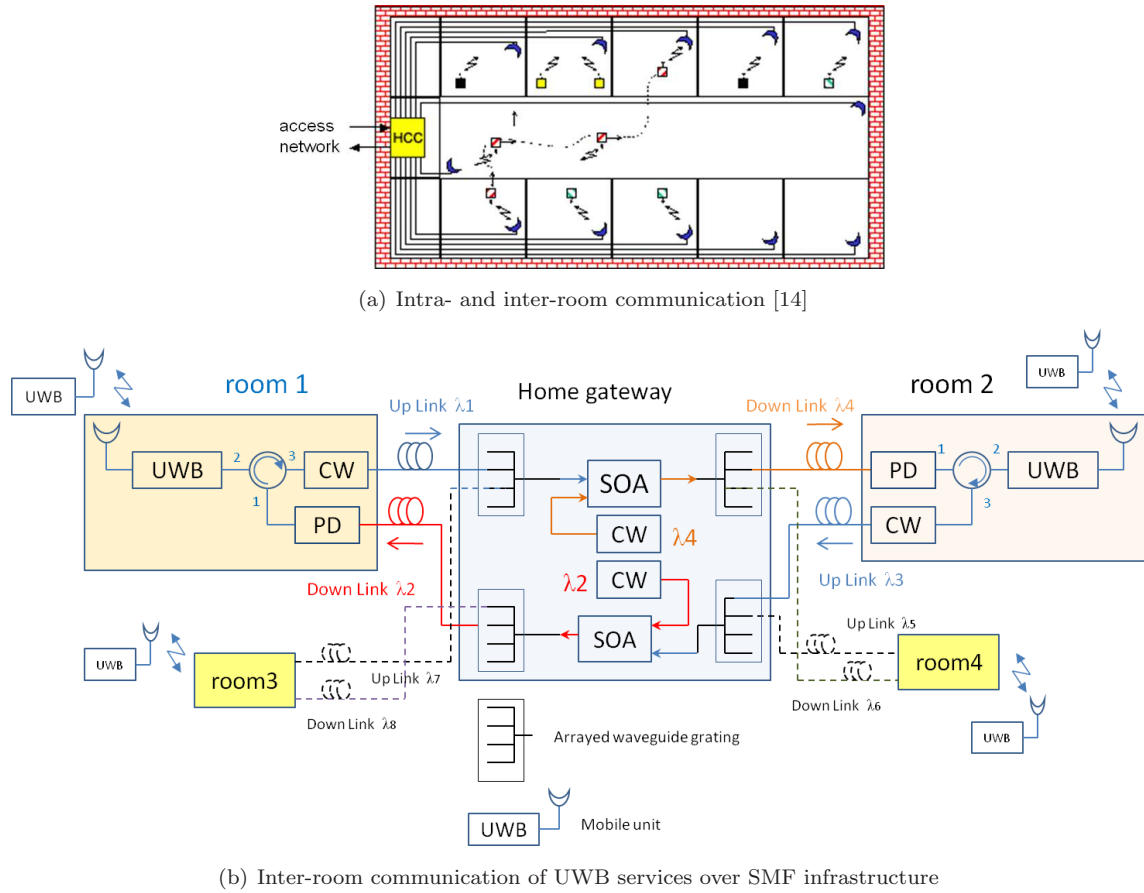


Figure 4.10: (a) In-room and inter-room transparent wireless communication using a transparently routed in-building optical network (b) Proposed inter-room communication of UWB services over SMF employing optical cross-connect. CW: continuous wave, PD: photo-detector, SOA: semiconductor optical amplifier.

4.4 Summary

In this chapter, the feasibility of optical switching techniques has been discussed for in-building networks. The simplest SOA-based wavelength conversion technique XGM has been briefly discussed, particularly for the analogue modulation format. Before the two-level dynamic routing approach is discussed, the experimental results have been addressed for one-level method in Section 4.2.1. By employing OFM the transmission of 18.3 GHz 52 sub-carriers OFDM signal of 36 Mbit/s data rate over 950 m MMF link has been successfully demonstrated. A mid-span all-optical routing within C-band (from 1552 to 1535 nm) with EVM less than 3% has been shown. It is observed that the penalties induced by the MMF modal dispersion are negligibly small, thanks to the OFM technique. In Section 4.2.2, a novel architecture has also been shown with improved flexibility for dynamic capacity allocation in the RoF links by combining optical routing with electrical SCM. The measured performance of such optical routing systems has been proved to be format transparent. Up to 192 Mbit/s data at 18.5 GHz distributed over 16 independent sub-carriers has been routed with less than 2 dB EVM penalty. Finally, an SMF-based inter-room cross-connect architecture is proposed for UWB services in a point-to-multi-point and bi-directional manner. The experimental verification can be performed in future work. This chapter presents an integrated dynamic capacity allocation approach for broadband in-building networks, enabling more flexible and efficient network management as well as more efficient use of radio network capacity.

4. OPTICAL DYNAMIC ROUTING IN RADIO-OVER-FIBRE LINKS

Chapter 5

High Capacity Baseband Data Links over POF

The optical backbone network as shown in Figure 1.2 in Section 1.2 should support wireless radio service, as well as provide baseband services such as HDTV or Ethernet. As discussed in Chapter 1 and 3, POF (especially polymethylmethacrylate (PMMA) POF) with large core diameters has gained lots of popularity for Gbit/s short range in-building networks, due to the cheap 'do-it-yourself' installation, easy maintenance and small bending radius. This chapter will present the experimental results on baseband high capacity data links employing POF and the advanced modulation format discrete multi-tone (DMT) [92, 93, 96].

The features of POF cables have been introduced in Chapter 1 and are summarised in Table 5.1¹. The contributions of this chapter on a high capacity transmission link based on different types of POFs are also indicated in the table. After a brief introduction of the DMT format, Section 5.2 addresses the demonstration of multi-Gbit/s transmission over PMMA GI-POF, employing two different types of receivers and Section 5.3 presents a comparison between PMMA single-core SI-, GI- and multi-core SI-POF. Section 5.4 presents a very high data rate transmission over perfluorinated (PF) GI-POF link.

5.1 Bit-Loading in DMT

Derived from the more general orthogonal frequency division multiplexing (OFDM), DMT is a baseband version [70, 121] that is widely applied in large scale to digital subscriber twisted-pair copper lines (ADSL,

¹This chapter is based on the results published in [116], [117], [118] and [119].

¹This summary is based on the most common products on the market. Other products such as low-NA MC-POF are not included. The product prices are approximate values.

5. HIGH CAPACITY BASEBAND DATA LINKS OVER POF

Type of POF	PMMA POF			PF POF
	Graded-index	Step-index		
		Single-core	Multi-core	
Loss per 100 m at 650 nm	20 dB	15 dB	15 dB	< 10 dB
Bandwidth × distance	3 GHz×50 m	100 MHz×50 m	300 MHz×50 m	>10 GHz×100 m
Bending radius	25 mm	20 mm	2 mm	5 mm
Numerical aperture	0.2	0.5	0.6	0.2
Approximate Price	\$1.45	\$0.7	\$1.3	\$1.27
Demonstration	Section 5.2	Section 5.3		Section 5.4

Table 5.1: Summary of features of different POF types and their application in this chapter. The bending radius is measured with loss increment <0.5 dB and the prices are evaluated per metre of POF with jackets [120].

VDSL, etc.) and power-line communication systems. The basic principle of DMT has been discussed in Section 3.2. This section is dedicated for the bit-loading feature in the DMT format.

An important feature of DMT is the possibility to allocate the number of bits per subcarrier according to its corresponding signal-to-noise ratio (SNR), typically known as bit-loading. Bit-loading can be divided into two categories: rate-adaptive and margin-adaptive. Rate-adaptive algorithms maximise the bit rate for a fixed bit-error ratio (BER) and a given received power constraint, while margin-adaptive algorithms minimise the BER for a given bit rate. In this chapter, rate-adaptive bit-loading will be considered in order to maximise the transmission rate over the POF links [96, 119].

The rate-adaptive bit-loading algorithm is a reformulation of the Shannon capacity formula [95] and can be expressed as a problem of maximising the total achievable bandwidth-normalised bit-rate b , which is the summation of the normalised bit-rates per subcarrier used for DMT transmission:

$$\begin{aligned}
 \max_{E_n}(b) &= \max_{E_n} \left[\sum_{n=1}^{N-1} \log_2 \left(1 + \frac{SNR_n}{\Gamma} \right) \right] \\
 &= \max_{E_n} \left[\sum_{n=1}^{N-1} \log_2 \left(1 + \frac{E_n \times g_n}{\Gamma} \right) \right]
 \end{aligned} \tag{5.1}$$

where $SNR_n = E_n \times g_n$ is the SNR per subcarrier, g_n represents the subcarrier SNR when unit energy is applied, Γ is the difference (gap) between the SNR needed to achieve maximum (Shannon) capacity and the SNR to achieve this capacity at a given bit error probability, and E_n is the allocated energy per subcarrier, subject to an energy constraint, given by [50]:

$$\sum_{n=1}^{N-1} E_n = E_{tot} \quad (5.2)$$

where E_{tot} is the fixed total available energy for transmission. The problem is now to find the optimum number of bits per subcarrier, and the corresponding energy distribution per subcarrier E_n , in order to maximise the bit-rate.

The solution to this bit-rate maximisation problem, based on the use of Lagrange multipliers, is commonly known as water-filling [99]. In [99], Chow proposed that the water-filling solution can be computed numerically and the finite bit-loading algorithm can be easily adapted for practical use. The algorithm, based on Equation 5.1, initially discards the sub-carriers that are the least energy-efficient from information transmission, and redistributes the energy to more efficient sub-carriers in order to support higher data rates. The non-integer number of allocated bits per subcarrier are then rounded to the nearest integer and the corresponding energy is dynamically adapted to support the newly-allocated number of bits at the same performance [50].

From Equation 5.1, notice that E_n of some of the sub-carriers can be set to zero in order to achieve the maximum normalised bit-rate b . Therefore, the optimal solution is not always to use all $N - 1$ available sub-carriers to transmit information. Chow's algorithm has been shown to achieve near-optimum performance [95, 99]. Chow's algorithm will be used to calculate the rate-adaptive bit-loading for the DMT over POF experiments described in the next sections. More details of the bit-loading of the DMT format can be found in [50].

5.2 Transmission over PMMA GI-POF Employing Different Photo-detectors

5.2.1 4.5 Gbit/s over 50 m PMMA GI-POF using APD

By employing the DMT format with bit-loading algorithm, the first transmission experiment over PMMA GI-POF in this section is addressed. The experimental system setup is shown in Figure 5.1, see also [116]. A low-cost 667 nm wavelength VCSEL from Firecomms (RVM665T), which was designed to have a bandwidth of 3 GHz, was directly modulated by the output of an arbitrary waveform generator (AWG) sampling at 5 GSamples/s. The bias current of the VCSEL was set to 6 mA, resulting in a peak-to-peak driving current of maximum 12 mA. The optical power of the VCSEL launched into the POF was measured to be -1 dBm. After transmitting the directly modulated signal over the 1 mm core diameter PMMA GI-POF of maximum 50 metres length, a -17 dBm optical power was received due to the 17 nm deviation from the POF minimum loss (0.2 dB/m at 650 nm). An avalanche photodiode (APD) receiver

5. HIGH CAPACITY BASEBAND DATA LINKS OVER POF

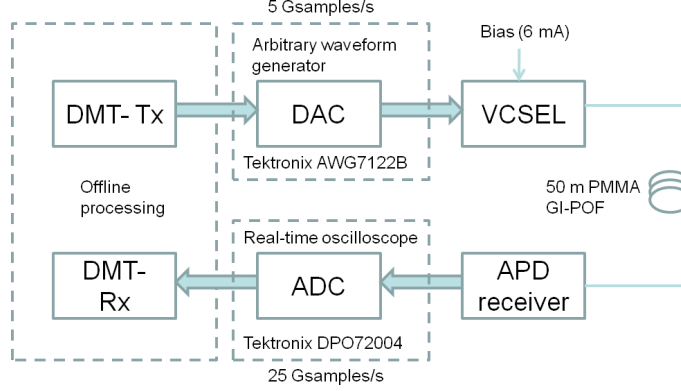


Figure 5.1: Experimental setup for the transmission of an DMT signal over PMMA GI-POF.

was used to detect the signal. The APD receiver consisted of a photodiode (model: Silicon Sensor APD 230-8, with an optimum gain factor of 60 dB) and two stages of amplifier (model: HP IVA-14228), requiring 130 V voltage supply. The received signal was sent to a real-time oscilloscope running at a sampling rate of 25 GSamples/s for off-line evaluation.

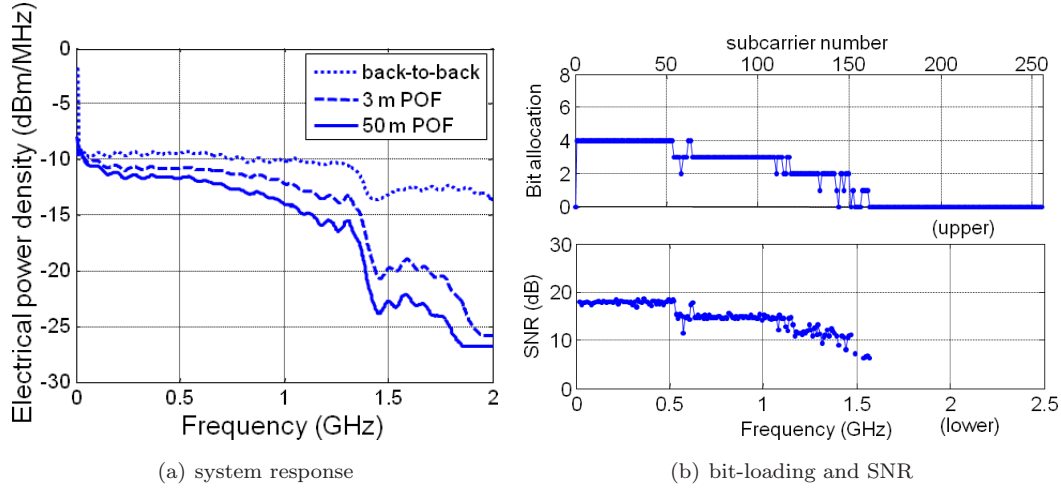


Figure 5.2: (a) Normalised frequency response of the system, (b) (upper) Bit allocation for 4.5 Gbit/s; (lower) SNR after 50 m transmission using bit loading.

The bandwidth of the investigated system is mainly limited by the APD detector, which has a -3 dB analogue bandwidth of 1.3 GHz as shown in Figure 5.2(a). By using the DMT technique in combination with the bit-loading algorithm, this limited bandwidth can be used in a most efficient manner. As described in Figure 5.1, the DMT (de)modulation is executed off-line to calculate the most efficient bit-loading parameters in an adaptive way. In this experiment, 256 equally spaced sub-carriers is chosen,

ranging from 0 to 2.5 GHz. In Figure 5.2(b)(upper), it is observed that there are no bits assigned to the 160th sub-carrier and beyond, therefore there is almost zero SNR beyond 1.6 GHz as shown in Figure 5.2(b)(lower). This is due to the strictly limited system bandwidth. Still, it can be seen in Figure 5.2(b)(upper), that 4 bits of information at maximum (i.e. 16-QAM) are allocated for some of the carriers, while others have 3 or less; this adaptive allocation is leading to the stair-like SNR after 50 m POF shown in Figure 5.2(b)(lower).

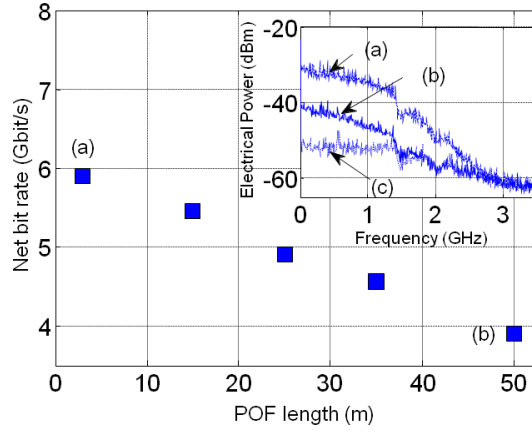


Figure 5.3: Transmitted netto bit rate for different lengths of POF. Inset: electrical spectra of the signal after (a) 3 m GI-POF; (b) 50 m and (c) background noise.

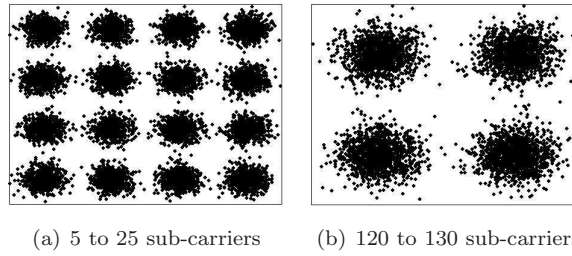


Figure 5.4: Constellation diagrams of the demodulated signal at sub-carrier between (a) 5 and 25; (b) 120 and 130.

Figure 5.3 shows the measured maximum bit rates which can be transmitted over 3, 15, 25, 35 and 50 metres of PMMA GI-POF, respectively, with BER values of less than 10^{-3} . This target BER is chosen based on the forward error correction (FEC) limit for error-free operations. After 50 m transmission, it is still possible to achieve 3.9 Gbit/s net bit rate (corresponding 4.5 Gbit/s including overhead). Meanwhile, for less than 30 m links, successful transmissions of more than 5 Gbit/s can be realised even though the system has only 1.3 GHz bandwidth. The inset of Figure 5.3 presents the electrical spectra of the received

5. HIGH CAPACITY BASEBAND DATA LINKS OVER POF

signals, for (a) 3 m (b) 50 m transmission and (c) background noise for comparison. It is noted that the SNR becomes less than 20 dB after 50 metres.

Finally, in Fig. 5.4 two sets of signal constellations of the demodulated signals are presented at different sub-carrier indices. From the sub-carrier 5 to 25, 4 bits/sub-carrier are allocated, corresponding to the 21 overlapping constellations of 16-QAM (see Fig. 5.4(a)), whereas from 120 to 130 only 2 bits/sub-carrier are allocated, giving 11 constellations of 4-QAM (see Fig. 5.4(b)). In both figures, separated constellation points predict the good quality of the received signal.

5.2.2 12.7 Gbit/s over 35 m PMMA GI-POF using PIN Diode

In the previous experiment, an APD receiver was employed which requires high-voltage supply (130 V). That was not suitable for the practical implementation for in-home systems. In contrast, in this experiment the APD was replaced by a low-voltage silicon PIN diode (model: Hamamatsu s5973) with 400 μm diameter active area equipped with an external broadband amplifier (model: SHF 100CPP) to detect the transmitted signal [117]. The -3 dB bandwidth of the PIN was approximately 1.5 GHz. The rest of the experimental setup remained the same as shown in Figure 5.1.

The maximum available -3 dB bandwidth of the system is approximately 1.5 GHz, which is also limited by the receiver (as shown in Figure 5.5(a)). In this experiment, 512 subcarriers are chosen, ranging from 0 to 3 GHz. The Chow's bit-loading algorithm measured the SNR per subcarrier. This SNR is a continuous curve as function of frequencies. Then, the algorithm allocated bits per subcarrier to obtain an optimum transmission rate. Therefore, the received SNR values become a stair-like curve truncated at frequencies where no bits are assigned. This principle is also the same as the one used in the previous experiment. In Figure 5.5(b), no bits are assigned beyond the 360th subcarrier or 2.2 GHz. This truncation is caused by the system bandwidth. Moreover, it is seen in Figure 5.5(b)(upper), that some of the carriers with the upper limit of 7 bits of information (i.e. 128-QAM) are allocated, while others are allocated less. The number of bits allocated matches the response of the system indicated in Figure 5.5(b). Results shown in Figure 5.5(b) are obtained after 15 m POF transmission.

Figure 5.6 shows the measured values of maximum bit rate which can be transmitted over 3, 10, 15, 25 and 35 m PMMA GI-POF respectively, for a bit error ratio (BER) of less than 10^{-3} . For less than 15 m POF, transmissions of more than 10.1 Gbit/s is realised based on a system which has a -3 dB bandwidth of only 1.5 GHz. For 10 m transmission 12.7 Gbit/s is achieved as gross data rate while for 35 m POF, it is still possible to achieve 6 Gbit/s. All bit rates mentioned include 7% FEC bits, cyclic prefix and preambles. The inset of Figure 5.6 presents the electrical spectra of the received signals, for (a) 3 m, (b) 35 m transmission and (c) background noise for comparison. In this experiment, the bending

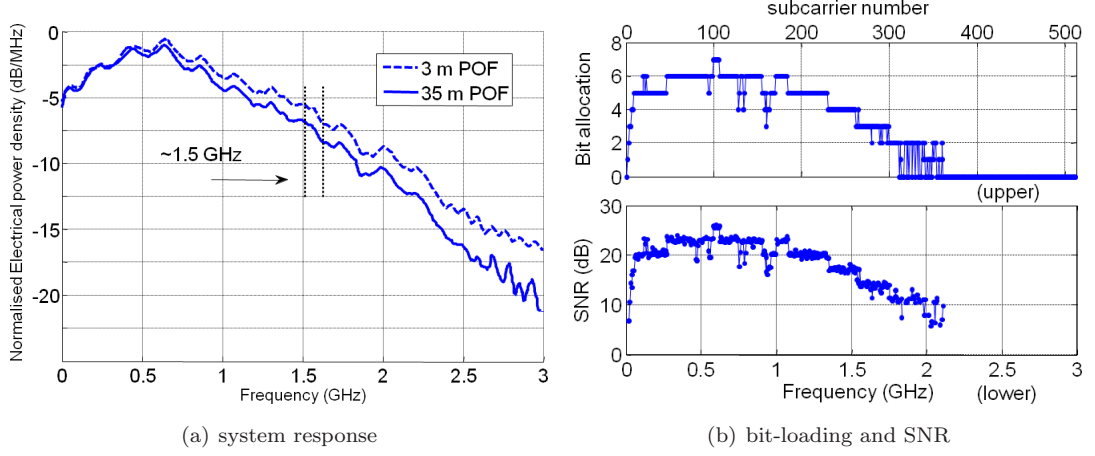


Figure 5.5: (a) Normalised frequency response of the system, (b) Transmission performance for 15 m: (upper) Bit allocation and (lower) SNR.

of the POF for a bending radius of 10 mm in 10 m transmission case is also implemented. It has been observed that the performance in terms of maximum bit rate is degraded by 10% for the bending radius of 10 mm. With this bending radius, the maximum achievable bit rate is still above 10 Gbit/s. This demonstrates the robustness of PMMA POF for in-home environments.

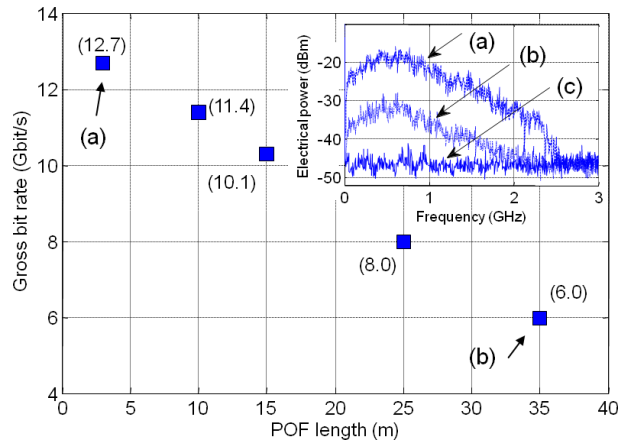


Figure 5.6: Transmitted bit rates for different lengths of POF. Inset: electrical spectra of the signal after (a) 3m; (b) 35 m and (c) background noise.

5.2.3 Discussion

Comparing Figure 5.3 and Figure 5.6, it is obvious that the system performance using PIN is much better than the one using APD for short range communications (e.g. less than 35 metres). This is because the bandwidth of the PIN is larger than the APD, although APD has a more flatten response and higher gain. However, by employing a PIN diode, a maximum transmission distance of only 35 metres can be reached due to its lower responsivity. The system performance, which can be seen as the channel capacity C , is affected by two determining factors: the SNR and the available bandwidth B , as expressed by Shannon's formula

$$C = B \times \log_2(1 + SNR) \quad (5.3)$$

Increasing the available bandwidth and/or improving the SNR will enhance the system performance. However, in the experiments reported above, the APD receiver has a larger gain for the signal compared with the PIN receiver (corresponding to a larger SNR in the APD case), while the PIN diode yields a larger bandwidth B . As shown in Equation 5.3, the bandwidth has a stronger influence on the maximum capacity. Therefore, by comparing the experimental results between an APD and a PIN detectors, it is found that the SNR from the APD is not so high that the gain could compensate the degradation of the capacity due to a smaller bandwidth.

Moreover, the APD has a higher gain, thus a better SNR when compared to PIN for sufficient input powers. Given the same bandwidth, according to Equation 5.3, SNR values are encapsulated in the logarithmic calculation, meaning that increase in SNR (or shorten the transmission distance) affects a logarithmic increase in the capacity. Based on this principle, a PMMA POF system using a PIN diode is in favor over an APD, provided with an integrated trans-impedance amplifier (TIA). In this experiment a PIN and an external amplifier (EA) is used. However, this 50-Ω external amplifier reduces the level of input signal before being amplified. To increase the signal output, integrated TIA with PIN is desired. Having such an PIN with an TIA, the transmission capacity can be enhanced furthermore.

5.3 Transmission over 50 m PMMA Multi-core SI-POF

PMMA SI-POF has been a subject of many laboratory research recently, due to its limited bandwidth. Much efforts have been spent to reach approximately >1.25 Gbit/s transmissions [96, 97, 122, 123]. To enhance the bandwidth, POF with the graded-index profile was introduced in order to achieve more than 1.25 Gbit/s or multi-Gbit/s transmission as discussed in Section 5.2.

Alternatively, another kind of PMMA POF, namely multi-core (MC) SI-POF, has been commercialised due to its advantages of low bending loss and large bandwidth as shown in Table 5.1. Figure 5.7 shows a snapshot of the end face of the 19-core SI-POF used in the experiments of this section. As shown in the figure, the MC SI-POF has 19 cores confined in 1 mm overall core diameter. The modulated light source is illuminated over the whole area and carried by all the cores to the other end of the POF link. The MC-POF has a smaller bending radius (2 mm compared to 20 mm for single-core POF) for the same incremental loss, as shown in Table 5.1. This is because each core of the multi-core POF has a smaller core diameter, thus the ratio between the bending radius and the fibre radius is larger for the same absolute bending radius [39]. The bandwidth of the MC-POF is also larger than that of the single-core POF. An extensive study on the main reasons for the bandwidth enhancement of MC-POF with a numerical aperture (NA) of 0.6 compared to SI-POF with a NA of 0.5 has not been yet published anywhere, to the best knowledge of the author. Nevertheless, a basic explanation takes into account two major aspects: modal dispersion and mode coupling. Since each core of the MC-POF is smaller than the single core of SI-POF, each core supports less modes thus leading to a lower modal dispersion [39, 124], although it is not possible to consider them as separate single core fibres because the cores are very close to each other. Another reason can be the enhanced mode coupling of the MC-POF compared to SI-POF due to the designed structure. In fact, increasing of bandwidth with stronger mode coupling has been proved for single core POF [39, 125, 126]. This section will discuss the performance of a 19-core SI-POF link, in comparison with a conventional PMMA single-core SI-POF and PMMA GI-POF link [118].



Figure 5.7: 19-core SI-POF, product model: SMCK-1000 from Asahi Kasei (illuminated by white light).

The experimental setup is again similar to the setup in Figure 5.1. In this experiment, a 19-core SI-POF with lengths up to 50 m was put between the VCSEL (RVM665T) and the APD (Silicon Sensor 230-8). Operational conditions of other equipments were in principle kept the same as Figure 5.1. In Figure 5.8(a) the measured bandwidth of the 19-core SI-POF system is shown. For comparison, two

5. HIGH CAPACITY BASEBAND DATA LINKS OVER POF

other curves belonging to conventional single-core SI-POF and GI-POF of the length of 50 m are also presented. The maximum available bandwidth for the 50 metre links of 19-core SI-POF is approximately 350 MHz. It is observed that the bandwidth of the 19-core SI-POF is between the bandwidth of the single core SI-POF and the single core GI-POF, where the latter has a more complex index profile, thus requires a more complicated manufacturing process. However, the prices of SI-POF, GI-POF and MC-SI-POF are more or less the same as shown in Table 5.1. In Figure 5.8(a), the three vertical gray lines show the -3 dB bandwidth for three different POF links.

In this experiment, 512 sub-carriers are chosen, ranging from 0 to 3 GHz, for the DMT format. In Figure 5.8(b), no bits are assigned beyond the 275th subcarrier at 1.6 GHz. This truncation is again caused by the system bandwidth. Moreover, it can be seen in Figure 5.8(b)(top), that some of the carriers are loaded with the upper limit of 5 bits/symbol (i.e. 32-QAM), while others with less. Again, same as the previous experiments, the number of bits allocated reflects the response of the system indicated in Figure 5.8(a) for the 19-core SI-POF.

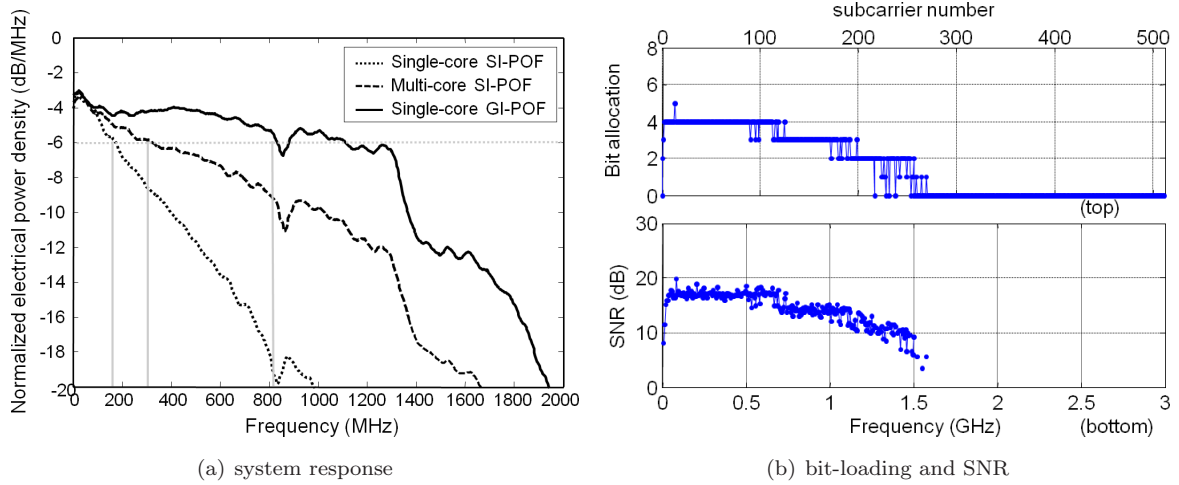


Figure 5.8: (a) Normalised frequency response of the system with 50 m of POF, (b) Transmission performance for 50 m of MC SI-POF: (top) bit allocation and (bottom) SNR.

Figure 5.9 shows the measured values of maximum bit rates for 50 m single-core SI-POF, 19-core SI-POF and single core GI-POF with a BER of less than 10^{-3} taken as the target assuming FEC. For a length of 2 m (considered here as a back-to-back setup), the performance of MC SI-, single-core SI- and GI-POF are very similar, due to the fact that the fibre bandwidth does not play a major role for this length. For a length of 50 m, the advantage of MC SI-POF over single core SI-POF is clearly shown in terms of transmission rate. For single-core SI-POF, less than 2 Gbit/s signal transmission rate is achieved. However, MC SI-POF is able to transmit more than twice the bit rate achieved with single

core SI POF due to its larger bandwidth. Moreover, it is worth to note that the maximum transmission rate of MC SI-POF is only 0.7 Gbit/s less than the GI POF rate thanks to its less loss. Considering the overall performance in bandwidth, bending property and attenuation, MC SI-POF can be presented as an attractive candidate for short-range POF links. In Figure 5.9, a data cluster for the -3 dB bandwidth of the 50 m length POF systems is also included. These numbers validate the curves shown in Figure 5.8(a). By employing the bit-loading algorithm, we transmitted 4.7 Gbit/s within the available bandwidth limitation of 1.5 GHz for MC SI-POF, resulting in a spectral efficiency of 3.1 bit/s/Hz.

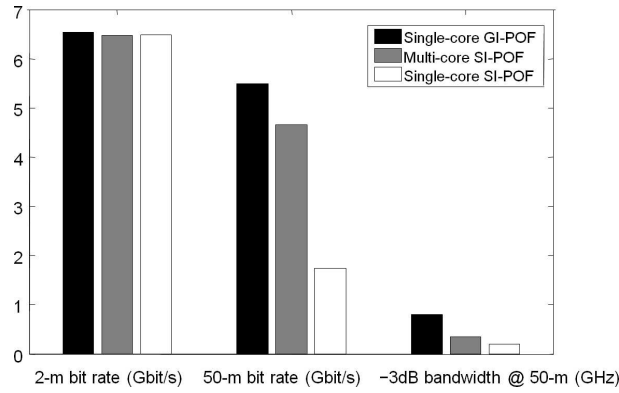


Figure 5.9: Maximum transmission rate for 2 and 50 m single-core SI-, MC SI- and single-core GI-POF, including the -3 dB bandwidth for 50 m POF systems as marked in Figure 5.8(a).

Finally, the demodulated signal constellation diagrams are shown for two sub-carrier index groups in Figure 5.10. As shown in Figure 5.10(a), 4 bits are allocated for the 41^{th} to 50^{th} sub-carrier, corresponding to the 16-QAM constellation while in Figure 5.10(b) only 2 bits (4-QAM) are assigned for the 201^{th} to 210^{th} sub-carrier. Sub-carrier indices are shown in Figure 5.8(b).

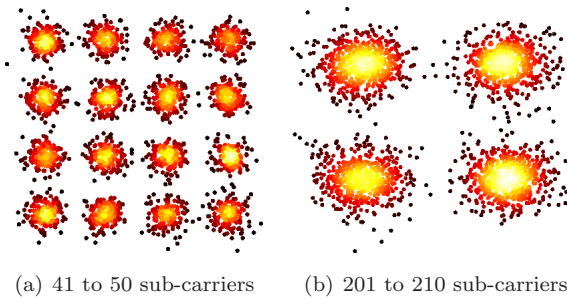


Figure 5.10: Constellation diagrams of the demodulated signal: (a) 64 QAM for 41^{th} to 50^{th} and (a) 4-QAM for 201^{th} to 210^{th} sub-carriers.

5.4 47.4 Gbit/s Transmission over 100 m PF GI-POF

In recent years, there has been an increasing use of commercial perfluorinated graded-index plastic optical fibre (PF GI-POF) with core diameters of 50, 62.5 μm or 120 μm for 10 Gbit/s short-reach applications such as low-cost interconnects in data centers, local area networks (LAN) and supercomputers [127]. For these applications, multimode fibres such as the PF GI-POF are preferred above single-mode fibre due to their large core diameter and numerical aperture. Due to the large alignment tolerances in transceiver components and fibre splices, multimode fibre is attractive for in-building networks as its installation is easy and at low cost. In addition, when compared to silica MMF, PF GI-POF offers further advantages such as smaller bending radius (5 mm), better tolerance to tensile load and stress, and simpler connectorisation.

Recent developments in the standardisation of higher-speed networking standards like 40 and 100 Gbit/s Ethernet also include silica MMF as physical medium [128], thereby paving the way for low-cost optical networking at speeds beyond 10 Gbit/s. Although current proposals consider parallel transmission of multiple 10 Gbit/s MMF links with multiple fibres or multiple wavelengths to achieve higher speeds, serial transmission using only one MMF is attractive because issues such as skew between parallel fibres, inter-channel crosstalk, and reduced reliability due to higher complexity can be avoided. Several research groups have demonstrated 40 Gbit/s serial transmission over PF GI-POF [125, 129, 130]. However, these results were obtained with expensive large-bandwidth (> 25 GHz) single-mode fibre components such as external Mach-Zehnder modulators and small-area high-bandwidth detectors [125, 129] as well as optical fibre amplifiers [130], which are neither practical nor suitable for low-cost applications. In this section, by employing DMT scheme, more than 40 Gbit/s can be achieved using direct modulation of a laser and a multimode receiver.

5.4.1 Experimental setup

In order to realise more than 40 Gbit/s transmission over PF GI-POF, the experimental setup depicted in Figure 5.11 was used.¹ The electrical ports of the setup were the same as in the previous sections. A distributed feedback (DFB) laser (model: NTT NLK5B5EBKA) was directly modulated (through an electrical variable attenuator and amplifier) by the output of the signal generator (AWG) at a sampling speed of 24 GSamples/s. To achieve this sampling speed, the two outputs of the AWG, both at 12 GSamples/s, were interleaved. The DFB laser, with a wavelength of 1302 nm and maximum output power of 10 dBm, was specified for up to 10 Gbit/s on-off keying transmission and had an electrical -3 dB

¹This is a joint experiment with S.C.J. Lee. Results and discussion can also be found in Lee's PhD thesis [50].

modulation bandwidth of approximately 12 GHz. The resulting intensity modulated optical signal was then either transmitted over 100 metres of 50 μm core diameter PF GI-POF, or directly coupled to the multimode variable optical attenuator in the back-to-back measurement case. After the multimode attenuator, the received optical signal was detected by a multimode-fibre-coupled photo-detector (PD) with a detection diameter of 21 μm and an integrated coupling lens (model: NewFocus 1434-50). The resulting received electrical signal was then amplified and captured using a real-time scope running at a sampling rate of 50 GSamples/s for demodulation and evaluation.

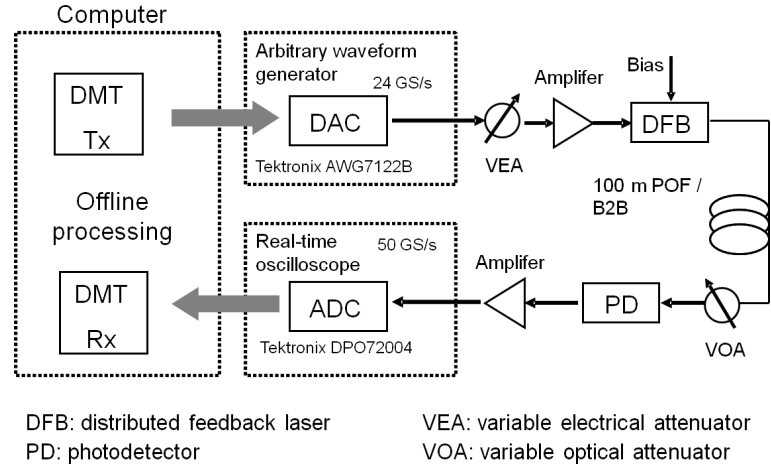


Figure 5.11: Measurement setup for DMT over 50 μm core diameter PF GI-POF transmission

5.4.2 Transmission results

In this section, details of the transmission performance of DMT for a net bit-rate of 47.4 Gbit/s (with gross rate of 51.6 Gbit/s) over 100 m PF GI-POF are presented. In the experiment, 1024 subcarriers are used for the DMT transmission, ranging from a frequency of 0 to 12 GHz. Figure 5.12(a)(upper) shows the measured SNR per subcarrier in the initialisation stage, prior to applying Chow's rate-adaptive bit-loading algorithm, and after transmission over 100 m PF GI-POF. The channel response is clearly adapted by the large amount of sub-carriers. The bit and power allocation per subcarrier, after applying rate-adaptive bit-loading, is depicted in Figure 5.12(b). For sub-carriers with the highest SNR, 6 bits are allocated for DMT transmission, which is realised by 64-QAM. The number of allocated bits per subcarrier decreases to 2, for those sub-carriers with the lowest SNR. This is equivalent to a modulation format of 4-QAM. By allocating a different amount of power to each individual subcarrier, the SNR per subcarrier can be fine-tuned to a fixed value, which is just enough to achieve a BER of 10^{-3} for the

5. HIGH CAPACITY BASEBAND DATA LINKS OVER POF

specific modulation format. The resulting SNR per subcarrier after rate-adaptive bit-loading is shown in Figure 5.12(a)(lower).

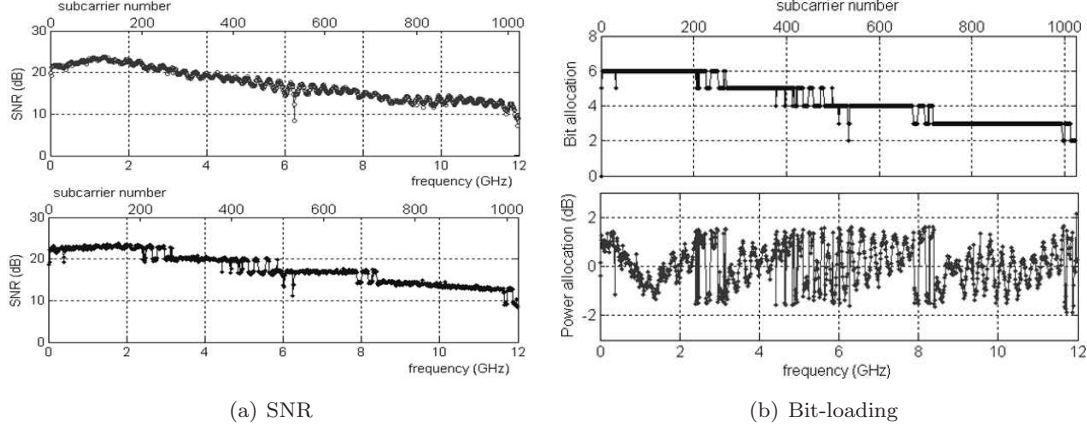


Figure 5.12: (a) Measured SNR per subcarrier for DMT transmission over 100 m GI POF, (upper) before (lower) after rate-adaptive bit-loading. (b) Rate-adaptive bit-loading parameters for DMT transmission over 100 m GI-POF using a total of 1024 sub-carriers.

Figure 5.13(a) presents the measured BER values as a function of the subcarrier index for the received 47.4 Gbit/s DMT signal. This value is under the FEC limit for error-free operation. In Figure 5.13(b), the electrical spectra of the signal as observed before and after 100 m transmission are presented. The available bandwidth for data transmission is seen to be less than 13 GHz, taking into account the bandwidth of the AWG and the DFB laser. However, the DMT scheme and the bit-loading algorithm allow us to successfully transmit 47.4 Gbit/s data through the available bandwidth of PF GI-POF. The dotted curve is the spectrum without data modulation, which indicates the noise floor of the system. The system performance in terms of BER as a function of received power optical can be found in [50, 119, 131].

5.4.3 Effect of parameters

Laser nonlinearity Besides the transmission results, the impact of laser nonlinearity is investigated in this section in order to achieve 47.4 Gbit/s data rate over PF GI-POF. Figure 5.14(a) shows schematically how the peak-to-peak driving current I_{pp} is varied for the DFB laser. The laser is always fully modulated starting from its threshold current I_{th} . The laser bias current, which is equal to $I_{pp}/2 + I_{th}$, is adjusted according to I_{pp} in order to ensure a full modulation of the DFB laser. The average received optical power is always fixed to the same value with the variable optical attenuator when I_{pp} is increased. By this method, the influence of thermal noise (resulting mainly from the electrical amplifier at the receiver) is kept constant when I_{pp} is varied. Figure 5.14(b) presents the effect of peak-to-peak electrical driving

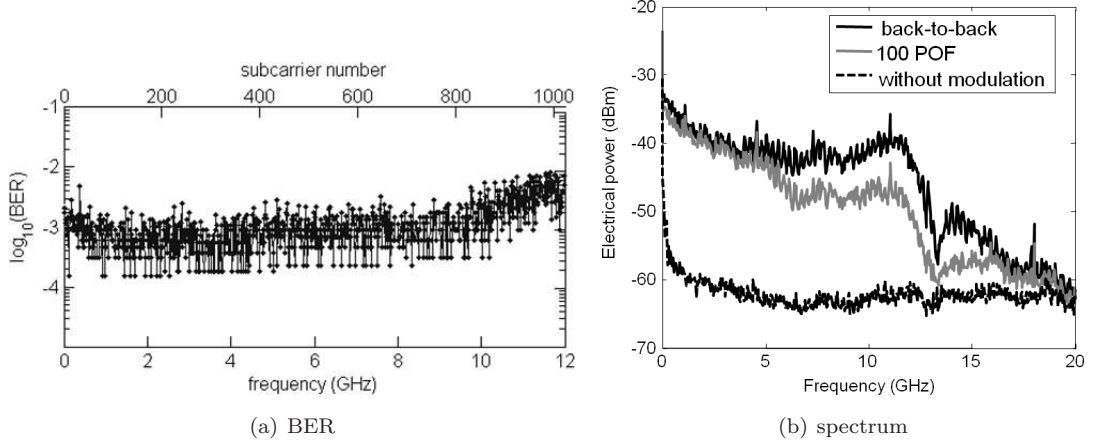


Figure 5.13: (a) BER performance per DMT subcarrier after transmission over 100 m GI-POF and (b) Received signal spectrum after 100 m POF, compared to the back-to-back case and the case without modulation.

current I_{pp} on the system performance in both back-to-back and PF GI-POF transmission system. In this measurement the laser bias level is fixed at 60 mA and thus the received optical power is fixed at +4 dBm. On the left vertical axis the maximum transmission rate for different peak-to-peak driving current levels up to 85 mA with adaptive bit loading is shown. The transmission rate is saturated for peak-to-peak driving currents of 70 mA and above, at which the maximum rate is achieved. On the right vertical axis, the BER is plotted versus different peak-to-peak driving currents for transmission. The laser bias level and received optical power are kept the same, as well as the bit loading parameters in transmission measurement. A similar floor in BER is observed for comparison with back-to-back case. This saturation in system performance is due to the DMT electrical clipping noise and laser non-linearity [50]. A separate investigation of DMT electrical clipping noise can be found in [131].

From the back-to-back measurement results of Figure 5.15(a), a similar performance is observed as in Figure 5.14(b). For a fixed driving current, the system performance increases for larger received optical power, which is apparent due to less influence of receiver (thermal) noise. However, at +4 dBm received optical power, performance seems to be limited and the achievable transmission rate seems to saturate at its maximum value. Possible reasons for this limit are saturation effects of the photo-detector at high received optical powers and the electrical DMT clipping noise resulting from clipping the electrical DMT signal in the digital domain before D/A conversion. More analysis and measurement results on the DMT clipping in this experiment can be found in [50, 131].

The results on laser nonlinearity from transmission experiments over 100 m PF GI-POF are investigated and shown in Figure 5.15(b). The corresponding back-to-back curves in Figure 5.15(a) are included

5. HIGH CAPACITY BASEBAND DATA LINKS OVER POF

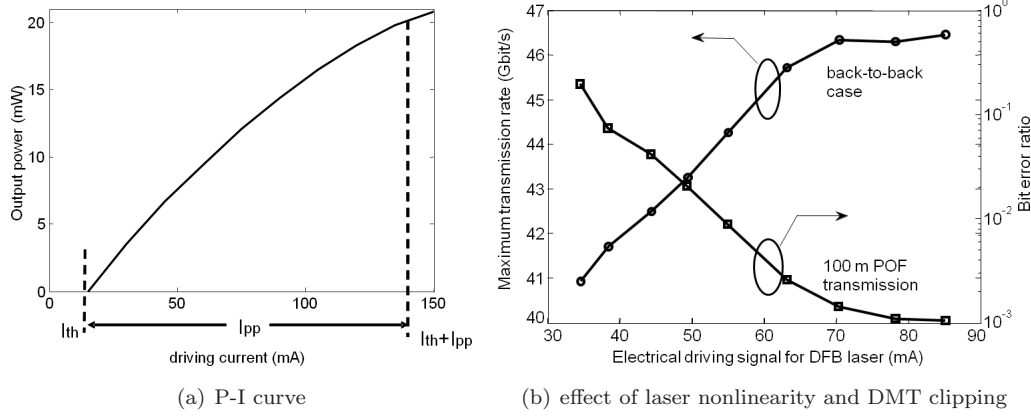


Figure 5.14: (a) Optical output power versus DFB driving currents used in the experiments. I_{th} : threshold current; I_{pp} : peak-to-peak driving current and (b) left axis: Transmission rate versus peak-to-peak driving current with rate-adaptive bit-loading; right axis: BER versus driving current with fixed bit-loading parameters.

for reference. The performance degrades for larger peak-to-peak laser drive currents in the case of transmission over 100 m PF GI-POF. The reduced transmission rate can be attributed to the change in the shape of the frequency response at higher laser currents, as shown in Figure 5.16. At higher laser currents, the frequency response leads to a reduced available bandwidth, hence reduces the achievable rate. Note that in Figure 5.15(b), at higher launch power powers the maximum transmission rate decreases. This can be attributed to differential modal attenuation (DMA) [132, 133], which is the effect that higher order modes propagating through the GI-POF experience higher attenuation than the fundamental modes. At low launch power, almost only the fundamental modes can be detected after 100 m PF GI-POF due to the DMA effect. However, for very high optical launch powers, the higher order modes are not attenuated enough at a distance of 100 m and are therefore also detected at the end of the PF GI-POF. This difference in mode attenuation profile leads to constructive/destructive modal interference, and affects in this case the PF GI-POF bandwidth in a negative way (as can be observed in Figure 5.16).

Number of sub-carriers In addition to the impact of laser non-linearity, the influence of the number of sub-carriers used for DMT transmission is also investigated experimentally. The same DMT parameters as in previous section are used, except that the total number of sub-carriers is now varied from 128 to 512. The received optical power is fixed at +4 dBm. Again, with rate-adaptive bit-loading, the power and bit-allocation per subcarrier is adapted to the transmission channel, thereby maximising the transmission rate for a fixed BER of 10^{-3} .

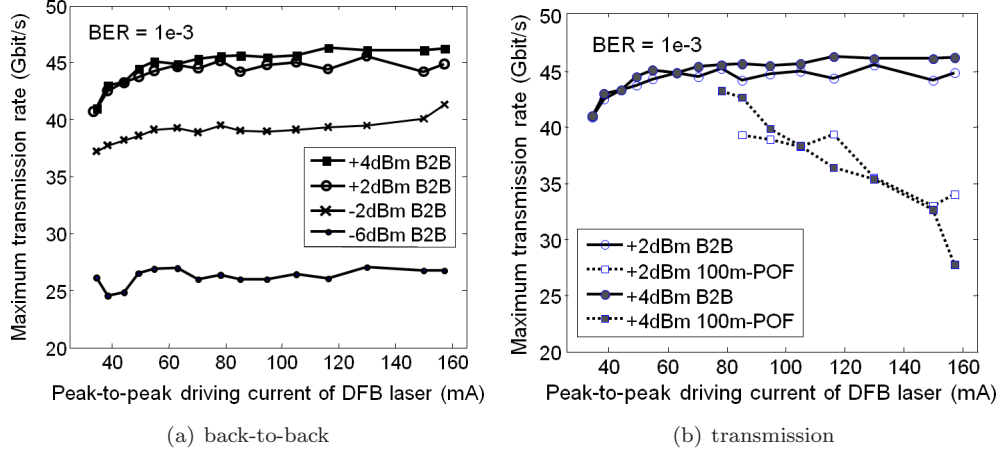


Figure 5.15: (a) Maximum achievable transmission rate at BER of 10^{-3} as a function of peak-to-peak laser drive currents for different received optical powers, back-to-back case (b) Maximum achievable transmission rate at BER of 10^{-3} versus peak-to-peak laser drive currents for different received optical powers.

Figure 5.17(a) shows the experimental results for the back-to-back case. As observed in Figure 5.17(a), the system performance improves when the number of DMT subcarriers is increased. To further investigate this, the total number of DMT sub-carriers is varied over a larger range for the same received optical power of +4 dBm. The peak-to-peak driving current I_{pp} of the DFB laser is fixed to 85 mA. The measurement results are plotted in Figure 5.17(b), for the case of back-to-back and 100 m of PF GI-POF. As shown in Figure 5.17(b), the transmission rate improves with the increase of the DMT subcarrier counts. This is true for back-to-back and for 100 m of PF GI-POF. The conclusion is that with a larger number of sub-carriers, the frequency response of the transmission channel can be more finely divided into more sub-channels, making the channel response of each subcarrier less dispersive. Consequently, every subcarrier experiences a better channel response and therefore the overall performance increases.

The performance gap between 100 m PF GI-POF and the back-to-back case is due to the extra bandwidth limitation of the PF GI-POF. The attenuation of PF GI-POF is not significant in Figure 5.17(b) because the received optical power and peak-to-peak laser driving current are both fixed to the same value for each measurement point. It can also be noted that the number of sub-carriers cannot be increased infinitely in order to have better performance, as the curve flattens after 512 sub-carriers.

Modal noise Up to an I_{pp} of 85 mA, modal noise is not observed. This is because light of a single-mode DFB laser with single mode pigtail (small launching area) is launched into the PF GI-POF, thereby exciting only lower order modes. Due to mode coupling in the PF GI-POF, higher order modes can

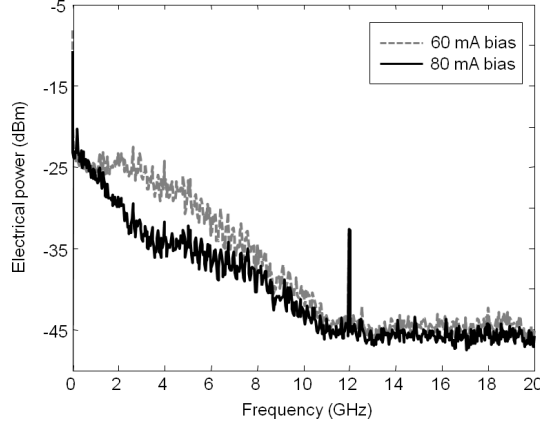


Figure 5.16: Measured frequency response of 100 m GI POF at 60 and 80 mA laser bias current

still exist but most are suppressed by DMA. Additionally, a commercial photo-detector with integrated coupling lens is used to couple most of the light from the end of the PF GI-POF into the detector. (The effective detector diameter is $21\ \mu\text{m}$.) For I_{pp} larger than 85 mA, beginning signs of modal noise can be observed, because of high laser launch power. Due to such high launching power (up to +10 dBm), DMA in the PF GI-POF is not large enough to suppress the higher order modes resulting from mode coupling in the PF GI-POF. Therefore, higher-order modes are present at the PF GI-POF end-face and some are not detected by the photo-detector, leading to beginning signs of modal noise. As the results are obtained at I_{pp} of 85 mA, these results do not suffer from modal noise. More discussion regarding modal noise can be found in [134–136].

In this section, by exploiting DMT with up to 64-QAM, off-the-shelf and low-cost components such as standard 1300 nm directly-modulated DFB laser diode (with 12 GHz bandwidth) and an MMF-coupled $21\ \mu\text{m}$ large diameter photo-detector, 47.4 Gbit/s net serial transmission over 100 m of $50\ \mu\text{m}$ core diameter PF GI-POF can be achieved. This demonstrates the potential of DMT for enabling highly spectral efficient transmission at high bit-rates over POF, while overcoming the fibre’s modal dispersion and allowing the use of conventional optical transceivers [119, 131]. It is therefore a promising solution for robust and high capacity PF GI-POF LAN links operating at data rates of 40 Gbit/s and beyond.

5.5 Summary

This chapter presents the experimental results on baseband transmission of DMT signal over PMMA and PF POF. First, the DMT and its bit-loading algorithm have been briefly summarised in Section 5.1. Section 5.2 includes two experiments for PMMA GI-POF by using a high voltage APD (130 V) and

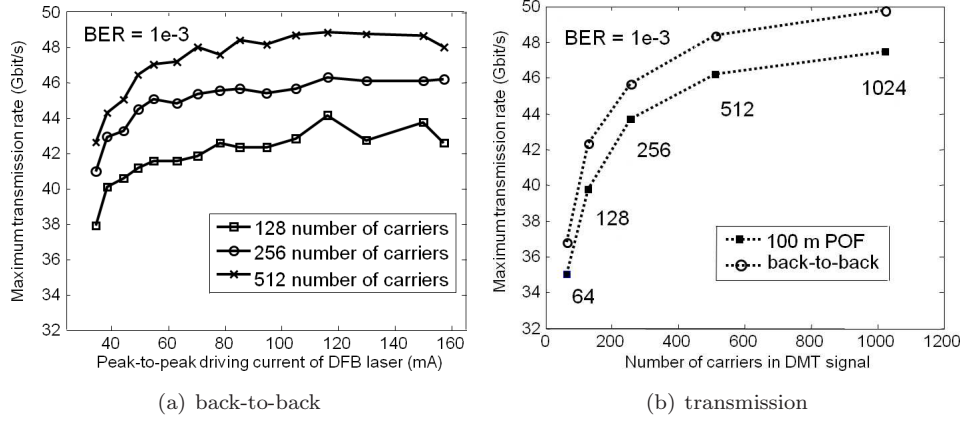


Figure 5.17: (a) Maximum achievable transmission rate at BER of 10^{-3} versus peak-to-peak laser drive currents for different number of sub-carriers and (b) Maximum achievable transmission rate at BER of 10^{-3} for different number of sub-carriers. Received optical power is fixed at +4 dBm.

a low voltage PIN photodiode (3.3 V), respectively. By employing DMT technique and APD receiver, 4.6 Gbit/s bit rate over 50 m PMMA POF has been demonstrated. The system -3 dB bandwidth is limited by the APD (< 1.3 GHz) giving 3 bit/s/Hz spectral efficiency, by employing adaptive bit-loading. In comparison, by employing PIN photodiode with a larger bandwidth, transmission capacities of up to 12.7 Gbit/s for 3 metres are demonstrated. The system -3 dB bandwidth is about 1.5 GHz. A smoother slope of the frequency response of the PIN photodiode, compared with the APD, results in a larger spectral efficiency of 6.3 bit/s/Hz for the case of PIN photodiode¹. Another type of PMMA POF, multi-core SI-POF, has been presented in Section 5.3. In Section 5.3, a robust transmission of 4.7 Gbit/s over 50 m PMMA 19-core SI-POF has been demonstrated. This transmission capacity is more than twice the transmission capacity of a single-core SI-POF. The performance of MC SI-POF has also been compared with a single-core GI-POF, resulting in a capacity difference of only 0.7 Gbit/s for 50 m transmission. In Section 5.4, the DMT transmission over PF GI-POF is presented. Due to its large bandwidth (approximately 10 GHz), a record transmission rate of 47.4 Gbit/s has been achieved. Different parameters in the DMT transmission for PF GI-POF have also been investigated, including laser nonlinearities, number of sub-carriers and etc. An abstract of the baseband transmission results over PMMA and PF-POF are summarised in Table 7.1 in Chapter 7.

Nevertheless, the complexity of DMT approach due to the digital signal processing largely increases the power consumption in practical implementation of DMT scheme. Other modulation formats such as OOK or PAM can offer a less complex system with lower power consumption and a compromise in transmission

¹Here the spectral efficiency is calculated using available bandwidth, instead of -3 dB bandwidth.

5. HIGH CAPACITY BASEBAND DATA LINKS OVER POF

capacity [123, 137, 138]. Alternative methods of DMT technique using either the combination of PAM and DMT [139] or a real-time field-programmable gate array (FPGA) implementation of DMT [50, 140] have also been addressed in literature in order to have a practically usable system. Towards a lower costly solution with lower power consumption, application-specific integrated circuit (ASIC) implementation of the DMT algorithm might be a good candidate. In conclusion, by engineering a good trade-off between DSP algorithm, modulation format and optical transceivers, DMT has proven to be a robust technique to provide multi-Gbit/s baseband data transmission system for in-building networks.

Chapter 6

Converged Multi-standard In-Building Networks

For in-building networks, multimode fibre, made from either silica or plastic material, has been gaining more and more attention and therefore been in a position to replace the copper twisted pair or Cat. 5 cable for home and enterprise customers [142]. Due to their inherent large bandwidth, EMI-immunity and other key advantages, optical fibres have been shown in the previous chapters to be strong candidates for transporting both baseband digital and microwave analogue signals with certain network functionalities such as signal routing. Chapter 2 to 5 have discussed the potential of delivering one high-capacity baseband signal or one wireless service for home users via fibre backbones.

As shown in Figure 1.2, one of the desired benefits of an optical backbone for in-home environments is to enable simultaneous multi-standard transmission of more than one wireless service or both wired and wireless services over single physical infrastructure [143–148]. As shown in Figure 1.2, the optical backbone, for example a POF infrastructure, is connected to external access networks via a residential gateway (RG), and delivers both high speed Internet and HDTV services together with WiFi and other short-range wireless services to end users by employing the same optical links [86, 146, 147]. Only in such infrastructures, the bandwidth advantage of optical fibres can be utilised to eventually bring the broadband experience to the end users in both baseband and RF domains. This Chapter is dedicated to discuss two possible scenarios of such infrastructures: Section 6.1 presents the multi-standard distribution system of more than one microwave wireless service over a silica MMF infrastructure and Section 6.2 addresses an integrated high capacity wired and wireless multi-standard system over POF [141].

This chapter is based on the results published in [141]

6.1 Multi-standard Wireless Distribution System over MMF

In this section, only multi-standard wireless signal transmission system is considered. The most common RF signals are chosen from today's wireless access services: WiFi, WiMax, UMTS signals and an upcoming short-range wireless service: ultra-wideband (UWB) MB-OFDM signal. Moreover, the market of 50 μm core diameter MMF is increasing worldwide, mainly due to the easy installation of enhanced bandwidth type fibres (OM2 type and above) [144]. Here a performance comparison of multi-standard radio-over-MMF system is presented for various WLAN and WPAN signals.

6.1.1 Experimental setup

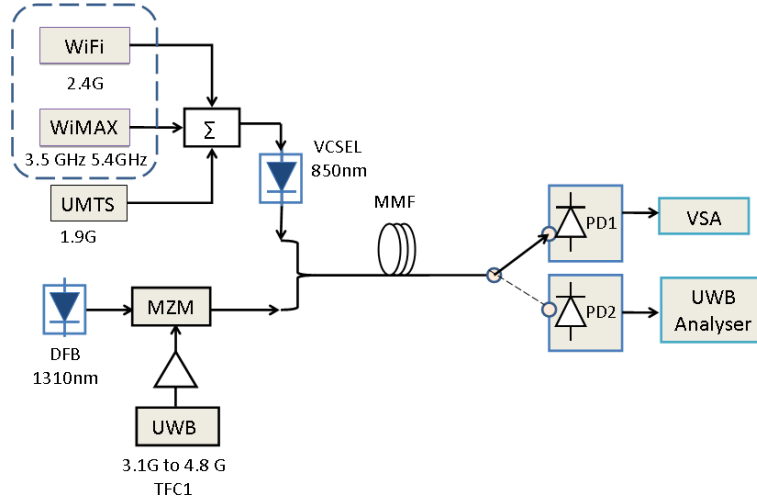


Figure 6.1: Experimental setup: multi-standard MMF system including four wireless services.

The experimental setup for a multi-standard wireless radio-over-fibre (RoF) system is shown in Figure 6.1.¹ Four sets of equipments were employed to generate the electrical wireless signals: a WiFi signal at 2.4 GHz, a WiMax signal at 3.5 or 5.4 GHz, a UMTS signal at 1.9 GHz and an MB-OFDM UWB signal centered at 3.96 GHz with 3 sub-bands (TFC 1: 3.168 to 4.752 GHz). Among these signals, WiFi and WiMax signals were generated by a vector signal generator; the UMTS signal was generated by another vector signal generator and the MB-OFDM UWB signal was generated by a WiMedia-compliant UWB transceiver (Wisair prototype). The WiFi signal was the standard IEEE 802.11n signal with a symbol rate of 50 MSym/s with the modulation format of 16-QAM (corresponding to 200 Mbit/s bit rate). For

¹This experiment was supported by the EU project EURO-FOS, and carried out in University Polytechnic Valencia, Spain, March 2010.

WiMax signal, a similar signal with 50 MSym/s 16-QAM signal at carrier frequency of 3.5 and 5.4 GHz was used. The UMTS signal generated was standard-compliant with a modulation format of QPSK and a chip rate of 3.84 Mc/s.¹ The UMTS signal had a channel bit rate of 5.76 Mbit/s. The MB-OFDM UWB signal was also standard-compliant with the bit rate of 200 Mbit/s.

In this experiment, two different light sources were used to carry the wireless data in order to avoid electrical spectrum overlap between UWB and WiMax signal at 3.5 GHz. An 850 nm VCSEL (output power: -4 dBm) was directly modulated by the WiFi, WiMax and UMTS data while a 1310 nm DFB laser (output power: 8 dBm) was externally modulated by the UWB data. In this experiment an MZM was employed for the feasibility demonstration of the multi-standard MMF system. Before transmission, a multi-mode optical coupler with 50:50 splitting ratio was used to couple the 850 and 1310 nm optical signals to a graded-index OM3 MMF with the core diameter of 50 μm . The input power of the MMF was measured around 0 dBm. The length of the MMF was chosen to be 400, 1100 or 1500 metres. At the receiver side, the wavelength division de-multiplexer was not used due to the large separation of two wavelengths. Instead, followed by a manual switch, two photo-detectors were employed to detect the signal in 850 and 1310 nm bands respectively. However, the signals were transmitted simultaneously through the fibre before being detected. A vector signal analyser and a UWB analyser were used to measure the quality of the signals respectively. In the future work, only one light source would be employed to investigate the robustness of UWB signal with respect to other microwave signals [86]. Moreover, the DFB laser can also be replaced by a directly modulated laser in order to further simplify the system.

6.1.2 Experimental results

The system performance for different signals at different frequencies transported over various lengths of MMF are summarised in Figure 6.2. The measured EVM is plotted as a function of the received optical power. The power of the electrical driving signals were all set to -9 dBm. As shown in Figure 6.2(a), the highest carrier frequency of WiMax signal at 5.4 GHz leads to the worst system performance over MMF due to the bandwidth limitation of MMF. The EVM penalty for WiMax data at 5.4 GHz is observed to be more than 2% with every increase in transmission length from back-to-back to 400 metres as well as from 400 to 1100 metres. The EVM values are more than 20% at 1500 metres case and thus are not plotted in the figure. In contrast, WiMax signals at 3.5 GHz experience a significant degradation from 400 metres transmission to 1100 metres as shown in Figure 6.2(b), while negligible penalty can be seen between 1100 m case and 1500 m case. This is probably due to a transmission dip in the frequency response of the 1100 m MMF around 3.5 GHz.

¹Chip rate is a measure of the speed with which encoding elements, called chips, are generated in direct sequence spread spectrum (DSSS) signals.

6. CONVERGED MULTI-STANDARD IN-BUILDING NETWORKS

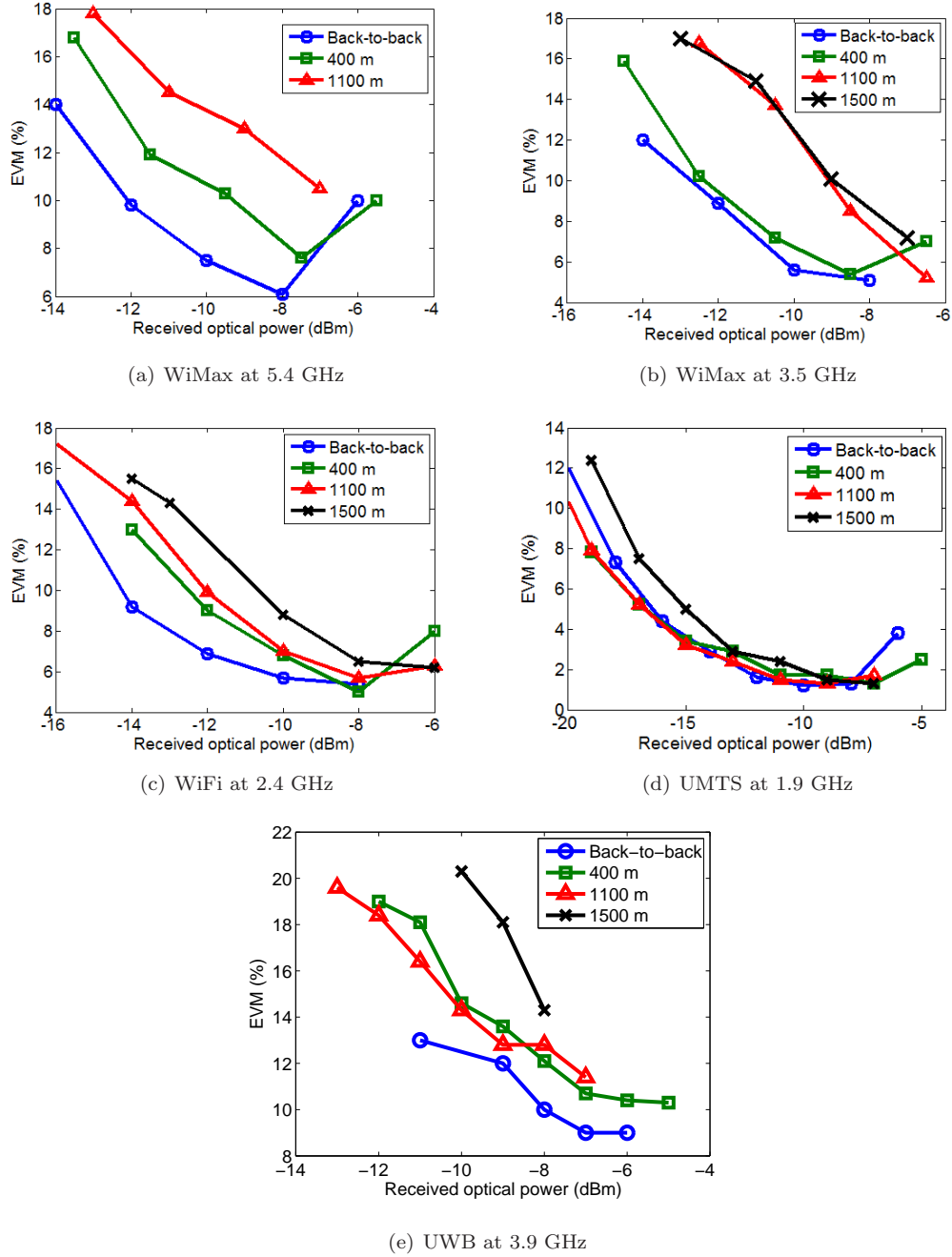


Figure 6.2: System performance of (a) WiMax at 5.4 GHz, (b) WiMax at 3.5 GHz, (c) WiFi at 2.4 GHz, (d) UMTS at 1.9 GHz and (e) UWB at 3.9 GHz, for back-to-back and transmission of 400, 1100 or 1500 metres MMF.

For the WiFi signal, as shown in Figure 6.2(c), the measured performance is similar to the case of the WiMax signal at 5.4 GHz but with less degradation due to a lower carrier frequency at 2.4 GHz, thus less degradation from the MMF bandwidth limitation. Due to an even lower carrier frequency (1.9 GHz) and a less data rate (7.8 Mbit/s) of the UMTS signal, the performance of UMTS is observed as the best among five examined signals as presented in Figure 6.2(d). Less than 2% EVM penalty can be seen even after 1500 m MMF transmission. Note that the EVM requirements for the 16-QAM WiFi and QPSK UMTS signals are 11.2% and 17.5% respectively. In contrast, the EVM requirement for WiMax data is more strict (2.8%). In this experiment, no electrical amplifier was used for the WiFi, WiMax and UMTS signal before modulating the laser and the powers of these three signals were all set as -9 dBm. To achieve a better performance for WiMax signal, a low-noise power amplifier (PA) can be inserted before the modulation of the VCSEL. Finally, Figure 6.2(e) shows the performance of the 3 sub-band UWB signal for different fibre lengths. The EVM requirement for UWB signal is 15.5% (-16 dB). Although the carrier frequency of the UWB signal (3.9 GHz) is relatively high compared to WiFi and UMTS, the system performance still complies with the standards requirement, given the received optical power is sufficiently large (≥ -8 dBm).

In conclusion, the feasibility of transmitting five types of RF signals over a single MMF link simultaneously has been investigated by employing two light sources at 850 and 1310 nm wavelengths. In the comparison of the performance between WiFi, UMTS, UWB signals and WiMax signals at two different frequencies, the UMTS signal has been observed to be the most robust one up to 1500 m fibre link due to its least data rate and lowest carrier frequency, with less than 1% EVM penalty. The WiMax and UWB signals have more EVM penalties due to the relatively large data rates and carrier frequencies. However, all the performance of the investigated RF signals are in line with the standard requirements if the fibre transmission length is less than 1 km. For a typical in-building network, this transmission length is sufficient for a multi-standard RF distribution system to the end users.

6.2 Wired and Wireless Multi-standard System over POF

Besides the multi-standard RoF systems which only convey RF signals, both wired and wireless signals should also be simultaneously transported over fibre infrastructure due to the increasing demand of high-speed internet and HDTV video. Targeting at the home network infrastructure, besides the silica MMFs, the PF GI-POF with a core diameter of $50\text{ }\mu\text{m}$ is also a good candidate thanks to its easy installation and small bending radius. Moreover, the transceivers for PF GI-POF can be identical to the ones used for silica MMF since the core fibre has the same dimension. In this section, the feasibility of simultaneously

6. CONVERGED MULTI-STANDARD IN-BUILDING NETWORKS

transmitting baseband discrete multi-tone (DMT) and UWB MB-OFDM signals over PF GI-POF will be discussed [141].

6.2.1 Experimental setup

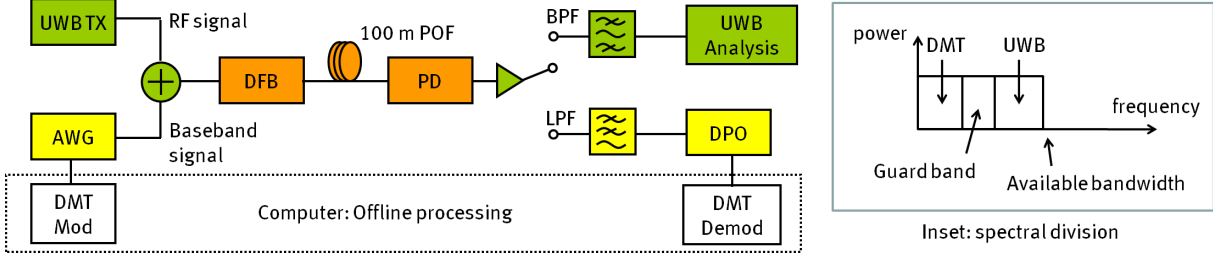


Figure 6.3: Experimental setup: multi-standard 50 μm PF GI-POF system for baseband DMT and UWB radio signals, inset: spectral division to accommodate DMT and UWB signals.

The experimental setup for wired and wireless system over PF GI-POF is shown in Figure 6.3 with an inset figure showing the spectral division scheme for multi-standard data with the guard band in between. The cost-effective intensity modulation and direct detection (IM/DD) approach was chosen to deliver both a baseband and a radio signal. A WiMedia-compliant UWB transmitter from Wisair was used to generate the MB-OFDM signal centered at 3.96 GHz with 3 sub-bands (TFC 1: 3.168–4.752 GHz). In the baseband region, the DMT modulation format with bit-loading was employed to maximise the data rate. Off-line processing was used to generate the DMT signal employing an AWG sampling at 3 GSamples/s. After combining the baseband DMT signal and the UWB radio signal electrically, a DFB laser (model: NTT NLK5B5EBKA) at 1302 nm wavelength was directly modulated to transmit both signals over 100 m long 50 μm core diameter PF GI-POF. The input power to the PF GI-POF link was around 7 dBm. The received optical signal was attenuated and detected by a lens-equipped 21 μm PIN photo-detector with a 62 μm multi-mode pigtail (model: NewFocus 1434-50). After amplification, the two signals were separated using a UWB band-pass filter (BPF) and a 3 GHz low-pass filter (LPF) respectively. The BPF had a central frequency of 4 GHz and a bandwidth of 2 GHz. The filtered signals were demodulated and analysed by a real-time oscilloscope (DPO). The employment of the DMT format enabled efficient utilisation of the available bandwidth up to 1.5 GHz, which was one half of the AWG sampling rate. In this experiment, the AWG sampling rate was set to be relatively small (3 GHz) so that the DMT signal did not occupy the whole bandwidth up to 3 GHz where the UWB signal was located. Therefore, sufficient guard between the DMT and UWB is guaranteed. Future investigation is possible for a smaller guard band. Figure 6.4 shows the received electrical signal before low-pass and band-pass

filtering. Besides the baseband DMT signal, the UWB radio signal from 3.1 GHz until 4.8 GHz can be seen. In this experiment, a manual switch in the receiver side of the link was employed. So the DMT and UWB data were separately demodulated. However, the data were simultaneously transported through the PF GI-POF and the bandpass and low-pass filters in the receiver side were utilised to separate the signals. Replacing the switch by a power divider will make the system more practical, while introducing 3 dB loss in the system. In this experiment, to obtain a higher received SNR the manual switch was temporarily used as shown in Figure 6.3 as a proof-of-concept.

6.2.2 Experimental results and discussion

The spectrum of the received electrical signal is shown in Figure 6.4. As same approach discussed in Chapter 5, the Chow's bit-loading algorithm is employed to efficiently utilise the spectrum of the DMT signal. Due to the channel response at the DMT receiver, the DMT signal experienced low-pass filtering until 3 GHz because of the LPF bandwidth. The UWB spectrum consisted of 3 sub-bands, centered at 4 GHz, corresponding to the time-frequency code 1 (TFC 1) of the WiMedia standard.

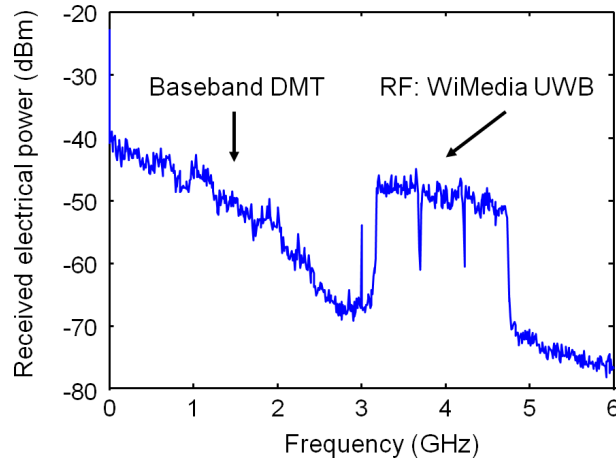


Figure 6.4: Received electrical signal after 100 m PF GI-POF transmission.

Figure 6.5(a) presents the detailed measurement results for the DMT signal using bit-loading. Figure 6.5(a)(upper) shows the bit allocation parameters used in the DMT modulation after 100 m transmission with a received optical power of 1 dBm. In this experiment, 256 sub-carriers are chosen, ranging from 0 to 1.5 GHz. It is seen in Figure 6.5(a)(upper), that 5 bits are allocated per symbol for most of the sub-carriers till the 130th. From the 131th sub-carrier, the bit allocation is set to 4 bits per symbol for most carriers. It should be noted that until the highest sub-carrier index, there are more than 2

6. CONVERGED MULTI-STANDARD IN-BUILDING NETWORKS

bits allocated. Therefore, the spectrum from 1.5 to 3 GHz shown in Figure 6.4 is actually the aliasing signal, which will be filtered out in the demodulation process. A gross bit rate of 6 Gbit/s is achieved by using the DMT format for the baseband signal. Figure 6.5(a)(lower) presents the measured bit error ratio (BER) as a function of sub-carrier index. The overall BER is measured as 4×10^{-5} in Figure 6.5(a), which falls within the forward error correction (FEC) limit of 1×10^{-3} .

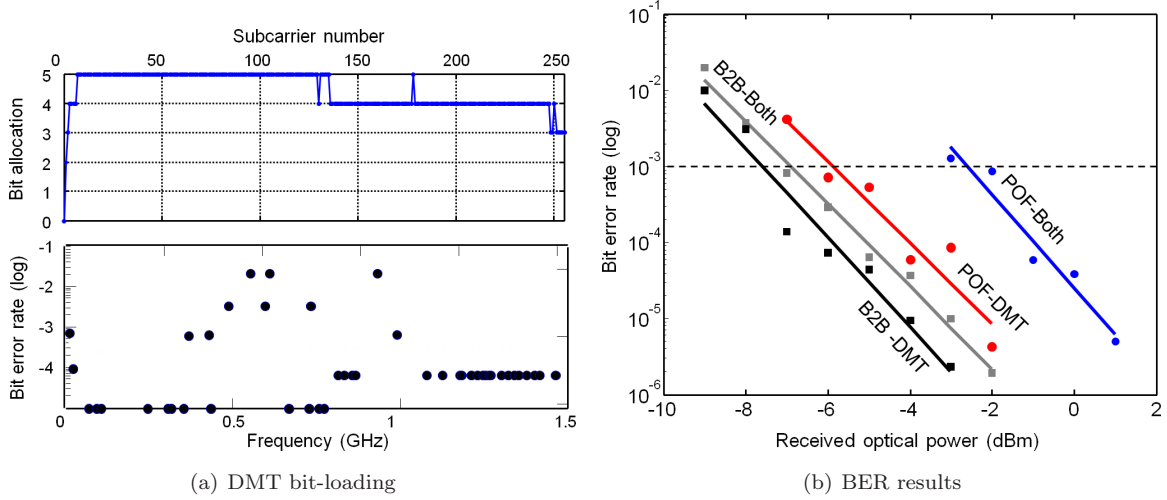


Figure 6.5: (a) Bit-loading parameters and the BER values of the 6 Gbit/s DMT signal vs. frequency, after 100 m PF GI-POF (when DMT and UWB signals coexist in the system) and (b) BER performance of 6 Gbit/s DMT signal; only DMT and DMT together with UWB, for both back-to-back and POF transmission cases.

In Figure 6.5(b), the BER of the DMT signal versus the received optical power for different transmission cases is shown: back-to-back with single or both signals and POF transmission with single or both signals. As indicated in the figure, in back-to-back case there is 1 dB power penalty between transmitting only DMT signal and transmitting both DMT and UWB signals. This penalty is attributed to a higher peak-to-average power ratio (PAPR) of the combined signal modulating the laser, leading to an enhanced nonlinear distortion of the signals. In the future work, carefully choosing of the clipping factors of the signals, the bias of the laser and the driving signal power can reduce such nonlinear distortion. For the case of transmitting only DMT signal over POF, a power penalty of 2 dB compared with the back-to-back case is observed, which is because of the modal dispersion of the PF GI-POF. When launching the UWB signal together with the DMT signal for transmission, the system performance is even more degraded with a power penalty of 4 dB compared with the back-to-back case. This degradation is due to the mixed effect of fibre dispersion and nonlinear distortion of the combined UWB and DMT signals. However,

with the received optical power of -2 dBm it is still possible to have BER of 10^{-3} which is within the FEC limit.

In contrast, Figure 6.6 shows the error vector magnitude (EVM) of the UWB signal as a function of the received optical power for different transmission cases. In the back-to-back case, there is less than 1 dB power penalty between the measurement for only UWB signal and the measurement of both UWB and DMT signals. This is again due to the distortion introduced by the high PAPR of the combined signal. For the same reason, in POF transmission case, the power penalty between the two curves (single UWB curve and both UWB/DMT curve) is less than 2 dB. However, the 100 m POF transmission introduces an EVM penalty of approximately 4 dB for the same optical received powers, because of the fibre modal dispersion. Moreover, in Figure 6.6 the WiMedia standard requirement (-16 dB) is shown as well as the measured electrical back-to-back EVM value. With more than -4 dBm received optical power, the overall EVM penalty of UWB signal after transmission is only around 3 dB, indicating a good system performance of UWB transmission over PF GI-POF.

Finally, in Figure 6.7 the received constellation diagrams are shown after 100 m POF with a received optical power of 0 dBm. For the DMT format, the plotted constellation is the overlap of 50 to 60 sub-carriers where 4 bits are allocated for each carrier; while the UWB constellation is an overlap of all 128 sub-carriers with a modulation format of QPSK. Both of the constellation diagrams indicate the low deviation in the EVM values.

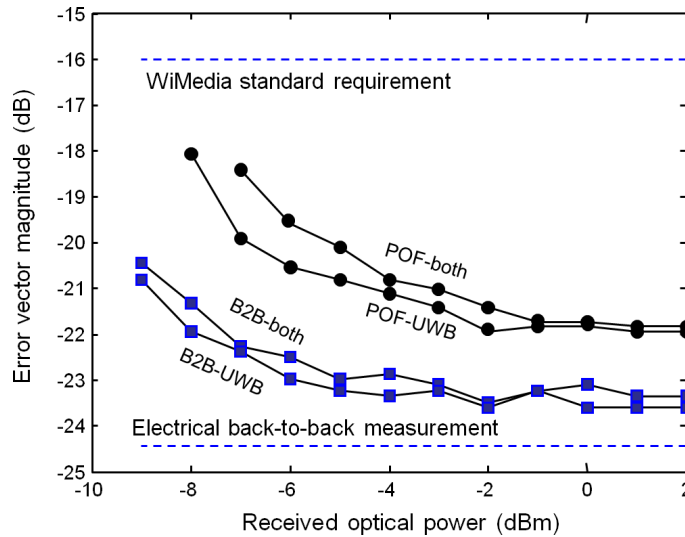


Figure 6.6: EVM performance of UWB signal; only UWB, and UWB together with DMT, for both back-to-back and PF GI-POF transmission cases.

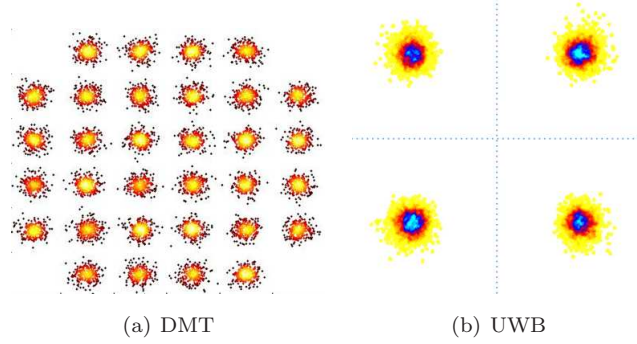


Figure 6.7: Constellation diagrams of the received signal after simultaneous transmission over 100 m POF; (a) DMT and (b) UWB.

6.3 Summary

In this chapter a single fibre infrastructure for in-building networks has been presented, which is able to deliver more than one wireless signal format. In addition, the coexistence of baseband and RF signals in a plastic optical fibre is also presented. In Section 6.1 successful transmission of three microwave services (UMTS, WiFi, WiMax) and one UWB wireless service has been demonstrated at two different wavelengths using different lengths of MMFs. System performance has been compared among all the wireless services for different lengths of fibre links, where UMTS signal experiences the least distortion due to its most narrow bandwidth (7.8 Mbit/s) and UWB (at 200 Mbit/s) is the most distorted signal to be carried through the fibres.

In Section 6.2, by employing DMT and UWB modulation formats, a simultaneous transmission of broadband signal at the baseband and RF over PF GI-POF has been experimentally demonstrated for the first time. The system bandwidth is efficiently employed using the DMT format, thus achieving bit rate of 6 Gbit/s with $\text{BER} < 10^{-3}$. Using the same POF link of 100 metre, 200 Mbit/s WiMedia-compliant UWB signal has also been delivered in coexistence with 6 Gbit/s DMT signal with only 3 dB EVM penalty. This work has demonstrated the feasibility of a POF backbone as a common infrastructure for wired and wireless services for broadband in-building networks. More recently, based on this work, similar investigations on the multi-standard system over PMMA POF have been reported in [149].

Chapter 7

Conclusions and Recommendations

7.1 Summary and Conclusion

Introducing optical fibre and optical techniques in in-building or home networks has been foreseen as a further step of penetrating fibre-optics from the doorstep into the inner building, enabling real broadband communications including both wired and wireless services to the users. In particular, the deployment of low-cost optical fibres, radio-over-fibre and other optical techniques offer an electro-magnetic interference (EMI) immunity, cost-effective and large bandwidth optical backbone to deliver multi-standard signals over a single physical infrastructure with certain service delivery mechanisms management such as broadcast-and-select or optical routing. In the framework of such optical solutions for future broadband in-building networks, the topics that have been investigated in this thesis are summarised in Table 7.1.

The transmission techniques for RF signals have been discussed in Chapter 2 and 3 in this thesis. First, the principle of the optical frequency multiplication (OFM) was explained in the frequency domain analysis in Chapter 2. The frequency domain approach provides a good insight into the harmonic generation by the means of heterodyne beating of the Bessel-valued harmonics. It has been mathematically proved that, in a phase-modulation and direct-detection system, the absence of the optical filter results in a cancelation of all the beating products in the frequency domain and only gives a DC component at the output of the photo-detector. However, with an optical filter, different orders of Bessel components in the frequency domain are distorted and the beating effect of the components leads to a series of OFM harmonics at higher frequencies. The phase noise of the generated harmonics linearly depends on the phase noise of the sinusoidal signal by a multiplication factor of p , which is the order of the harmonic. The transmission of RF signal over optical fibre by employing the OFM approach has been presented in Chapter 2. The use of multi-carrier SCM has been investigated in an OFM system employing MMF.

7. CONCLUSIONS AND RECOMMENDATIONS

Transmission of more than 210 Mbit/s 64-QAM data in the SCM format with 18 GHz sub-carrier frequency over 4.4 km MMF has been demonstrated. The impact of parameters in the SCM configuration on the performance of such multi-carrier RoF system has also been investigated. It has been found that the system performance is not affected by the number of sub-carriers but only depends on the total transmitted bit rate. A linear relation between the EVM values and the total bit rate has been found by the measurements, despite the number of carriers employed in SCM. In Chapter 2 the impact of the transmitter nonlinearity on the multi-carrier RoF system employing OFM has been investigated. A comparative study on OFDM and single-carrier QAM has been conducted to examine the effect of modulation format on the system performance. Both analytical and experimental results indicate that an OFDM signal is less tolerant to transmitter nonlinearity than the single-carrier format. By employing an MZM as the external modulator and keeping the received optical power less than 0 dBm, a 2 dB power difference has been observed for an EVM penalty of 1% between OFDM and single-carrier QAM signal. In Chapter 2, only microwave services have been considered and the transmission medium is silica MMF with a 50 μm core diameter.

After the investigation of the transmission technique for microwave RF services employing OFM, in Chapter 3, a simpler technique, intensity modulation and direct detection, has been presented for the transmission of ultra-wideband (UWB) signals in the format of MB-OFDM via another type of low-cost fibre, plastic optical fibre (POF). A UWB signal in baseband has been transmitted over the bandwidth-limited PMMA GI-POF. Only the bandwidth and the number of carriers are compliant with the UWB industry standard. However, by using the off-line processing in an AWG and DPO, a very large SNR of the signal has been realised yielding a large transmission capacity for the proposed PMMA POF system. 2.1 Gbit/s was achieved by employing a visible light VSCEL and an APD receiver with a bit error ratio of 10^{-3} . This error ratio can be seen to be error-free after implementation of FEC algorithm. In Section 3.3, the system has been improved in such a way that the transmitted UWB signal is totally standard-compliant according to ECMA-368 or Wireless-USB standard. The author believes this is the first demonstration of standard-compliant UWB services over low-cost 1 mm PMMA GI-POF. The last part of Chapter 3 is dedicated to bi-directional transmission of UWB signals over PF GI-POF system. A full-duplex bi-directional transmission over a single fibre has been experimentally shown for the first time. The coexistence of two UWB sub-bands centered at 3.4 GHz and 4.5 GHz has been shown for down- and up-link respectively, leading to a very small transmission penalty in EVM (1 and 2%) with and without POF.

Chapter 4 presents the network functionality of an RoF system, namely the traffic routing and dynamic capacity allocation by employing SOA-based wavelength conversion. After a brief introduction of SOA-

Transmission in RoF system	<ul style="list-style-type: none"> • optical frequency multiplication approach for narrow-band signals (using MMF): > 200 Mbit/s 64-QAM signal over 4.4 km MMF at 18 GHz. • intensity modulation and direct detection for ultra-wideband signals (using POF): 200 Mbit/s UWB signal over 100 m large core POF, bidirectional UWB over PF POF. 	Chapter 2 and 3
Routing of RoF system	<ul style="list-style-type: none"> • XGM-based wavelength conversion and SCM addressing (using MMF, SMF): 36 Mbit/s OFDM signal over 950 m MMF with mid-span routing. • inter-room cross-connect for UWB services (proposed). 	Chapter 4
Baseband transmission over POF	<ul style="list-style-type: none"> • DMT system on different types of photo-detector (using 1 mm core diameter PMMA POF): 4.5 Gbit/s over 50 m using APD; 6 Gbit/s over 35 m using PIN. • DMT system on different types of POF (using 1 mm multi-core, single-core SI- or GI-PMMA and 50 μm PF POF): 2 Gbit/s over single core SI-POF, 4.7 Gbit/s over multi-core SI-POF, 5.5 Gbit/s over single core GI-POF, 47.4 Gbit/s over PF GI-POF. 	Chapter 5
Multi-standard transmission	<ul style="list-style-type: none"> • wireless multi-standard system (using MMF): Standard WiFi, WiMax, UMTS and UWB coexistent over up to 1 km MMF. • wired and wireless dual-standard system (using POF): 6 Gbit/s baseband DMT and 200 Mbit/s UWB coexistent over 100 m PF POF. 	Chapter 6

Table 7.1: Summary of the topics investigated in this thesis

7. CONCLUSIONS AND RECOMMENDATIONS

based cross-gain modulation (XGM), an RoF system with a mid-span optical routing has been presented in Section 4.2. It has been demonstrated that the RF services generated by the OFM approach can be routed by means of the desired wavelength and the wavelength conversion based on SOA XGM is totally transparent for the format of analogue signals. A 52 sub-carrier OFDM signal of 36 Mbit/s has been transmitted over 950 m MMF at 18.3 GHz with an overall EVM penalty of less than 3%. In Section 4.3, another routing demonstration employing electrical SCM and optical wavelength conversion has been proposed and investigated. The parameters of the SCM have been investigated for the wavelength conversion. For a data rate of 192 Mbit/s over 16 sub-carriers, an EVM value of 5.8% has been obtained at a received optical power of -3 dBm. The combination of SCM and optical wavelength conversion enables a larger flexibility for the signal routing in RoF networks by adding one more dimension of freedom, namely electrical frequencies. Finally in Chapter 4, the scenario of an inter-room communication of UWB services for PAN in RoF system has been proposed including up-links, down-links and optical cross-connect. The proposed experimental setup consists of 2 rooms interacting to each other based on the wavelength conversion technique. However, due to the large complexity of the optical cross-connect unit and the nature of the PAN communication, higher layer control in a time-division multiplexing manner may be considered in practice. Future work can be continued in this direction towards an experimental demonstration of the proposed system.

Apart from the RoF system discussed in Chapter 2, 3 and 4, future broadband in-building services should also be provided by baseband data streams from and to the end users such as HDTV, Ethernet, etc. Therefore, Chapter 5 is dedicated to the baseband transmission in in-building optical backbone networks. Apparently, the transmission backbone for an in-building network should maintain flexibility in deployment and inexpensive while at the same time be able to provide multi-Gbit/s capacity as well as transport baseband and RF signals. The above characteristics can be found in POF cable, especially 1 mm PMMA POF for baseband and IF data transmission or 50 μ m PF GI-POF for baseband and RF data. Chapter 5 has investigated the feasibility of delivering multi-Gbit/s, 10 Gbit/s or even above 40 Gbit/s via POF links by employing the advanced modulation format discrete multi-tone (DMT) technique. Different system components have been examined including photo-detector and several types of POF (i.e. 1 mm SI-, GI- or multi-core SI-POF). By employing an APD receiver and 1 mm PMMA GI-POF, 4.6 Gbit/s transmission has been demonstrated for a 50 m POF link. In contrast, a PIN photodiode having a slightly larger bandwidth than APD leads to 6 Gbit/s transmission over 35 m long 1 mm core diameter PMMA GI-POF. An interesting comparison has been made in Section 5.2.3 between an APD and a PIN photodiode. It is concluded that for PMMA POF system, a PIN photodiode is recommended over APD from both the system performance and power consumption respect. Nevertheless, the integrated

trans-impedance amplifier (TIA) of a PIN receiver is desired to improve the power budget of the system. This thesis has also investigated a new type of PMMA POF, namely multi-core SI-POF. A comparison is presented in Section 5.3 to discuss the performance of multi-core SI-POF, single-core SI-POF and single-core GI-POF. 4.7 Gbit/s transmission capacity has been demonstrated by using 19-core, in total 1 mm core diameter PMMA POF for 50 m link. The transmission capacity is more than twice the rate of a 1 mm single-core SI-POF. The performance of multi-core SI-POF has also been compared with a 1 mm single-core GI-POF, resulting in a capacity difference of only 0.7 Gbit/s for a 50 m link. In Section 5.4, DMT transmission employing PF GI-POF with 50 μm core diameter has also been addressed. The data rate as high as 47 Gbit/s has been demonstrated for PF GI-POF due to its large bandwidth. Considering the features of PF GI-POF such as core diameter, attenuation and modulation bandwidth, the PF GI-POF is closer to silica MMF rather than the POF made by PMMA material. However, the significant advantage in small bending rate of the PF GI-POF makes it very suitable for in-building networks.

Finally in Chapter 6, the converged multi-standard operation for in-building networks has been presented. By combining different wireless standard services and high capacity baseband signal, Chapter 6 demonstrates an integrated network operating over a single physical backbone. In Section 6.1 various wireless services (both narrow-band and wide-band) have been integrated over MMF by using two wavelength windows and two modulation schemes (direct modulation of VCSEL and external modulation). Successful transmission of four wireless signal types, UMTS, WiFi, WiMax and UWB signals have been demonstrated. In comparison, Section 6.2 presents a more challenging proposal and a demonstration for transmission of both multi-tone wired and ultra-wideband multi-tone wireless services over PF GI-POF. A 6 Gbit/s baseband DMT signal has been successfully transmitted simultaneously with a UWB MB-OFDM wireless signal of 200 Mbit/s over 100 m PF GI-POF. The received UWB signal was also well in line with the standard WiMedia requirement with an EVM value of -22 dB. Further investigation of the same concept has also been shown for 1 mm PMMA POF [149].

As been discussed in this thesis, optical techniques for broadband in-building networks can be concluded as follows.

- optical fibre, especially low-cost silica MMF and POF;
- optical generation of microwave carriers;
- intensity modulation and direct detection;
- wavelength conversion technique by XGM in SOA;
- advanced modulation formats applied to optical communications for wired transmission of services;

7. CONCLUSIONS AND RECOMMENDATIONS

- wavelength division multiplexing technique;
- other optical techniques

These listed techniques have shown their attractive and powerful advantages to overcome the bottleneck of broadband in-building networks which is in contrast to their counterparts in the electrical domain such as twisted copper pair or Cat. 5 cable. Besides the very high data rate realised over the optical fibre backbone network, integrated and converged service delivery can be easily conveyed in the optical backbone in a considerably cost-effective manner as well. In addition to that, a single optical infrastructure offers more advantages in the network maintenance and management, compared with the situation of having more than two or three different operating networks in nowadays in-building environment.

7.2 Outlook and Future Work

Many challenges are still existing in the potential solution of using optical techniques for in-building networks. First of all, carrying services at high frequency carriers such as 40 GHz or beyond 60 GHz has an inherent issue with uplink modulation and transmission in RoF systems. For the downlink connection, the transmitter is located at residential gateway so that the devices can be shared among several users. Therefore, the cost of the downlink transmitter is not as critical as that of the uplink. For the uplink, due to the fact that nobody else could pay for the home network device but only the subscriber himself, the cost requirement for RAU in the RoF system remains very strict. Therefore, only intensity modulation and direct detection should be considered. However, to modulate a high frequency millimeter wave RF signal, the electrical bandwidth of the external optical modulator or laser should be considerably large thus leading to relatively expensive installation and maintenance. Low-cost solutions have been proposed by remote delivery of the uplink carrier wavelength [150] or by replacing the transceiver using a reflective-SOA (RSOA) [151] to simplify the RAUs in the system. Nevertheless, the whole system cannot be symmetric between up- and down-links in terms of complexity and functionality. Therefore, the cost concern would be the most significant factor to be considered for a practical RoF system with the top priority.

Second, regarding the low-cost infrastructure of POF, today's status of the POF application remains in the point-to-point system. There have been a lot of discussions on POF networking [152, 153] by employing POF splitters and couplers. However, due to the extra high loss of such devices, the high power budget of such POF networks severely limit the system performance. POF couplers and splitters are expected to be improved by the POF device manufactures. Another similar issue with a PMMA

POF system is the bandwidth of the visible light, large area photo-detector (PD). As has been seen in Chapter 5, the system bandwidth is more limited by the PD bandwidth instead of by the POF itself. To extend the bandwidth limitation of PMMA POF system from 1 GHz to, for instance, 3 GHz, the bandwidth of the PD is a major issue to be solved by the device manufactures in the near future. Moreover, the results reported in Chapter 5 were obtained with non-perfect devices, such as VCSEL wavelength misalignment and noisy receivers. Therefore the use of 650 nm VCSEL and low noise receivers such as A³PICS series [154] would improve the SNR by several dB each furthermore.

As discussed in Chapter 5, DMT format plays an important role in the multi-Gbit/s transmission over short-range POF links. In these IM/DD optical communication systems employing advanced modulation formats such as DMT and OFDM, electrical clipping is essential to reduce the peak-to-average power ratio (PAPR) for operating in the linear regime of the signal modulation. However, the clipping noise given by a large crest factor in such modulation schemes will reduce the modulation depth and therefore degrading the receiver performance, hence the link margins [155]. On the other hand, conventional multi-level modulation formats such as pulse amplitude modulation (PAM), e.g. 4-PAM, do not suffer from the effects of PAPR and could also provide transmission systems with an improved spectral efficiency. Therefore, for certain system designs, an m-PAM scheme could provide higher link margins compared to the DMT format for the similar channel bandwidth-bitrate ratio and the bit-error probability [155]. Interesting experimental verification can be conducted with respect to the theory proposed in [155] to find the optimum modulation format for IM/DD short-range optical communications.

Another issue in network layer for low-cost multimode infrastructures is the mode compatibility. Supposing the fibre deployment from the home gateway to the end users makes use of multimode silica or plastic fibres so that more than one mode (i.e. 10 or 20 modes) are active in the transmission fibre. However, in the cross-connect unit at the gateway, most of the active networking devices such as wavelength convertors require single-mode operation as discussed in Chapter 4. To avoid the mode filtering in the system, the network should confine itself to either all-single-mode or all-multi-mode operations [150]. However, for all multi-mode operation the network functionality is largely reduced because of the component limitation of the passive devices. Finally, a common open question is the integration of IP layer protocol and the physical layer infrastructure [56, 156]. This is a typical inter-disciplinary area where the gap between higher network layers and the physical layer should be resolved. Furthermore, characterisation of the signal quality should not only limit to SNR or EVM values. More requirements such as noise level, adjacent channel leakage ratio (ACLR), peak code domain error (CDE) and etc. need to be considered as well in the future radio-over-fibre research.

7. CONCLUSIONS AND RECOMMENDATIONS

In conclusion, in spite of the challenges stated above, optical techniques discussed in this thesis have shown a great potential to enable future broadband in-building networks. In the future they will be very strong candidates to support a converged broadband infrastructure to provide multi-standard services, in an energy-efficient and cost-effective way, to wired and wireless user terminals for the next generation in-building networks.

Appendix A

Modeling of XGM Effect on an Analogue RF Signal in SOA

Direct Modulation of a Laser using RF signal The laser rate equation with one mode is given by

$$\begin{aligned}\frac{dS}{dt} &= (\Gamma g - \frac{1}{\tau_p})S \\ \frac{dN}{dt} &= \frac{I}{e} - \frac{N}{\tau_c} - \Gamma g S \\ g &= \xi(N - N_t)\end{aligned}\tag{A.1}$$

where S and N are the photon and carrier density respectively, Γ is the confinement factor, g is the gain of the laser, τ_p is the photon lifetime, τ_c carrier lifetime, I is the injected current, ξ is the differential gain coefficient, and N_t is the carrier density at transparency. In this analysis, the injected current to modulate the laser take the form of

$$I = I_0 + \epsilon I_{QAM}(t)\tag{A.2}$$

where I_0 is the DC level, I_{QAM} is the modulation part, and ϵ is related to the modulation index.

By using the perturbation approach, we are searching for solutions having the form of [111]

$$\begin{aligned}S(t) &= S_0 + \epsilon S_1(t) + \epsilon^2 S_2(t) + \dots \\ N(t) &= N_0 + \epsilon N_1(t) + \epsilon^2 N_2(t) + \dots\end{aligned}\tag{A.3}$$

A. MODELING OF XGM EFFECT ON AN ANALOGUE RF SIGNAL IN SOA

Substitute Equation A.3 into the laser rate equations Equation A.1, we have [111]

$$\begin{aligned}\frac{dS_0}{dt} + \epsilon \frac{dS_1}{dt} + \dots &= (\Gamma\xi[N_0 - \epsilon N_c(t) + \dots - N_t] - \frac{1}{\tau_p}) \cdot (S_0 + \epsilon S_1(t) + \dots) \\ \frac{dN_0}{dt} + \epsilon \frac{dN_1}{dt} + \dots &= \frac{I_0 + \epsilon I_{QAM}(t)}{e} - \frac{N_0 + \epsilon N_1(t) + \dots}{\tau_c} - \Gamma\xi[N_0 + \epsilon N_1(t) - N_t](S_0 + \epsilon S_1(t) + \dots)\end{aligned}\quad (\text{A.4})$$

By solving Equation A.4 in the steady state, the solution is given by [111]

$$\begin{aligned}S_0 &= \tau_p \left(\frac{I_0}{e} - \frac{N_t}{\tau_c} - \frac{1}{\Gamma\xi\tau_p\tau_c} \right) \\ N_0 &= N_t + \frac{1}{\Gamma\xi\tau_p}\end{aligned}\quad (\text{A.5})$$

Recognising that the terms with the first order of ϵ in Equation A.4 have to be equal, we have the first order solution given by [111]

$$\begin{aligned}S_1(t) &= S_{1h}(t) + S_{1p}(t) \\ &= C_1 e^{\alpha t} \Gamma\xi \cos(\beta t) + C_2 e^{\alpha t} \Gamma\xi S_0 \sin(\beta t) + P_1(t) e^{i\omega_c t} + Q_1(t) e^{-i\omega_c t}\end{aligned}\quad (\text{A.6})$$

where β and ω_c are the modulation index and the carrier frequency of the QAM-formatted RF signal, and α is the loss of the waveguide. The terms with $P_1(t)$ and $Q_1(t)$ present the RF carrier phase shift of the QAM signal.

XGM for QAM-format RF Signal The SOA rate equation for the carrier number can be written as

$$\begin{aligned}\frac{dN}{dt} &= \frac{I}{e} - \frac{N}{\tau_c} - \Gamma v_g g(S_{QAM} + S_{CW}) \\ g &= \xi(N - N_t)\end{aligned}\quad (\text{A.7})$$

Similarly as with the previous derivation, we have the solution

$$N(t) = M_0 + \epsilon(M_h(t) + V e^{i\omega t} + W e^{-i\omega t}) \quad (\text{A.8})$$

In the meantime, the SOA rate equation for the photon number of the wavelength-converted signal can be written as

$$\begin{aligned}\frac{dS_{CW}}{dz} &= (\Gamma g - \alpha_{int}) S_{CW} \\ g &= \xi(N - N_t)\end{aligned}\quad (\text{A.9})$$

Using Equation A.8 in Equation A.9, we finally have the solution for the wavelength-converted signal through XGM as following [111]

$$S_{CW}(z, t) = S_{CW} e^{(\Gamma\xi[M_0 - N_t] - \alpha_{int})z} + \Gamma\xi M_1(t) S_{CW} z e^{(\Gamma\xi[M_0 - N_t] - \alpha_{int})z} + \dots \quad (\text{A.10})$$

Appendix B

UWB WiMedia Analysis Report

Parameters	Received signal	Test criteria
EVM (band 3, RMS)	−16.21 dB	−16 dB (PASS)
Frequency tolerance	−6.702 ppm	0 ± 20 ppm (PASS)
Preamble sync (sym. 1)	95.74%	$\geq 87\%$ (PASS)
ACPR (band3-1, band3-2)	32.72 dB, 28.59 dB	≥ 20 dB (PASS)
Spectral mask hit	0	no mask hit (PASS)
Rel. Pwr, PS/FS-CE	−0.143 dB	0 ± 2 dB (PASS)
Rel. Pwr, PS/FS-PLCP	0.053 dB	0 ± 2 dB (PASS)
Rel. Pwr, PS/PF-Payload	−0.035 dB	0 ± 2 dB (PASS)
Rel. Pwr, CE-PLCP	0.196 dB	0 ± 2 dB (PASS)
Rel. Pwr, CE-Payload	0.109 dB	0 ± 2 dB (PASS)
Rel. Pwr, PLCP-Payload	−0.088 dB	0 ± 2 dB (PASS)

Table B.1: Summary of the analysis report for the received MB-OFDM signal after 50 m PMMA POF transmission, corresponding to the result shown in Figure 3.8(a).

B. UWB WIMEDIA ANALYSIS REPORT

References

- [1] B. Reboul. A Global Overview of FTTH. In *FTTH Council APAC Annual Conference*, Seoul, May 2010. available on-line at www.ftthcouncilap.org. 1
- [2] L. Hutcheson. FTTH/FTTB in Asia-Pacific. In *FTTH Conference 2009 FTTH In Asia Pacific*, Melbourne, May 2009. available on-line at www.ftthcouncilap.org. 1
- [3] N. Anderson. Who's #1 in broadband? 1 Gbps fiber for \$26 in hong kong, Apr. 2010. available on-line at <http://arstechnica.com/>. 1
- [4] M. Popov. Qos provisioning in home networks: how to integrate fiber, wireless and all the others. In *Optical Fiber Communication (OFC), collocated National Fiber Optic Engineers Conference, 2010 Conference on (OFC/NFOEC)*, Mar. 2010. 1
- [5] H. Al-Raweshidy and S. Komaki. *Radio Over Fiber Technologies for Mobile Communications Networks*. Artech House, 2002. 2
- [6] A.M.J. Koonen and A. Ng'oma. *Integrated broadband optical fibre/wireless LAN access networks, in Broadband Optical Access Networks and Fiber-to-the-Home: System Technologies and Development Strategies*. Wiley, 2006. 2, 13
- [7] A.M.J. Koonen, H. van den Boom, E. Tangdionga, H.D. Jung, and P. Guignard. Designing in-building optical fiber networks. In *Optical Fiber Communication (OFC), collocated National Fiber Optic Engineers Conference, 2010 Conference on (OFC/NFOEC)*, pages 1 –3, Mar. 2010. 2, 7, 9
- [8] The Working Group for WLAN Standards. Wireless Local Area Networks. available on-line at <http://www.ieee802.org/11/>. 3
- [9] IEEE 802.15 WPAN Task Group 1. IEEE 802.15.1 Standard for Wireless Personal Area Networks. available on-line at <http://www.ieee802.org/15/>. 3

REFERENCES

- [10] IEEE 802.16 WPAN Working Group on Broadband Wireless Access Standards. IEEE 802.16 Standard for Wireless Metropolitan Area Networks. available on-line at <http://www.ieee802.org/16/>. 3
- [11] IEEE 802.15 WPAN Task Group 3. IEEE 802.15.1 Standard for High Data Rate Wireless Personal Area Networks. available on-line at <http://www.ieee802.org/15/>. 3
- [12] J.E. Mitchell. Radio over fibre networks: Advances and challenges. In *Optical Communication, 2009. ECOC '09. 35th European Conference on*, pages 1 –4, Sep. 20-24 2009. 4
- [13] D. Wake. Trends and prospects for radio over fibre picocells. In *Microwave Photonics, 2002. International Topical Meeting on*, pages 21 – 24, Oct. 5-8 2002. 4
- [14] IOP Generic Communication. Future home networks. <http://www.senternovem.nl>. 4, 7, 51, 65, 66
- [15] P. Hartmann, X. Qian, R.V. Penty, and I.H. White. Broadband multimode fibre (MMF) based IEEE 802.11a/b/g WLAN distribution system. In *Microwave Photonics, 2004. MWP'04. 2004 IEEE International Topical Meeting on*, pages 173 – 176, Oct. 4-6 2004. 5
- [16] T. Kuri, K. Kitayama, A. Stohr, and Y. Ogawa. Fiber-optic millimeter-wave downlink system using 60 GHz-band external modulation. *Lightwave Technology, Journal of*, 17(5):799 –806, May 1999. 5
- [17] P.A. Rosher, M.K. Compton, and A.D. Georgiou. Dispersive considerations in microwave optical systems. In *Microwave Optoelectronics, IEE Colloquium on*, pages 12/1 –12/6, Oct. 26 1990. 6
- [18] A. Ng'oma and M. Sauer. Opportunities and challenges in optical generation and distribution of 60 GHz wireless signals. In *Microwave Conference, 2008. APMC 2008. Asia-Pacific*, pages 1 –4, Dec. 2008. 6
- [19] G.H. Smith, D. Novak, and Z. Ahmed. Overcoming chromatic-dispersion effects in fiber-wireless systems incorporating external modulators. *Microwave Theory and Techniques, IEEE Transactions on*, 45(8):1410 –1415, Aug. 1997. 6
- [20] B. Davies and J. Conradi. Hybrid modulator structures for subcarrier and harmonic subcarrier optical single sideband. *Photonics Technology Letters, IEEE*, 10(4):600 –602, Apr. 1998. 6
- [21] A. Stöhr, R. Heinzelmann, A. Malcoci, and D. Jager. Optical heterodyne millimeter-wave generation using 1.55 μm traveling-wave photodetectors. *Microwave Theory and Techniques, IEEE Transactions on*, 49(10):1926 –1933, Oct. 2001. 6

-
- [22] R.P. Braun, G. Grosskopf, D. Rohde, and F. Schmidt. Low-phase-noise millimeter-wave generation at 64 GHz and data transmission using optical sideband injection locking. *Photonics Technology Letters, IEEE*, 10(5):728–730, May 1998. 6
- [23] L.N. Langley, M.D. Elkin, C. Edge, M.J. Wale, U. Gliese, X. Huang, and A.J. Seeds. Packaged semiconductor laser optical phase-locked loop (OPLL) for photonic generation, processing and transmission of microwave signals. *Microwave Theory and Techniques, IEEE Transactions on*, 47(7):1257–1264, Jul. 1999. 6
- [24] L.A. Johansson and A.J. Seeds. Generation and transmission of millimeter-wave data-modulated optical signals using an optical injection phase-lock loop. *Lightwave Technology, Journal of*, 21(2):511–520, Feb. 2003. 6
- [25] N.G. Walker, D. Wake, and I.C. Smith. Efficient millimetre-wave signal generation through FM-IM conversion in dispersive optical fibre links. *Electronics Letters*, 28(21):2027–2028, Aug. 1992. 6
- [26] Y. Le Guennec, G. Maury, J. Yao, , and B. Cabon. New optical microwave up-conversion solution in radio-over-fiber networks for 60-GHz wireless applications. *Lightwave Technology, Journal of*, 24(3):1277–1282, Mar. 2006.
- [27] A. Ng’oma. *Radio over Fiber Technology for Broadband Wireless Communication Systems*. PhD thesis, Eindhoven University of Technology, Department of Electrical Engineering, 2005. 13, 16, 58
- [28] A.M.J. Koonen and M.G. Larrode. Radio-over-MMF Techniques Part II: Microwave to millimeter-wave systems. *Lightwave Technology, Journal of*, 26(15):2396–2408, Aug. 2008. 6, 7, 13, 58
- [29] G.K. Chang, J. Yu, and Z. Jia. Architectures and enabling technologies for super-broadband radio-over-fiber optical-wireless access networks. In *Microwave Photonics, 2007 IEEE International Topical Meeting on*, pages 24–28, Oct. 3-5 2007. 7
- [30] R.A. Griffin, P.M. Lane, and J.J. O’Reilly. Radio-over-fiber distribution using an optical millimeter-wave/DWDM overlay. In *Optical Fiber Communication Conference, 1999, and the International Conference on Integrated Optics and Optical Fiber Communication. OFC/IOOC ’99. Technical Digest*, volume 2, pages 70–72 vol.2, 1999. 7
- [31] P.O. Hedekvist, B.E. Olsson, and A. Wiberg. Microwave harmonic frequency generation utilizing the properties of an optical phase modulator. *Lightwave Technology, Journal of*, 22(3):882–886, Mar. 2004. 7

REFERENCES

- [32] G. Qi, J. Yao, J. Seregelyi, S. Paquet, and C. Belisle. Optical generation and distribution of continuously tunable millimeter-wave signals using an optical phase modulator. *Lightwave Technology, Journal of*, 23(9):2687 – 2695, Sep. 2005. 7, 15
- [33] A.M.J. Koonen, A. Ng’oma, H. van den Boom, I. Monroy, P. Smulders, and G. Khoe. Carrying microwave signals in a GIPOF-based wireless LAN. In *POF 2001*, 2001. 7, 8, 13
- [34] R. Davey, J. Kani, F. Bourgart, and K. McCammon. Options for future optical access networks. *Communications Magazine, IEEE*, 44(10):50 –56, Oct. 2006. 7
- [35] A.M.J. Koonen. Trends in optical access and in-building networks. In *Optical Communication, 2008. ECOC 2008. 34th European Conference on*, pages 1 –31, Sep. 2008. 7
- [36] A.M.J. Koonen, H. Yang, H.D. Jung, Y. Zheng, J. Yang, H.P.A. van den Boom, and E. Tangdiongga. Recent research progress in hybrid fiber-optic in-building networks. In *Opto-Electronics and Communications Conference, 2008 and the 2008 Australian Conference on Optical Fibre Technology. OECC/ACOFT 2008. Joint conference of the*, pages 1 –2, Jul. 2008. 7
- [37] Z. Genc, G.M. Olcer, E. Onur, and I. Niemegeers. Improving 60 GHz indoor connectivity with relaying. In *Communications (ICC), 2010 IEEE International Conference on*, pages 1 –6, May 23-27 2010. 8
- [38] L. Ding, T. Melodia, S.N. Batalama, J.D. Matyjas, and M.J. Medley. Cross-layer routing and dynamic spectrum allocation in cognitive radio Ad Hoc networks. *Vehicular Technology, IEEE Transactions on*, 59(4):1969 –1979, May 2010. 8
- [39] O. Ziemann, P.E. Zamzow, and W. Daum. *POF Handbook: optical short range transmission systems*. Springer, 2001. 8, 9, 10, 77
- [40] <http://www.byteflight.com/>. 8
- [41] Intel Corp. Industry Leaders Develop: Superspeed USB Interconnect, 2007. available on-line at <http://www.usb.org/home>. 8
- [42] B. Wittmann, M. Johnck, A. Neyer, F. Mederer, R. King, and R. Michalzik. POF-based interconnects for intracomputer applications. *Selected Topics in Quantum Electronics, IEEE Journal of*, 5(5):1243 –1248, Sep. 1999. 8

-
- [43] J. Lambkin. In-home plastic optical fibre (POF) networks: Redefining the X in FTTX. In *Transparent Optical Networks, 2008. ICTON 2008. 10th Anniversary International Conference on*, volume 2, pages 202 –202, Dec. 22-26 2008. 8
- [44] M. O’Gorman, M. Scholles, and J. Faller. Simply POF: High-end Connectivity with Plastic Optical Fiber, White Paper. available on-line at <http://www.firecomms.com>.
- [45] I. Möllers, D. Jager, R. Gaudino, A. Nocivelli, H. Kragl, O. Ziemann, N. Weber, T. Koonen, C. Lezzi, A. Bluschke, and S. Randel. Plastic optical fiber technology for reliable home networking: overview and results of the EU project POF-ALL. *Communications Magazine, IEEE*, 47(8):58 –68, Aug. 2009. 36
- [46] B. Rollins and A. Mallya. Options for Current and Future POF Home Networks, 2010. available on-line at <http://www.comoss.com/press>. 8
- [47] K. Makino, T. Ishigure, and Y. Koike. Waveguide parameter design of graded-index plastic optical fibers for bending-loss reduction. *Lightwave Technology, Journal of*, 24(5):2108 – 2114, May 2006. 9
- [48] <http://www.firecomms.com/>. 9
- [49] H.A. Hmida, G.C. Cordner, A. Amer, and F.F. Shalan. FTTH design and deployment guidelines for civil work, fiber distribution and numbering. In *Optical Fiber Communication Conference, 2006 and the 2006 National Fiber Optic Engineers Conference. OFC 2006*, page 10 pp., Mar. 5-10 2006. 9
- [50] Jeffrey Lee. *Discrete multitone modulation for short-range optical communications*. PhD thesis, Eindhoven University of Technology, Department of Electrical Engineering, 2009. 10, 70, 71, 80, 82, 83, 88
- [51] H. Yang, M.G. Larrode, G.J. Rijckenberg, A. Ng’oma, E. Tangdiongga, and A.M.J. Koonen. Radio-over-fibre transmission of multi-carrier 64-QAM radio signal at 18 GHz. In *Broadband Europe*, Dec. 2007. 13, 20
- [52] E. Vos. Frequency Domain Approach for Optimizing Optical Frequency Multiplication System using Mach-Zehnder and Fabry-Perot Interferometer. Master’s thesis, Eindhoven University of Technology, Department of Electrical Engineering, 2008. 13, 15, 16, 17, 18, 19

REFERENCES

- [53] H. Yang, J. Zeng, Y. Zheng, H.D. Jung, B. Huiszoon, J.H.C. van Zantvoort, E. Tangdionga, and A.M.J. Koonen. Evaluation of effects of MZM nonlinearity on QAM and OFDM signals in RoF transmitter. In *Microwave Photonics, 2008. Jointly held with the 2008 Asia-Pacific Microwave Photonics Conference. MWP/APMP 2008. International Topics Meeting on*, pages 90 –93, Sep. 2008. 13, 26
- [54] M.G. Larrode, A.M.J. Koonen, J.J.V. Olmos, and E.J.M. Verdurmen. Microwave signal generation and transmission based on optical frequency multiplication with a polarization interferometer. *Lightwave Technology, Journal of*, 25(6):1372 –1378, Jun. 2007. 13
- [55] M.G. Larrode and A.M.J. Koonen. Theoretical and experimental demonstration of OFM robustness against modal dispersion impairments in radio over multimode fiber links. *Lightwave Technology, Journal of*, 26(12):1722 –1728, Jun. 2008. 60
- [56] M.G. Larrode. *Radio over Fiber Distribution Antenna Systems for In-building Broadband Wireless Services*. PhD thesis, Eindhoven University of Technology, Department of Electrical Engineering, 2008. 13, 20, 105
- [57] L.W. Couch. *Digital and Analog Communication Systems*. 1997. 14
- [58] B. Girod. *Signals and Systems*. Wiley New York, 2001. 14
- [59] G. N. Watson. *A Treatise of the Theory of Bessel Functions*. Cambridge University Press, 1966. 15, 16
- [60] J. Marti, F. Ramos, V. Polo, J.M. Fuster, and J.L. Corral. Chirped fiber gratings for MMW generation and processing. In *Lasers and Electro-Optics Society 2000 Annual Meeting. LEOS 2000. 13th Annual Meeting. IEEE*, volume 1, pages 264 –265 vol.1, 2000. 15
- [61] Light Reading. Who Makes What: GPON & WDM-PON Equipment, Jun. 2009. available on-line at <http://www.lightreading.com/>. 18
- [62] Q. Pan and R.J. Green. AM-SCM-PCM lightwave CATV transmission systems. *Electronics Letters*, 30(14):1155 –1156, Jul. 1994. 18
- [63] H. Yang, H.D. Jung, C. Okonkwo, E. Tangdionga, and A.M.J. Koonen. High capacity radio-over-fiber systems for multicarrier signals with dynamic routing. In *LEOS Annual Meeting Conference Proceedings, 2009. LEOS '09. IEEE*, pages 444 –445, Oct. 2009. 20, 61

-
- [64] Bas Huiszoon. *Optically transparent multiple access networks employing incoherent spectral codes*. PhD thesis, Eindhoven University of Technology, 2008. 20
- [65] K.A. Persson, C. Carlsson, A. Alping, A. Haglund, J.S. Gustavsson, P. Modh, and A. Larsson. WCDMA radio-over-fibre transmission experiment using singlemode VCSEL and multimode fibre. *Electronics Letters*, 42(6):372 – 374, Mar. 2006. 21, 23
- [66] ANRITSU. Adjacent channel power ratio (acpr): application note. available on-line at <http://www.us.anritsu.com/downloads/files/11410-00264.pdf>. 23
- [67] C.S. Oh and W. Gu. Fiber induced distortion in a subcarrier multiplexed lightwave system. *Selected Areas in Communications, IEEE Journal on*, 8(7):1296 –1303, Sep. 1990. 24
- [68] J. Armstrong. OFDM for optical communications. *Lightwave Technology, Journal of*, 27(3):189 –204, Feb. 2009. 24
- [69] T. Keller and L. Hanzo. *OFDM and MC-CDMA: A Primer*. Wiley, 2007. 24
- [70] D. Matiae. OFDM as a Possible Modulation Technique for Multimedia Applications in the Range of mm Waves, 1998. available on-line at www.ubicom.tudelft.nl/MMC/Docs/introOFDM.pdf. 25, 26, 69
- [71] L. Cheng, S. Aditya, Z. Li, and A. Nirmalathas. Generalized analysis of subcarrier multiplexing in dispersive fiber-optic links using Mach-Zehnder external modulator. *Lightwave Technology, Journal of*, 24(6):2296 – 2304, Jun. 2006. 27
- [72] T. Cho and K. Kim. Effect of third-order intermodulation on radio-over-fiber systems by a dual-electrode Mach-Zehnder modulator with ODSB and OSSB signals. *Lightwave Technology, Journal of*, 24(5):2052 – 2058, May. 2006.
- [73] P. Horvath and I. Frigyes. Effects of the nonlinearity of a Mach-Zehnder modulator on OFDM radio-over-fiber transmission. *Communications Letters, IEEE*, 9(10):921 – 923, Oct. 2005. 27
- [74] G.P. Agrawal. *Fiber-Optic Communication Systems*. Wiley, 2002. 27
- [75] H. Yang, E. Tangdionga, S.C.J. Lee, S. Randel, and A.M.J. Koonen. 2.1 Gbit/s ultra-wide-band transmission over 50 m GI-POF using low-cost VCSEL. In *Microwave Photonics, 2009. MWP '09. International Topical Meeting on*, pages 1 –3, Oct. 2009. 33, 37, 38

REFERENCES

- [76] H. Yang, Y. Shi, W. Wang, C.M. Okonkwo, H.P.A. van den Boom, A.M.J. Koonen, and E. Tangdionga. Wimedia-compliant UWB transmission over 1 mm core diameter plastic optical fibre. *Electronics Letters*, 46(6):434 –436, Mar. 2010. 33, 41
- [77] C.M. Okonkwo, H. Yang, Y. Shi, R. Alemany, R. Sambaraju, J. Herrera Llorente, A.M.J. Koonen, and E. Tangdionga. Bi-directional transmission of WiMedia-compliant UWB over 100 m perfluorinated graded-index plastic optical fiber. *Photonics Technology Letters, IEEE*, 2010. accepted for publication. 33, 45
- [78] W. Siri Wongpairat and K. Liu. *Ultra-Wideband Communications Systems : Multiband OFDM Approach*. Wiley, 2007. 33
- [79] M. Welborn. DS-UWB vs. 802.11n: What’s the best connectivity option?, 2005. available on-line at <http://www.eetimes.com/>. 33, 34
- [80] X. Shen, M. Guizani, R.C. Qiu, and T. Le-Ngoc. *Ultra-Wideband Wireless Communications and Networks*. Wiley, 2006. 34
- [81] M.B. Nejad. *Ultra Wideband Impulse Radio for Wireless Sensing and Identification*. PhD thesis, Royal Institute of Technology of Sweden, 2008. 34
- [82] N. Dinur and D. Wulich. Peak-to-average power ratio in high-order OFDM. *Communications, IEEE Transactions on*, 49(6):1063 –1072, Jun. 2001. 34
- [83] ECMA. High Rate Ultrawideband PHY and MAC Standard, Standard ECMA-368, Dec. 2007. available on-line at <http://www.ecma-international.org/publications/standards/Ecma-368>. 34
- [84] www.wimedia.org. 35
- [85] G. Heidari. *WiMedia UWB: Technology of Choice for Wireless UWB and Bluetooth*. Wiley, 2008. 35
- [86] M.P. Thakur, T. Quinlan, S. Dudley, M. Toyman, C. Bock, S.D. Walker, D.W. Smith, A. Borghesani, D. Moodie, R. Llorente, M. Ran, and Y. Ben-Ezra. Bi-directional, 480 Mbps, ultra-wideband, radio-over-fibre transmission using a 1310/1564 nm reflective electro-absorption transducer and commercially-available components. In *Optical Communication, 2008. ECOC 2008. 34th European Conference on*, pages 1 –2, Sep. 2008. 36, 45, 89, 91

-
- [87] Y.X. Guo, V.H. Pham, M.L. Yee, and L.C. Ong. Performance evaluation of multiband orthogonal frequency division multiplexing ultra-wideband signal transmission over multimode fibre. *Optoelectronics, IET*, 4(3):113–120, Jun. 2010. 36
 - [88] Y. Le Guennec, A. Pizzinat, S. Meyer, B. Charbonnier, P. Lombard, M. Lourdiane, B. Cabon, C. Algani, A.L. Billabert, M. Terre, C. Rumelhard, J.L. Polleux, H. Jacquinet, S. Bories, and C. Sillans. Low-cost transparent radio-over-fiber system for in-building distribution of UWB signals. *Lightwave Technology, Journal of*, 27(14):2649–2657, Jul. 2009.
 - [89] M. Ran, B.I. Lembrikov, and Y.B. Ezra. Ultra-wideband radio-over-optical fiber concepts, technologies and applications. *Photonics Journal, IEEE*, 2(1):36–48, Feb. 2010. 36
 - [90] C. Lethien, C. Loyez, J.P. Vilcot, R. Kassi, N. Rolland, C. Sion, and P.A. Rolland. Review of glass and polymer multimode fibers used in a Wimedia ultrawideband MB-OFDM adio over fiber system. *Lightwave Technology, Journal of*, 27(10):1320–1331, May. 2009. 36
 - [91] C. Lethien, C. Loyeza, J.P. Vilcota, L. Clavier, M. Bocqueta, and P.A. Rollanda. Indoor coverage improvement of MB-OFDM UWB signals with radio over POF system. *Optics Comm.*, 282(24):4706–4715, 2009. 36, 45
 - [92] S. Randel, A.M.J. Koonen, S.C.J. Lee, F. Breyer, M.G. Larrode, J. Yang, A. Ng’oma, G.J. Rijckenberg, and H.P.A. van den Boom. Advanced modulation techniques for polymer optical fiber transmission. In *Optical Communication, 2007. ECOC 2007. 33th European Conference on*, Sep. 2007. Th 4.1.4. 36, 69
 - [93] S.C.J. Lee, F. Breyer, S. Randel, J. Zeng, H.P.A. van den Boom, and A.M.J. Koonen. Discrete multi-tone modulation for low-cost and robust 10-Gb/s transmission over polymer optical fibre. In *Optical Communication, 2007. ECOC 2007. 33th European Conference on*, Sep. 2007. Th 9.6.4. 36, 69
 - [94] <http://www.optimedia.co.kr>. 36
 - [95] J.M. Cioffi. A multicarrier primer, Jun. 2008. available online at <http://www-isl.stanford.edu/~cioffi/pdf/multicarrier.pdf>. 37, 70, 71
 - [96] S.C.J. Lee, F. Breyer, S. Randel, R. Gaudino, G. Bosco, A. Bluschke, M. Matthews, P. Rietzsch, R. Steglich, H.P.A. van den Boom, and A.M.J. Koonen. Discrete multitone modulation for maximizing transmission rate in step-index plastic optical fibers. *Lightwave Technology, Journal of*, 27(11):1503–1513, Jun. 2009. 37, 69, 70, 76

REFERENCES

- [97] S.C.J. Lee, F. Breyer, S. Randel, H.P.A. van den Boom, and A.M.J. Koonen. High-speed transmission over multimode fiber using discrete multitone modulation. *Journal of Optical Networking*, 7(2):183–196, 2008. 37, 38, 76
- [98] R. van Nee and R. Prasad. *OFDM for Wireless Multimedia Communications*. Norwood, MA: Artech House, 2000. 37
- [99] P.S. Chow, J.M. Cioffi, and J.A.C. Bingham. A practical discrete multitone transceiver loading algorithm for data transmission over spectrally shaped channels. *Communications, IEEE Transactions on*, 43(234):773–775, Feb. 1995. 38, 71
- [100] J. Stott. The effects of phase noise in COFDM. In *BBC Research and Development Technical Review*, 1998. 45
- [101] A.G. Armada and M. Calvo. Phase noise and sub-carrier spacing effects on the performance of an OFDM communication system. *Communications Letters, IEEE*, 2(1):11–13, Jan. 1998. 45
- [102] H. Yang, H.D. Jung, Y. Zheng, B. Huiszoon, J.H.C. van Zantvoort, E. Tangdiongga, and A.M.J. Koonen. OFDM radio-over-fibre systems employing routing in multi-mode fibre in-building networks. In *Optical Communication, 2008. ECOC 2008. 34th European Conference on*, pages 1–2, Sep. 2008. 51, 57
- [103] H. Yang, Y. Shi, C.M. Okonkwo, E. Tangdiongga, and A.M.J. Koonen. Dynamic capacity allocation in radio-over-fiber links. In *Microwave Photonics, 2010. MWP/APMP 2008. International Topics Meeting on*, Oct. 2010. 51, 57, 61
- [104] A. Mecozzi. Small-signal theory of wavelength converters based on cross-gain modulation in semiconductor optical amplifiers. *Photonics Technology Letters, IEEE*, 8(11):1471–1473, Nov. 1996. 52
- [105] J.M. Wiesenfeld. Wavelength conversion techniques in optical networks. In *Vertical-Cavity Lasers, Technologies for a Global Information Infrastructure, WDM Components Technology, Advanced Semiconductor Lasers and Applications, Gallium Nitride Materials, Processing, and Devi*, pages 42–43, Aug. 1997. 52, 53
- [106] J.M. Wiesenfeld, B. Glance, A.H. Gnauck, L.Y. Lin, J.A. Nagel, J.S. Perino, S.L. Woodward, L.H. Spiekman, U. Koren, C.A. Burrus, M.D. Chien, K. Dreyer, T.L. Koch, B.I. Miller, X. Pan, and G. Raybon. Wavelength conversion techniques for optical networks. In *Optical Communication, 1998. 24th European Conference on*, volume 1, pages 655–656 vol.1, Sep. 1998. 52

-
- [107] T. Durhuus, B. Mikkelsen, C. Joergensen, S. Lykke Danielsen, and K.E. Stubkjaer. All-optical wavelength conversion by semiconductor optical amplifiers. *Lightwave Technology, Journal of*, 14 (6):942–954, Jun. 1996. 52, 53, 54, 55
- [108] J.M. Wiesenfeld, J.S. Perino, A.H. Gnauck, and B. Glance. Bit error rate performance for wavelength conversion at 20 Gbit/s. *Electronics Letters*, 30(9):720–721, Apr. 1994. 52
- [109] M. Galili, L.K. Oxenlowe, H.C. Hansen Mulvad, A.T. Clausen, and P. Jeppesen. Raman-assisted XPM wavelength conversion at 320 Gb/s. In *Optical Communications, 2006. ECOC 2006. European Conference on*, pages 1–2, Sep. 2006. 52, 53
- [110] M. Galili, H.C.H. Mulvad, L. Gruner-Nielsen, J. Xu, L.K. Oxenlowe, A.T. Clausen, and P. Jeppesen. 640 Gbit/s optical wavelength conversion using FWM in a polarisation maintaining HNLF. In *Optical Communication, 2008. ECOC 2008. 34th European Conference on*, pages 1–2, Sep. 2008. 53
- [111] Y. Zheng. Modelling of XGM effect on an analog RF signal in SOA, 2009. Internal report, COBRA Research Institute, Departement of Electrical Engineering, Eindhoven University of Technology. 53, 54, 55, 107, 108
- [112] N. Calabretta, H.D. Jung, J. Herrera Llorente, E. Tangdionga, and H.J.S. Dorren. All-optical label swapping techniques for data packets beyond 160 Gb/s. In *LEOS Annual Meeting Conference Proceedings, 2009. LEOS '09. IEEE*, pages 467–468, Oct. 2009. 55
- [113] H.D. Jung, N. Calabretta, E. Tangdionga, H.J.S. Dorren, and A.M.J. Koonen. All-optical routing architecture of radio signals using label processing technique for in-building optical networks. In *Optical Communication, 2008. ECOC 2008. 34th European Conference on*, pages 1–2, Sep. 2008. 55
- [114] S.T. Abraha, N.C. Tran, C.M. Okonkwo, H. Chen, E. Tangdionga, and A.M.J. Koonen. Service multicasting by all-optical routing of 1 Gb/s IR UWB for in-building networks. In *Optical Fiber Communication 2011. OFC 2011. Conference on*, Mar. 2011. accepted for publication. 65
- [115] M.G. Larrode and A.M.J. Koonen. All-fiber full-duplex multimode wavelength-division-multiplexing network for radio-over-multimode-fiber distribution of broadband wireless services. *Microwave Theory and Techniques, IEEE Transactions on*, 56(1):248–255, Jan. 2008. 65

REFERENCES

- [116] H. Yang, E. Tangdiongga, S.C.J. Lee, S. Randel, H.P.A. van den Boom, and A.M.J. Koonen. 4 Gbit/s over 50-m large core diameter GI-POF using low-cost VCSEL. In *Optical Communication, 2009. ECOC '09. 35th European Conference on*, pages 1 –2, Sep. 2009. 69, 71
- [117] H. Yang, S.C.J. Lee, C.M. Okonkwo, S.T. Abraha, H.P.A. van den Boom, F. Breyer, S. Randel, A.M.J. Koonen, and E. Tangdiongga. Record high-speed short-range transmission over 1 mm core diameter POF employing DMT modulation. *Optics Letters*, 35(5):730 –732, 2010. 69, 74
- [118] H. Yang, E. Tangdiongga, S. Lee, C. Okonkwo, H. van den Boom, S. Randel, and A.M.J. Koonen. 4.7 Gbit/s transmission over 50 m long 1 mm diameter multi-core plastic optical fiber. In *Optical Fiber Communication (OFC), collocated National Fiber Optic Engineers Conference, 2010 Conference on (OFC/NFOEC)*, pages 1 –3, Mar. 2010. 69, 77
- [119] H. Yang, S.C.J. Lee, E. Tangdiongga, F. Breyer, S. Randel, and A.M.J. Koonen. 40-Gb/s transmission over 100 m graded-index plastic optical fiber based on discrete multitone modulation. In *Optical Fiber Communication - includes post deadline papers, 2009. OFC 2009. Conference on*, pages 1 –3, Mar. 2009. 69, 70, 82, 86
- [120] available on-line at <http://www.fiberfin.com/> and <http://www.thorlabs.de/>. 70
- [121] J.A.C. Bingham. Multicarrier modulation for data transmission: an idea whose time has come. *Communications Magazine, IEEE*, 28(5):5 –14, May. 1990. 69
- [122] S. Randel, S.C.J. Lee, B. Spinnler, F. Breyer, H. Rohde, J. Walewski, A.M.J. Koonen, and A. Kirstiater. 1 Gbit/s transmission with 6.3 bit/s/Hz spectral efficiency in a 100 m standard 1 mm step-index plastic optical fiber link using adaptive multiple sub-carrier modulation. In *Optical Communication, 2006. ECOC 2006. 32th European Conference on*, Sep. 2006. PDP Th4.4.1. 76
- [123] F. Breyer, S.C.J. Lee, S. Randel, and N. Hanik. 1.25 Gbit/s transmission over up to 100 m standard 1 mm step-index polymer optical fiber using FFE or DFE equalisation schemes. In *Optical Communication, 2007. ECOC 2007. 33th European Conference on*, Sep. 2007. 9.6.6. 76, 88
- [124] Christian Alexander Bunge. *Polymerfaser-Dmpfungs- und Ausbreitungsmodell (Telekom D02)*. PhD thesis, TU Berlin, 1999. 77
- [125] A. Polley, R.J. Gandhi, and S.E. Ralph. 40 Gbps links using plastic optical fiber. In *Optical Fiber Communication and the National Fiber Optic Engineers Conference, 2007. OFC/NFOEC 2007. Conference on*, pages 1 –3, Mar. 2007. 77, 80

-
- [126] Y. Koike, T. Ishigure, and E. Nihei. High-bandwidth graded-index polymer optical fiber. *Lightwave Technology, Journal of*, 13(7):1475–1489, 1995. 77
- [127] G. Giaretta, W. White, M. Wegmuller, and T. Onishi. High-speed (11 Gbit/s) data transmission using perfluorinated graded-index polymer optical fibers for short interconnects (100 m). *Photonics Technology Letters, IEEE*, 12(3):347–349, Mar. 2000. 80
- [128] IEEE P802.3ba 40 Gb/s and 100 Gb/s Ethernet Task Force. <http://www.ieee802.org/3/ba/>. 80
- [129] S. Schöllmann, C. Wree, A. Joshi, and W. Rosenkranz. First experimental transmission over 50 m GI-POF at 40 Gb/s for variable launching offsets. In *Optical Communication, 2007. ECOC 2007. 33th European Conference on*, Sep. 2007. PDP 3.7. 80
- [130] J. Yu. 42.8 Gb/s chirp-managed signal transmission over 100 m graded-index plastic optical fiber. *Optical Fiber Communication (OFC), collocated National Fiber Optic Engineers Conference, 2010 Conference on (OFC/NFOEC)*, page PDP28, Mar. 2008. 80
- [131] H. Yang, S.C.J. Lee, E. Tangdiongga, C. Okonkwo, H.P.A. van den Boom, F. Breyer, S. Randel, and A.M.J. Koonen. 47.4 Gb/s transmission over 100 m graded-index plastic optical fiber based on rate-adaptive discrete multitone modulation. *Lightwave Technology, Journal of*, 28(4):352–359, Feb. 2010. 82, 83, 86
- [132] G. Yabre. Theoretical investigation on the dispersion of graded-index polymer optical fibers. *Lightwave Technology, Journal of*, 18(6):869–877, Jun. 2000. 84
- [133] T. Ishigure, H. Kano, and Y. Koike. Which is a more serious factor to the bandwidth of GI POF: differential mode attenuation or mode coupling? *Lightwave Technology, Journal of*, 18(7):959–965, Jul. 2000. 84
- [134] A.M.J. Koonen. Bit-error-rate degradation in a multimode fiber optic transmission link due to modal noise. *Selected Areas in Communications, IEEE Journal on*, 4(9):1515–1522, Dec. 1986. 86
- [135] T. Kanada. Evaluation of modal noise in multimode fiber-optic systems. *Lightwave Technology, Journal of*, 2(1):11–18, Feb. 1984.
- [136] G.C. Papen and G.M. Murphy. Modal noise in multimode fibers under restricted launch conditions. *Lightwave Technology, Journal of*, 17(5):817–822, May 1999. 86

REFERENCES

- [137] F. Breyer, S.C.J. Lee, S. Randel, and N. Hanik. Comparison of OOK- and PAM-4 modulation for 10 Gbit/s transmission over up to 300 m polymer optical fiber. In *Optical Fiber communication/National Fiber Optic Engineers Conference, 2008. OFC/NFOEC 2008. Conference on*, pages 1 –3, Feb. 2008. 88
- [138] C.M. Okonkwo, E. Tangdiongga, H. Yang, D. Visani, S. Loquai, R. Kruglov, B. Charbonnier, M. Ouzzif, I. Greiss, O. Ziemann, R. Gaudino, and A.M.J. Koonen. Recent results from the EU POF-PLUS project: Multi-Gigabit transmission over 1 mm core diameter plastic optical fibers. *Lightwave Technology, Journal of*, 2010. accepted for publication. 88
- [139] S.C.J. Lee, S. Randel, F. Breyer, and A.M.J. Koonen. PAM-DMT for intensity-modulated and direct-detection optical communication systems. *Photonics Technology Letters, IEEE*, 21(23):1749 –1751, Dec. 2009. 88
- [140] S.C.J. Lee, F. Breyer, D. Cardenas, S. Randel, and A.M.J. Koonen. Real-time Gigabit DMT transmission over plastic optical fibre. *Electronics Letters*, 45(25):1342 –1343, Dec. 2009. 88
- [141] H. Yang, D. Visani, C.M. Okonkwo, Y. Shi, G. Tartarini, E. Tangdiongga, and A.M.J. Koonen. Multi-standard transmission of converged wired and wireless services over 100 m plastic optical fibre. In *Optical Communication, 2010. ECOC 2010. 36th European Conference on*, Sep. 2010. We.7.B.3. 89, 94
- [142] Cisco. White paper: 10 GBASE-LRM and EDC: Enabling 10 GB deployment in the enterprise. available on-line at <http://www.cisco.com/en/US>. 89
- [143] M. Garcia Larrode, A.M.J. Koonen, J.J. Vegas Olmos, I. Tafur Monroy, and T.C.W. Schenk. RF bandwidth capacity and SCM in a radio-over-fibre link employing optical frequency multiplication. In *Optical Communication, 2005. ECOC 2005. 31st European Conference on*, volume 3, pages 681 – 682 vol.3, Sep. 2005. 89
- [144] J.P. Vilcot, C. Lethien, C. Loyez, and C. Sion. Radio over fiber systems: towards low-cost multi-standard and high data rate wireless applications. In *Microwave Symposium (MMS), 2009 Mediterranean*, pages 1 –3, Nov. 2009. 90
- [145] C. Lethien, C. Loyez, and J.P. Vilcot. Potentials of radio over multimode fiber systems for the in-buildings coverage of mobile and wireless LAN applications. *Photonics Technology Letters, IEEE*, 17(12):2793 – 2795, Dec. 2005.

-
- [146] P.A. Gamage, A. Nirmalathas, C. Lim, E. Wong, D. Novak, and R. Waterhouse. Multi-services distribution using power-efficient low-cost VCSELs. In *Microwave Photonics, 2008. Jointly held with the 2008 Asia-Pacific Microwave Photonics Conference. MWP/APMP 2008. International Topics Meeting on*, pages 169–172, Sep. 2008. 89
- [147] I. Gasulla and J. Capmany. Simultaneous baseband and radio over fiber signal transmission over a 5 km MMF link. In *Microwave Photonics, 2008. Jointly held with the 2008 Asia-Pacific Microwave Photonics Conference. MWP/APMP 2008. International Topics Meeting on*, pages 209–212, Sep. 2008. 89
- [148] C.K. Sim, M.L. Yee, B. Luo, L.C. Ong, and M.Y.W. Chia. Performance evaluation for wireless LAN, Ethernet and UWB coexistence on hybrid radio-over-fiber picocells. In *Optical Fiber Communication Conference, 2005. Technical Digest. OFC/NFOEC*, Mar. 2005. 89
- [149] D. Visani, Y. Shi, C.M. Okonkwo, H. Yang, G. Tartarini, H.P.A. van den Boom, E. Tangdionga, and A.M.J. Koonen. Towards converged broadband wired and wireless in-home optical networks. In *15th International Conference on Optical Network Design and Modeling*, Feb. 2011. accepted for publication. 98, 103
- [150] M.G. Larrode and A.M.J. Koonen. All-fiber full-duplex multimode wavelength-division-multiplexing network for radio-over-multimode-fiber distribution of broadband wireless services. *Microwave Theory and Techniques, IEEE Transactions on*, 56(1):248–255, Jan. 2008. 104, 105
- [151] Y.Y. Won, H.S. Kim, and S.K. Han. 1.25 Gbit/s millimetre-wave band wired/wireless radio-over-fibre system based on RSOA using injection-locking effect. *Electronics Letters*, 45(7):365–366, Mar. 2009. 104
- [152] Y. Shi, H. Yang, D. Visani, C.M. Okonkwo, H.P.A. van den Boom, H. Kragl, G. Tartarini, S. Randel, A.M.J. Koonen, and E. Tangdionga. First demonstration of high capacity large-core POF-based broadcasting for in-home networks. In *Optical Communication, 2010. ECOC 2010. 36th European Conference on*, Sep. 2010. We.6.B.2. 104
- [153] A. Antonino, D. Zeolla, J. Vinogradov, and R. Gaudino. First demonstration of bidirectional Gigabit transmission over a single step-index plastic optical fibre. In *Optical Fiber Communication (OFC), collocated National Fiber Optic Engineers Conference, 2010 Conference on (OFC/NFOEC)*, pages 1–3, Mar. 2010. 104

REFERENCES

- [154] A³PICs. Advanced asics, analog and photonics integrated circuits. available on-line at <http://www.a3pics.com>. 105
- [155] S. Randel, F. Breyer, S.C.J. Lee, and J.W. Walewski. Advanced modulation schemes for short-range optical communications. *Selected Topics in Quantum Electronics, IEEE Journal of*, 16(5): 1280 –1289, Sep. 2010. 105
- [156] B. Kalantari-Sabet, M. Mjeku, N.J. Gomes, and J.E. Mitchell. Performance impairments in single-mode radio-over-fiber systems due to MAC constraints. *Lightwave Technology, Journal of*, 26(15): 2540 –2548, Aug. 2008. 105

Acronyms

Abbreviation	Description
3DTV	three dimension television
APD	avalanche photo-detector
AWG	arbitrary waveform generator
AWG	arrayed waveguide grading
B2B	back to back
BER	bit error ratio
BPF	band-pass filter
CAT-5	catalogue 5
CATV	cable television
CW	continuous wave
DC	direct current
DFB	distributed feedback
DMT	discrete multi-tone
DPO	digital phosphor oscilloscopes
DSB	double side band
DSL	digital subscriber line
DVD	digital video disc
EC	electrical circulator
ECMA	European computer manufacturers association
E/O	electrical to optical
EVM	error vector magnitude
FDM	frequency division multiplexing
FEC	forward error correction
FFT	fast Fourier transform
FM-IM	frequency modulation to intensity modulation
FSR	free spectral range
FTTH	fibre to the home
GI-POF	graded-index plastic optical fibre
GSM	global system for mobile communications

continued on the next page –

REFERENCES

– continued from previous page

Abbreviation	Description
HCC	home communication controller
HDTV	high definition television
IEEE	institute of electrical and electronics engineers
IF	intermediate frequency
IFFT	inverse Fourier transform
IM	intensity modulation
IM/DD	intensity modulation and direct detection
IPTV	internet protocol television
ISI	inter-symbol interference
LAN	local area network
LD	laser diode
LED	light emitting diode
MB-OFDM	multi-band orthogonal frequency division multiplexing
MC-POF	multi-core plastic optical fibre
MMF	multi-mode fibre
MOST	multimedia-oriented system transport
MZI	Mach-Zehnder interferometer
MZM	Mach-Zehnder modulator
NA	numerical aperture
OC	optical circulator
O/E	optical to electrical
OFDM	orthogonal frequency division multiplexing
OFM	optical frequency multiplication
OPLL	optical phase lock loop
PAN	personal area network
PD	photo-detector
PF	perfluorinated
PIN	postive-intrinsic-negative
PM	phase modulation
PMMA	poly-methyl-methacrylate
POF	plastic optical fibre
PON	passive optical network
QAM	quadrature amplitude modulation
RAU	remote antenna unit
RC-LED	resonate-cavity light emitting diode
RF	radio frequency
RG	residential gateway
RoF	radio-over-fibre
SCM	sub-carrier multiplexing
SI-POF	step-index plastic optical fibre

continued on the next page –

– continued from previous page

Abbreviation	Description
SMF	single-mode fibre
SNR	signal-to-noise ratio
SOA	semiconductor optical amplifier
SSB	single-side band
TDM	time division multiplexing
TFC	time-frequency code
TIA	trans-impedance amplifier
UMTS	universal mobile telecommunication system
USB	universal serial bus
UTP	unshielded twisted pair
UWB	ultra-wideband
VCSEL	vertical cavity surface emitting laser
VSG	vector signal generator
VSA	vector signal analyser
WDM	wavelength division multiplexing
WDM-PON	wavelength division multiplexed passive optical network
WiFi	wireless fidelity
WiMax	worldwide interoperability for microwave access
WLAN	wireless local area network
WPAN	wireless personal area network
WWAN	wireless wide area network

REFERENCES

List of publications

Journals

1. D. Visani, C.M. Okonkwo, S. Loquai, H. Yang, Y. Shi, H.P.A. van den Boom, S.C.J. Lee, S. Randel, E. Tangdionga and A.M.J. Koonen, "Beyond 1 Gbit/s Transmission over 1 mm Core Diameter Plastic Optical Fiber employing DMT for In Home Communication Systems", submitted to *IEEE Journal of Lightwave Technology*, 2010
2. C.M. Okonkwo, E. Tangdionga, H. Yang, D. Visani, S. Loquai, R. Kruglov, B. Charbonnier, M. Ouzzif, I. Greiss, O. Ziemann, R. Gaudino and A.M.J. Koonen, "Recent Results from the EU POF-PLUS Project: Multi-Gigabit Transmission over 1 mm Core Diameter Plastic Optical Fibers", *IEEE Journal of Lightwave Technology*, 2010, accepted for publication
3. C.M. Okonkwo, H. Yang, Y. Shi, R. Alemany, R. Sambaraju, J. Herrera, E. Tangdionga and A.M.J. Koonen, "Bi-directional Transmission of WiMedia-Compliant UWB Signals over 100m Per-fluorinated Graded Index-Plastic Optical Fibre for In-Building Networks", *IEEE Photonics Technology Letters*, 2010, accepted for publication
4. Y. Shi, H. Yang, C.M. Okonkwo, E. Tangdionga and A.M.J. Koonen, "Optical frequency multiplication using a fiber ring resonator", *IET Electronics Letters*, Vol. 46, No. 11, Page 781 - 783, May, 2010
5. H. Yang, Y. Shi, W. Wang, C.M. Okonkwo, H.P.A. van den Boom, E. Tangdionga and A.M.J. Koonen, "WiMedia-compliant UWB transmission over 1-mm core diameter plastic optical fiber", *IET Electronics Letters*, Vol. 46, No. 6, Page 434 - 436, March, 2010
6. H. Yang, S.C.J. Lee, E. Tangdionga, C.M. Okonkwo, H.P.A. van den Boom, F. Breyer, S. Randel and A.M.J. Koonen, "47.4 Gb/s Transmission Over 100 m Graded-Index Plastic Optical Fiber

REFERENCES

Based on Rate-Adaptive Discrete Multitone Modulation", *IEEE Journal of Lightwave Technology*, Vol. 28, No. 4, Page 352 - 359, February 2010

7. H. Yang, S.C.J. Lee, C.M. Okonkwo, S.T. Abraha, H.P.A. van den Boom, F. Breyer, S. Randel, E. Tangdiongga and A.M.J. Koonen, "Record high speed short-range transmission over 1-mm core diameter POF employing DMT technique", *OSA Optics Letters*, Vol. 35, No. 3, Page 730-732, February 2010

International conferences

8. Y. Shi, D. Visani, C.M. Okonkwo, H. Yang, H. P. A. van den Boom, G. Tartarini, E. Tangdiongga and A.M.J. Koonen, "First Demonstration of HD Video Distribution over Large-Core POF employing UWB for In-Home Networks", Optical Fiber Communication/National Fiber Optic Engineers Conference (*OFC/NFOEC 2011*), LA, C.A., March 2011, accepted for publication
9. E. Tangdiongga, C.M. Okonkwo, Y. Shi, D. Visani, H. Yang, H.P.A. van den Boom and A.M.J. Koonen, "High-Speed Short-Range Transmission over POF [invited]", Optical Fiber Communication Conference (*OFC 2011*), LA, C.A., March 2011, accepted for publication
10. D. Visani, Y. Shi, C.M. Okonkwo, H. Yang, G. Tartarini, H.P.A. van den Boom, E. Tangdiongga and A.M.J. Koonen, "Towards Converged Broadband Wired and Wireless In-home Optical Networks", 15th International Conference on Optical Network Design and Modeling (*ONDM 2011*), Bologna, Italy, February 8, 2011, accepted for publication
11. A.M.J. Koonen, H. Yang, C.M. Okonkwo, Y. Shi, S.T. Abraha, E.O. Martinez and E. Tangdiongga, "Converged in-building networks using POF - economics and advanced techniques [invited]", 19th International Conference on Plastic Optical Fibers (*POF 2010*), Yokohama, Japan, 19 - 21, October 2010, TH3
12. H. Yang, Y. Shi, C.M. Okonkwo, E. Tangdiongga and A.M.J. Koonen, "Dynamic Capacity Allocation in Radio-over-fiber Links", 2010 IEEE International topical meeting on microwave photonics (*MWP 2010*), Montreal, Canada, 5 - 9 October 2010, TH2-3
13. Y. Shi, H. Yang, C.M. Okonkwo, D. Visani, G. Tartarini, E. Tangdiongga and A.M.J. Koonen, "Multimode Fiber Transmission of Up-Converted MB-OFDM UWB Employing Optical Frequency Multiplication", 2010 IEEE International topical meeting on microwave photonics (*MWP 2010*), Montreal, Canada, 5 - 9 October 2010, TH4-3-2

-
14. H. Yang, D. Visani, C.M. Okonkwo, Y. Shi, G. Tartarini, E. Tangdiongga and A.M.J. Koonen, "Multi-standard Transmission of Converged Wired and Wireless Services over 100m Plastic Optical Fiber", 36th European Conference on Optical Communications (*ECOC 2010*), Torino, Italy, 19 - 23 September 2010, paper We.7.B.3
 15. Y. Shi, H. Yang, D. Visani, C.M. Okonkwo, H.P.A. van den Boom, H. Kragl, G. Tartarini, S. Randel, A.M.J. Koonen and E. Tangdiongga, "First Demonstration of High Capacity Large-Core POF-based Broadcasting for In-Home Networks", 36th European Conference on Optical Communications (*ECOC 2010*), Torino, Italy, 19 - 23 September 2010, paper We.6.B.2
 16. H. Yang, Y. Shi, W. Wang, C.M. Okonkwo, H.P.A. van den Boom, A.M.J. Koonen and E. Tangdiongga, "Multiband OFDM UWB Transmission over 1-mm Core Diameter Graded-Index Plastic Optical Fiber", OSA Access Networks and In-house Communications (*OSA ANIC*), paper AThA3, Karlsruhe, Germany, 21 - 24 June, 2010
 17. R. Alemany, Y. Shi, H. Yang, R. Sambaraju, C.M. Okonkwo, E. Tangdiongga, A.M.J. Koonen and J. Herrera, "UWB Radio over MMF Transmission with Optical Frequency up-Conversion to the 24 GHz Band", OSA Access Networks and In-house Communications (*OSA ANIC*), post-deadline paper AThD1, Karlsruhe, Germany, 21 - 24 June, 2010
 18. H. Yang, E. Tangdiongga, S.C.J. Lee, C.M. Okonkwo, H.P.A. van den Boom, S. Randel and A.M.J. Koonen, "4.7 Gbit/s Transmission over 50 m Long 1 mm Diameter Multi-Core Plastic Optical Fiber", Optical Fiber Communication Conference (*OFC 2010*), San Diego, C.A., 21 - 25 March 2010, paper OWA4
 19. D. Visani, C.M. Okonkwo, S. Loquai, H. Yang, Y. Shi, H.P.A. van den Boom, A.M.H. Ditewig, G. Tartarini, B. Schmauss, S. Randel, A.M.J. Koonen and E. Tangdiongga, "Record 5.3 Gbit/s Transmission over 50m 1mm Core Diameter Graded-Index Plastic Optical Fiber", Optical Fiber Communication/National Fiber Optic Engineers Conference (*OFC/NFOEC 2010*), San Diego, C.A., 21 - 25 March 2010, post-deadline paper PDPa3
 20. E. Tangdiongga, H. Yang, S.C.J. Lee, C.M. Okonkwo, H.P.A. van den Boom, S. Randel and A.M.J. Koonen, "Low-cost and high-capacity short-range optical interconnects using graded-index plastic optical fiber", Optical Fiber Communication/National Fiber Optic Engineers Conference (*OFC/NFOEC 2010*), San Diego, C.A., 21 - 25 March 2010, post-deadline paper JWA64

REFERENCES

21. S.T. Abraha, H. Yang, C.M. Okonkwo, H.P.A. van den Boom, E. Tangdionnga and A.M.J. Koonen, "Novel generation and transmission of 2 Gbps impulse radio ultra wideband over MMF for in-building networks application", Optical Fiber Communication/National Fiber Optic Engineers Conference (*OFC/NFOEC 2010*), San Diego, C.A., 21 - 25 March 2010, OML4
22. A.M.J. Koonen, S.C.J. Lee, H.D. Jung, H. Yang, E. Tangdionnga and H.P.A. van den Boom, "Optical fiber in-building networks - architectures and techniques (invited)", 2009 Intelligent Buildings and Smart Homes Conference, Taipei, Taiwan, 18-20 November, pp. 622-623
23. H. Yang, H.D. Jung, C.M. Okonkwo, E. Tangdionnga and A.M.J. Koonen, "High Capacity Radio-over-Fiber Systems for Multicarrier Signals with Dynamic Routing", 22nd Annual Meeting of the IEEE Photonics Society (*Photonics Annual 2009*), Antalya, Turkey, 4 - 8 October 2009, Paper WG3
24. A.M.J. Koonen, H. Yang, H.D. Jung, S.C.J. Lee, E. Tangdionnga, C.M. Okonkwo, H. van den Boom, "Optical in-building network techniques [invited]", 2009 IEEE LEOS Annual Meeting Conference (*Photonics Annual 2009*, Antalya, Turkey, 4 - 8 October 2009, Paper ThC2
25. S.T. Abraha, H. Yang, E. Tangdionnga and A.M.J. Koonen, "Novel generation and transmission of FCC-compliant impulse radio ultra wideband signals over 100-m GIPOF", 2009 IEEE International topical meeting on microwave photonics (*MWP 2009*), Valencia, Spain, 14 - 16 October 2009, Paper Th4.15
26. H. Yang, E. Tangdionnga, S.C.J. Lee, S. Randel and A.M.J. Koonen, "2.1 Gbit/s MB-OFDM UWB system over 50 m GI-POF", 2009 IEEE International topical meeting on microwave photonics (*MWP 2009*), Valencia, Spain, 14 - 16 October 2009, Paper Th4.10
27. H. Yang, E. Tangdionnga, S.C.J. Lee, S. Randel, H.P.A. van den Boom and A.M.J. Koonen, "4 Gbit/s over 50 m larger core GI-POF using low-cost VCSEL", 35th European Conference on Optical Communications (*ECOC 2009*), Vienna, Austria, 20 - 24 September 2009, Paper 3.5.1
28. S.T. Abraha, H. Yang, E. Tangdionnga and A.M.J. Koonen, "Generation and transmission of FCC compliant impulse radio ultra wideband signals over 100 m GIPOF", 35th European Conference on Optical Communications (*ECOC 2009*), Vienna, Austria, 20 - 24 September 2009, Paper P6.22
29. A.M.J. Koonen, H.D. Jung, H. Yang, C.M. Okonkwo, Y. Zheng, S.T. Abraha and E. Tangdionnga, "Techniques for flexible radio-over-fibre networks (invited)", 2009 International Conference on Photonics in Switching (*PS 2009*), Pisa, Italy, 15 - 20 September 2009, pp. 1-4

-
30. A.M.J. Koonen, S.C.J. Lee, H. Yang, H.D. Jung, E. Tangdiongga, H.P.A. van den Boom and S. Randel, "Research trends in optical in-building networks (invited)", 2009 Lasers & Electro Optics & The Pacific Rim Conference on Lasers and Electro-Optics (*CLEO/PACIFIC RIM 2009*), Shanghai, China, 31 August - 3 September, 2009, Shanghai, China, pp. ThG2-4-1-2
31. H. Yang, S.C.J. Lee, E. Tangdiongga, F. Breyer, S. Randel and A.M.J. Koonen, "40 Gb/s transmission over 100 m graded-index plastic optical fiber based on discrete multitone modulation", Optical Fiber Communication/National Fiber Optic Engineers Conference (*OFC/NFOEC 2009*), San Diego, C.A., 24 - 26 March 2009, post-deadline paper PDPd8
32. H. Yang, H.D. Jung, Y. Zheng, B. Huiszoon, J.H.C. van Zantvoort, E. Tangdiongga, and A.M.J. Koonen, "OFDM radio-over-fibre systems employing routing in multi-mode fibre in-building networks", 34th European Conference on Optical Communications (*ECOC 2008*), Brussels, Belgium, 21 - 25 September 2008, paper Tu4F6
33. H. Yang, J. Zeng, Y. Zheng, H.D. Jung, B. Huiszoon, J.H.C. van Zantvoort, E. Tangdiongga and A.M.J. Koonen, "Evaluation of effects of MZM nonlinearity on QAM and OFDM signals in RoF transmitter", 2008 IEEE International topical meeting on microwave photonics (*MWP 2008*), Gold coast, Australia, 30 September -3 October 2008, pp 90 - 93
34. E.R. Alonso, H. Yang, J.H. Llorente, B. Huiszoon, J.H.C. van Zantvoort and A.M.J. Koonen, "Generation and transmission of high frequency radio signals through fiber links up to 125 km by means of the Optical Frequency Multiplication technique", 2008 IEEE International topical meeting on microwave photonics (*MWP 2008*), Gold coast, Australia, 30 September -3 October 2008, pp 205 - 208
35. A.M.J. Koonen, H. Yang, H.D. Jung, Y. Zheng, J. Yang, H.P.A. van den Boom and E. Tangdiongga, "Recent research progress in hybrid fiber-optic in-building networks (invited)", optoelectronics and communications conference and 2008 Australian conference on optical fiber technology (*OECC 2008*), Sydney, Australia, 7 - 10 July, 2008, paper ONBA3
36. A.M.J. Koonen, H. Yang, H. D. Jung, Y. Zheng, H.P.A. van den Boom and E. Tangdiongga, "Flexible in-building radio-over-fiber networks", 13th European Conference on Networks and Optical Communications (*NOC 2008*), Krems, Austria, 1 - 3 July 2008, pp. 195-202

REFERENCES

37. A.M.J. Koonen, M.G. Larrode, A. Ng'Oma, K. Wang, H. Yang, Y. Zheng and E. Tangdionga, "Perspectives of radio over fiber technologies (invited)", Conference on Optical Fiber Communication/National Fiber Optic Engineers Conference (*OFC/NFOEC 2008*), San Diego, CA, 24 - 28 February 2008, paper OThP3
38. H. Yang, M.G. Larrode, G.J. Rijckenberg, A. Ng'oma, E. Tangdionga and A.M.J. Koonen, "Radio-over-fibre transmission of multi-carrier 64-QAM radio signal at 18 GHz", Broadband Europe (*BBEurope*), Antwerp, Belgium, 3 - 6 December, 2007, paper We2B4
39. H. Yang, C. Peucheret, T. Tokle and P. Jeppesen, "Comparison of practical implementation limitations for different electronic pre-distortion transmitter structures", 32rd European Conference on Optical Communications (*ECOC 2006*), Cannes, France, 24 - 28 September, 2006, Paper We1.5.2, pp. 43

Regional conferences and workshops

40. H. Yang, E. Tangdionga and A.M.J. Koonen, "Simulations of modulator nonlinear effects in radio-over-fibre systems", 12th Annual Symposium of the IEEE/LEOS Benelux Chapter, Brussels, Belgium, 17-18 December 2007, pp. 139-142
41. H. Yang, Y. Zheng, H.D. Jung, E. Tangdionga and A.M.J. Koonen, "Simulation of multi-band OFDM UWB radio over multimode fibre using pre-distortion technique", 13th annual symposium of the IEEE/LEOS Benelux Chapter, Enschede, The Netherlands, 27 - 28 November 2008, pp. 91-94
42. Y. Zheng, H. Yang, H.D. Jung, E. Tangdionga and A.M.J. Koonen, "SOA-based wavelength converter for multi-service radio-over-fiber signals", 13th annual symposium of the IEEE/LEOS Benelux Chapter, Enschede, The Netherlands, 27 - 28 November 2008, pp. 75-78
43. Y. Shi, H. Yang, C.M. Okonkwo, E. Tangdionga and A.M.J. Koonen, "Performance evaluation of multi-band OFDM systems for short-haul optical communications", 14th Annual Symposium of the IEEE Photonics Benelux Chapter, Brussels, Belgium, 5 - 6 November 2009, pp. 125-128
44. H. Yang, E.R. Alonso, Y. Zheng, E. Tangdionga and A.M.J. Koonen, "Radio-over-fibre system for multi-carrier RF signals", FTTH, Wireless Communications and their interaction, 6th Workshop organized by the Network of Excellence ISIS, Stockholm, Sweden, 2 - 3, June 2-3, 2008

Acknowledgements

I am very grateful to my promotor Prof. Ton Koonen for offering me the opportunity to start this PhD project since January 2007. I also want to thank him for the inspiring guidance and valuable support in the past four years. I would like to thank Dr. Eduward Tangdionga, my co-promotor, for his guidance, advices and numerous technical discussion. Without him, every single step of the progress during the project would have been much more difficult.

I would like to give my acknowledgement to the Dutch Senter Novem (now Agentschap NL) organisation of the Dutch Ministry of Economics Affairs, for funding my work in the IOP Generieke Communicatie project Future Home Networks. I would like to thank Prof. Ignas Niemegeers from TU/Delft for coordinating Future Home Networks project, and my colleague Jing Wang for leading most of the project reports. A significant part of my work was involved to the EU project POF-PLUS, for which I would like to express my appreciation to Dr. Roberto Gaudino, Prof. Olaf Ziemann, Dr. Benoit Charbonnier and the other POF-PLUS partners. I am also very grateful to all the members of my PhD committee for reviewing, commenting and approving this work. I appreciate your time and kind considerations.

I would like to thank all the members from the ECO group, especially Henrie van den Boom for the consistent help in the lab regarding the practical problems and Dr. Huug de Waardt for the very kind technical and managemental advices. I am very grateful to Susan de Leeuw, José Hakkens and Audrey van Dinter for their warm assistance on administrative matters. I would also like to thank our ex-colleagues Anthony Ng'oma, Maria Garcia Larrode, Bas Huiszoon and Patryk Urban for all the great time we used to spend and very helpful discussions in the area of radio-over-fibre and access networks. Special thanks to Jeffrey Lee for the great ideas and collaborative work we have made on POF. I also want to say thank-you to Chigo Okonkwo, Solomon Abraha, Yan Shi and Davide Visani, for all the successful late evenings in the lab 11.11 and 11.15. Special thank-you owed to Abhinav Rohit, Jorge Rivas and Dr. Prasanna Gamage for sharing the office room and making it enjoyable.

Finally, I would like to dedicate this thesis to my beloved parents, who have been loving, supporting and encouraging me throughout years and to my dear Jiafan for the faithful support and encouragement.

Curriculum Vitae

Hejie Yang was born in Tianjin, China on January 15, 1982. He received his B.Eng. degree in University of Science and Technology, Beijing, China in 2004 and his M.Sc. degree in Telecommunication from Technical University of Denmark (DTU) in 2006. He started his research on the topic of electrical pre-distortion techniques for optical communications in 2005 in COM research center at DTU (now DTU Fotonik). During the M.Sc. thesis he published his first paper at ECOC '06 in Cannes, France.

In January 2007, he started working towards the Ph.D. degree in the ECO group of COBRA research institute in Eindhoven University of Technology (TU/e), The Netherlands, in the area of optical techniques for in-building networks including radio-over-fibre (RoF) and low-cost plastic optical fibre (POF) techniques. His Ph.D. work has been performed in the framework of Dutch national IOPGenCom program Future Home Networks. Some parts of his work have also been contributed to the EU FP6 project ISIS and the FP7 projects ALPHA, POF-PLUS and EURO-FOS.

During his Ph.D. studies, he has authored and co-authored more than 40 publications in international journals and conferences as well as a featured interview in *IET Electronics Letters*. He is also a peer reviewer for *IET Electronics Letters*.